

UNIVERSITY OF OKLAHOMA

GRADUATE COLLEGE

SCALABLE MICROCRYSTAL MEDIUM FOR STATIC 3D DISPLAY

A DISSERTATION

SUBMITTED TO THE GRADUATE FACULTY

in partial fulfillment of the requirements for the

Degree of

DOCTOR OF PHILOSOPHY

By

BADIA KOUDSI

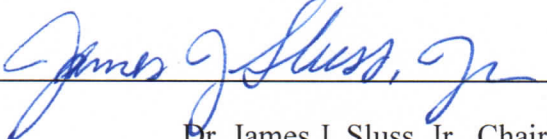
Norman, Oklahoma

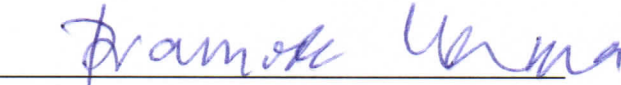
2012


SCALABLE MICROCRYSTAL MEDIUM FOR STATIC 3D DISPLAY

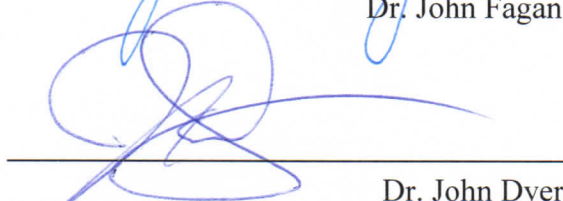
A DISSERTATION APPROVED FOR THE
SCHOOL OF ELECTRICAL AND COMPUTER ENGINEERING

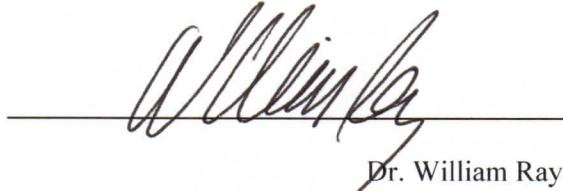
BY


Dr. James J. Sluss, Jr., Chair


Dr. Pramode Verma


Dr. John Fagan


Dr. John Dyer


Dr. William Ray

© Copyright by BADIA KOUDSI 2012

All Rights Reserved

ACKNOWLEDGMENTS

I would like to thank Dr. James Sluss, my advisor for his guidance and support during my PhD.

I am also grateful to my husband Dr. Hakki Refai for his guidance, passion and love.

I would have never been able to go far without the support and trust of my family, particularly my dad, my lovely mom, my brother Yousef and Juji.

Furthermore, I am grateful to Dr. Hazem Refai and his wife Amal for their moral support and encouragement.

I convey many heartfelt thanks to my overseas friends Dima, Hala, lama, Kinda and 2 Jasmine for their love and support.

In addition, I would like to thanks 3DIcon Corporation and OCAST, which funded my research.

TABLE OF CONTENTS

Table of contents	v
List of tables	vii
List of figures	viii
Abstract	xii
Chapter 1: Introduction	1
1.1 Depth cue	2
1.2 Various types of 3D displays	4
1.2.1 Stereoscopic display.	5
1.2.2 Autostereoscopic display.	6
1.2.3 Multiview autostereoscopic.	7
1.2.4 Integral imaging.	7
1.2.5 Holography.	8
1.2.6 Volumetric display.	9
1.3 Dissertation outline.	12
Chapter 2: CSpace [®] display.	14
Chapter 3: Physical Background of Materials.	18
3.1 Photon conversion.	18
3.1.1. Down-conversion.	18
3.1.2 Quantum cutting.	18
3.1.3 Up-conversion.	18
3.1.3.1 Up-conversion mechanism in Er-Yb co-doped systems.	23
3.1.3.2 Up-conversion mechanism in Tm ⁺³ -Yb ⁺³ co-doped systems.	25
Chapter 4: Scalable Medium for CSpace display.	26
4.1 Crystal size	26
4.1.1 Nanocrystal	26
4.1.2 Micro crystal.	27
4.1.3 Bulk crystal	28
4.2 Experimental setup.	28
4.2.1 Sample preparation procedure:	28
4.2.1.1 Preparation of 10% wt microcrystals with different refractive index liquid.	28
4.2.2 Structural characterization.	29
4.2.3 Optical characterization.	30
4.2.3.1 Transmission or Scattering	30
4.2.3.2 Green emission strength.	32
Chapter 5: Microcrystal Testing.	36
5.1 1% Er: NaYF ₄ 10 wt% microcrystals with different refractive index.	36
5.1.1 SEM Measurement:	36
5.1.2 Transmission measurement.	37

5.1.3 Green emission strength.	40
5.2 0.5% Er: KY ₃ F ₁₀ 10 wt% microcrystal with different refractive index liquids:	48
5.2.1 SEM Measurement.	48
5.2.2 Transmission measurement	49
5.2.3 Green emission strength measurement.	51
5.3 0.5% Er: LLF 10 wt% microcrystal with different refractive index liquids:	59
5.3.1 SEM measurement.	59
5.3.2 Transmission measurement	60
5.3.3 Green emission strength measurements	62
Chapter 6: Different particle concentration.	71
6.1 1%Er: NaYF ₄ 20 wt% dispersed in 1.468.	71
6.1.1 Transmission measurement:	71
6.1.2 Green emission measurement	74
6.2 1%Er: NaYF ₄ 30 wt%.	74
6.2.1 Transmission measurement.	75
6.2.2 Green emission strength measurement	76
6.3 0.5% Er: KY ₃ F ₁₀ 20 wt%.	77
6.3.1 Transmission measurement	77
6.3.2. Green emission strength measurement	78
6.4 0.5% Er: KY ₃ F ₁₀ 30 wt%	78
6.4.1 Transmission measurement	78
6.4.2 Green emission strength measurement	79
6.5 Transparency.	80
6.5.1 1%Er: NaYF ₄ .	80
6.5.2 0.5% Er: KY ₃ F ₁₀ .	81
Chapter 7: Bulk crystals	82
7.1 1%Er:NaYF ₄ bulk crystal.	82
7.2 2%Er: NaYF ₄ .	83
7.3 0.5% Er:KY ₃ F ₁₀ .	84
7.4 0.5% Er: YLF.	85
7.5 Data analysis.	85
Chapter 8: Review of results and analysis, and 3D Image constructed using the CSpace [®] display	88
8.1 Volumetric 3D image inside special image space constructed using CSpace display_	91
Chapter 9: Conclusion and Future work.	95
9.1 Conclusion	95
9.2 Future works	97
References	98

LIST OF TABLES

Table 3.1.3.1: Comparison between the different up conversion processes regarding their efficiencies [9].

Table 5.1.3.1: The average green emission strength for the sample 1%Er: NaYF₄ 10 wt% microcrystal dispersed in different refractive index liquid.

Table 5.2.3.1: Average green emission measurements for the sample 0.5% Er: KY₃F₁₀ 10 wt% dispersed in different refractive index liquid.

Table 5.3.2.1: Average green emission strength for the microcrystal 0.5% Er: LLF 10 wt% dispersed in different refractive index liquids.

Table 7.5.1: Green emission measurements for the studied bulk crystal.

Table 7.5.2: Green emission for the sample 0.5% Er: KY₃F₁₀

Table 8.1: Green emission measurements for the studied samples.

LIST OF FIGURES

- Figure 1.1.1: Depth cue categories.
- Figure 1.2.1: Schematic for 3D display types.
- Figure 1.2.1.1: Anaglyph principle [3].
- Figure 1.2.2.1: Type of Autostereoscopic Display (a) lenticular and (b) parallax barrier [5].
- Figure 1.2.4.1: Integral imaging. [6]
- Figure 1.2.5.1: Recording and decoding the hologram [4].
- Figure 1.2.6.1: Swept volumetric display: a) Perspecta spatial 3D system b) Felix 3D[?].
- Figure 1.2.6.2: Static volumetric displays examples. A) DepthCube [26 from master]. B) Elizabeth Downing volumetric display [29 from master].
- Figure 2.1: 3D volumetric display using two DLP projectors.
- Figure 2.2:
3D volumetric Display where image space can be seen from all directions.
- Figure 2.3: 3D Volumetric display using four DLP projectors.
- Figure 3.1.3.1: General diagram for a simple three-level system.
- Figure 3.1.3.2: Various up conversion mechanisms.
- Figure 3.1.3.3: Up conversion mechanism in Er^{+3} - Yb^{+3} co-doped systems [7].
- Figure 3.1.3.4: Up-conversion mechanism in Tm^{+3} - Yb^{+3} co-doped systems [7].
- Figure 4.1.1.1: 3D image in silicone [20].
- Figure 4.2.2.1: Observation with SEM (from the SEM brochure).
- Figure 4.2.3.1.1: Scattering setup schematic.
- Figure 4.2.3.2.1: Measurement setup for green emission strength.
- Figure 4.2.3.2.2: Green emission strength setup measurement.
- Figure 4.2.3.2.3: Telescope measuring the green emission voxel inside the placed sample.
- Figure 5.1.1.1: a) low resolution SEM images of 1% Er: NaYF₄ with 50 μm scale bar, B) high resolution SEM image with 4 μm scale bars.
- Figure 5.1.2.1: 2-28 μm 1%Er: NaYF₄10%wt dispersed in 1.45,1.456,1.46 refractive index liquids, b) 1%Er: NaYF₄10%wt dispersed in 1.464,1.468,1.472, c) 1%Er: NaYF₄10%wt dispersed in 1.47,1.474, 1.476, d) 1%Er: NaYF₄10%wt dispersed in 1.48,1.484,1.49.
- Figure 5.1.2.2: Comparison between 2-28 μm size 1%Er:NaYF₄10%wt particles dispersed in 1.47 and 1.49 index match liquid.
- Figure 5.1.2.3: Comparison between 2-28 μm size 1%Er: NaYF₄ 10%wt particles dispersed in 1.45 and 1.468 index match liquid.
- Figure 5.1.2.4: Scattering measurement setup.
- Figure 5.1.2.5: Transmission setup for the sample 1%Er: NaYF₄ dispersed in a 1.48 refractive index liquid.
- Figure 5.1.2.6: Transmission measurement for 1%Er: NaYF₄ in different refractive index liquid samples.

Figure 5.1.3.1: Green emission strength for the sample 1%Er: NaYF₄ 10wt% microcrystal dispersed in 1.45 refractive index liquid.

Figure 5.1.3.2: Green emission strength for the sample 1%Er: NaYF₄ 10wt% microcrystal dispersed in 1.456 refractive index liquid.

Figure 5.1.3.3: Green emission strength for the sample 1%Er: NaYF₄ 10wt% microcrystal dispersed in 1.46 refractive index liquid.

Figure 5.1.3.4: Green emission strength for the sample 1%Er: NaYF₄ 10wt% microcrystal dispersed in 1.464 refractive index liquid.

Figure 5.1.3.5: Green emission strength for the sample 1%Er: NaYF₄ 10wt% microcrystal dispersed in 1.468 refractive index liquid.

Figure 5.1.3.6: Green emission strength for the sample 1%Er: NaYF₄ 10 wt% microcrystal dispersed in 1.47 refractive index liquid.

Figure 5.1.3.7: Green emission strength for the sample 1%Er: NaYF₄ 10 wt% microcrystal dispersed in 1.472 refractive index liquid.

Figure 5.1.3.8: Green emission strength for the sample 1%Er: NaYF₄ 10 wt% microcrystal dispersed in 1.474 refractive index liquid.

Figure 5.1.3.9: Green emission strength for the sample 1%Er: NaYF₄ 10 wt% microcrystal dispersed in 1.476 refractive index liquid.

Figure 5.1.3.10: Green emission strength for the sample 1%Er: NaYF₄ 10 wt% microcrystal dispersed in 1.48 refractive index liquid.

Figure 5.1.3.11: Green emission strength for the sample 1%Er: NaYF₄ 10 wt% microcrystal dispersed in 1.484 refractive index liquid.

Figure 5.1.3.12: Green emission strength for the sample 1%Er: NaYF₄ 10 wt% microcrystal dispersed in 1.49 refractive index liquid.

Figure 5.1.3.13: Green emission strength for samples of 1%Er: NaYF₄ 10 wt% microcrystal dispersed in different refractive index liquids.

Figure 5.2.1.1: SEM measurement for 0.5% Er: KY₃F₁₀ 10 wt% .

Figure 5.2.1.2: a) 0.5% Er: KY₃F₁₀ 10 wt% dispersed in 1.45,1.456,1.46 refractive index liquids, b) 0.5% Er: KY₃F₁₀ 10 wt% dispersed in 1.464,1.468,1.47, c) 0.5% Er: KY₃F₁₀ 10 wt% dispersed in 1.47,1.474, 1.476,, d) 0.5% Er: KY₃F₁₀ 10 wt% dispersed in 1.48,1.484,1.49.

Figure 5.2.1.3: Comparison between the sample 0.5% Er: KY₃F₁₀ 10 wt% dispersed in 1.47 and 1.49 refractive index liquid.

Figure 5.2.1.4: Transmission measurement for the sample 0.5% Er: KY₃F₁₀ 10 wt% dispersed in 1.46 refractive index liquid.

Figure 5.2.1.5: Transmission measurement for 0.5% Er: KY₃F₁₀ 10 wt%: in different refractive index liquids.

Figure 5.2.3.1: Green emission strength for 0.5% Er: KY₃F₁₀ 10 wt% dispersed in 1.45 refractive index liquid.

Figure 5.2.3.2: Green emission strength for 0.5% Er: KY₃F₁₀ 10 wt% dispersed in 1.456 refractive index liquid.

Figure 5.2.3.3: Green emission strength for 0.5% Er: KY₃F₁₀ 10 wt% dispersed in 1.46 refractive index liquid.

Figure 5.2.3.4: Green emission strength for 0.5% Er: KY₃F₁₀ 10 wt% dispersed in 1.464 refractive index liquid.

Figure 5.2.3.5: Green emission strength for 0.5% Er: KY₃F₁₀ 10 wt% dispersed in 1.468 refractive index liquid.

Figure 5.2.3.6: Green emission strength for 0.5% Er: KY₃F₁₀ 10 wt% dispersed in 1.47 refractive index liquid.

Figure 5.2.3.7: Green emission strength for 0.5% Er: KY₃F₁₀ 10 wt% dispersed in 1.474 refractive index liquid.

Figure 5.2.3.8: Green emission strength for 0.5% Er: KY₃F₁₀ 10 wt% dispersed in 1.476 refractive index liquid.

Figure 5.2.3.9: Green emission strength for 0.5% Er: KY₃F₁₀ 10 wt% dispersed in 1.48 refractive index liquid.

Figure 5.2.3.10: Green emission strength for 0.5% Er: KY₃F₁₀ 10 wt% dispersed in 1.484 refractive index liquid.

Figure 5.2.3.11: Green emission strength for 0.5% Er: KY₃F₁₀ 10 wt% dispersed in 1.49 refractive index liquid.

Figure 5.2.3.12: Green emission strength measurement for the sample 0.5% Er: KY₃F₁₀ 10 wt% dispersed in different refractive index liquids.

Figure 5.3.1.1: High magnification SEM images for the sample 0.5% Er: LLF 10 wt%.

Figure 5.3.2.1: a) 0.5% Er: LLF10 wt% dispersed in 1.45,1.456,1.46 refractive index liquids, b) 0.5% Er: LLF 10 wt% dispersed in 1.464,1.468,1.47, c) 0.5% Er: LLF 10 wt% dispersed in 1.47,1.474, 1.48,, d) 0.5% Er: LLF 10 wt% dispersed in 1.484,1.49.

Figure 5.3.2.2. Comparison for the sample 0.5% Er: LLF10 wt% dispersed in 1.45 and 1.47 refractive index liquid.

Figure 5.3.2.3: Measurement setup for the scattering test.

Figure 5.3.2.4: Transmission measurements for 0.5% Er: LLF 10 wt% dispersed in different refractive index liquids.

Figure 5.3.3.1: Measurement green emission setup for 0.5% Er: LLF 10 wt% samples.

Figure 5.3.2.2: Green emission strength for 0.5% Er: LLF 10 wt% dispersed in 1.45 refractive index liquid.

Figure 5.3.2.3: Green emission strength for 0.5% Er: LLF 10 wt% dispersed in 1.456 refractive index liquid.

Figure 5.3.2.4: Green emission strength for 0.5% Er: LLF 10 wt% dispersed in 1.46 refractive index liquid.

Figure 5.3.2.5: Green emission strength for 0.5% Er: LLF 10 wt% dispersed in 1.464 refractive index liquid.

Figure 5.3.2.6: Green emission strength for 0.5% Er: LLF 10 wt% dispersed in 1.468 refractive index liquid.

Figure 5.3.2.7: Green emission strength for 0.5% Er: LLF 10 wt% dispersed in 1.467 refractive index liquid.

Figure 5.3.2.8: Green emission strength for 0.5% Er: LLF 10 wt% dispersed in 1.472 refractive index liquid.

Figure 5.3.2.9: Green emission strength for 0.5% Er: LLF 10 wt% dispersed in 1.474 refractive index liquid.

Figure 5.3.2.10: Green emission strength for 0.5% Er: LLF 10 wt% dispersed in 1.48 refractive index liquid.

Figure 5.3.2.11: Green emission strength for 0.5% Er: LLF 10 wt% dispersed in 1.484 refractive index liquid.

Figure 5.3.2.12: Green emission strength for 0.5% Er: LLF 10 wt% dispersed in 1.49 refractive index liquid.

Figure 5.3.2.13: Green emission measurement for the 0.5% Er: LLF 10 wt% microcrystal dispersed in collection of refractive indices liquids.

Figure 6.1.1.1: Scattering measurement setup.

Figure 6.1.1.2: Transmission result for the sample 1%Er: NaYF₄ 20 wt% dispersed in 1.468.

Figure 6.1.2.1: Green emission strength for 1%Er: NaYF₄ 20 wt% dispersed in 1.468.

Figure 6.2.1.1: Transmission measurement for the sample 1%Er: NaYF₄ 30 wt% dispersed in 1.468.

Figure 6.2.2.1: Green emission strength for 1%Er: NaYF₄ 30 wt% dispersed in 1.468.

Figure 6.3.1.1: Transmission measurement for the sample 0.5% Er: KY₃F₁₀ 20 wt% dispersed in 1.49.

Figure 6.3.2.1: Green emission strength for 0.5% Er: KY₃F₁₀ 20 wt% dispersed in 1.49.

Figure 6.4.1.1: Transmission measurement for the sample 0.5% Er: KY₃F₁₀ 30 wt% dispersed in 1.49 .

Figure 6.4.2.1: Green emission strength measurement for 0.5% Er: KY₃F₁₀ 30 wt% dispersed in 1.49.

Figure 6.5.1.1: Comparison between 1%Er: NaYF₄ 20 wt% and 30% wt dispersed in 1.468.

Figure 6.5.2.1: Comparison between 0.5% Er: KY₃F₁₀ 30wt% and 20% dispersed in 1.49.

Figure 8.1.1: 1%Er: NaYF₄ bulk crystal.

Figure 8.2.1: 2%Er: NaYF₄ bulk crystal.

Figure 8.3.1: 0.5% Er: KY₃F₁₀ bulk crystal.

Figure 8.4.1: 0.5% Er: YLF bulk crystal.

Figure 9.1.1: Scalable medium for CSpace[®] display.

Figure 9.1.2: The desired image “gear”.

Figure 9.1.3: Six slices for the gear image.

Figure 9.1.4: The gear with depth “6 slices”.

Figure 9.1.5: The scalable medium placed in CSpace[®] display.

Figure 9.1.6: the desired image “gear” in 3D using CSpace[®] display.

Figure 9.1.7: The desired image from different directions.

Abstract

Efficient up-conversion emitters are necessary to generate full color 3D display. Rare-earth, co-doped fluorides that convert diode laser light from near infrared to visible red, green, and blue light by sequential two photon absorption are necessary to accomplish this. An up-conversion medium for 3D display, particularly the CSpace[®] “static volumetric display”, can be fabricated by grinding rare-earth-doped fluoride bulk crystals into a powder, and then dispersing the resultant microcrystals within an index matched host. This technique leads to a reduction in display cost, weight, and growing time, as well as provides display scalability. To demonstrate a scalable medium for the CSpace[®] display, several rare-earth-doped fluoride bulk crystals were ground into a microcrystal powder and then dispersed in different refractive index liquids, including 1.45, 1.456, 1.46, 1.464, 1.468, 1.47, 1.474, 1.476, 1.48, 1.484, and 1.49. Fluorescence strength and transmission measurements were taken. Different particle concentrations were tested and demonstrated, as well. Detailed experiments for these measurements are described in this dissertation. A real volumetric 3D image was constructed inside a prototype display medium of 40 x 40 x 10 mm³ using the CSpace[®] display. A potential future solution is presented, and suggestions to improve the scalable medium are given.

Chapter 1

Introduction

Several industries have been targeted for employing three dimensional (3D) display technologies; however, none have yet to take initiative for development. Due to the increasing interest and the need for 3D display systems in medicine, defense, education, and baggage scanning, competition for market share will soon be substantial [1].

A promising static volumetric 3D display system called CSpace[®] is currently under development as part of an ongoing public-private collaboration supported by the University of Oklahoma. The CSpace[®] display can produce up to an 800 million voxel 3D image in real time with full range view without the use of visual aids. Because 3D images are drawn in a medium, the medium itself is the most important factor in the functionality of the CSpace[®] system. The medium must be characterized with good brightness, transparency, optical properties, uniformity, and must also be reproducible in any size at a reasonable cost. The CSpace[®] medium currently used is 1% Er: NYF₄ bulk crystal with a dimension of approximately 4 x 4 x 10 cm³. The image space consists of four pieces of the bulk crystal, each sized approximately 2 x 2 x 10 cm³. The four pieces are optically glued to create a medium 4 x 4 x 10 cm³ in size. This solution is expensive, and its size has not yet reached minimum requirements. As such, it is doubtful the technique will be efficient enough for practical use, especially when medium fabrication is needed to manufacture a significant number of image spaces for commercial purposes.

The research conducted in this dissertation is primarily concerned with the scalability of the 3D display medium and the possibility of easily fabricating a large 3D display medium at a reasonable cost. An up-conversion medium for 3D display,

particularly for CSpace[®], has been fabricated by grinding rare-earth-doped fluoride bulk crystals and then dispersing resultant microcrystals within an index match host. This innovation led to a reduction in display cost, weight, and growing time, and facilitated display scalability. The study evaluated the impact of refractive index matching on scattering; refractive index matching on green emission strength; changing weight percentage (wt %) of particles on both scattering and green emission strength; and the creation of a 3D image within the resultant prototype display medium.

The contributions of this work are conclusions based on supporting experimental data in which grinding bulk crystals into microcrystal and placing them in an index matching host lead to a significant increase in the size of the 3D display medium while retaining the desired optical properties. Also, a real volumetric 3D image was rendered inside a prototype display medium sized 40 x 40 x10 mm³. To the best of the author's knowledge, these are the first reported results of this kind.

1.1 Depth cue

The phenomena “three dimension,” i.e., an object with width, height, and depth, has become well known. Depth perception is inherent in the human visual system and enables observable relationships between objects. Although the retina of each human eye produces merely a two-dimensional (2D) image of its surroundings, the human brain processes these two images into a 3D image. Accomplishing this task largely depends on a significant number of cues to evaluate distance, depth, and object shape in a 3D environment.

Depth cues can be classified into three categories, as shown in Figure 1.1.1.

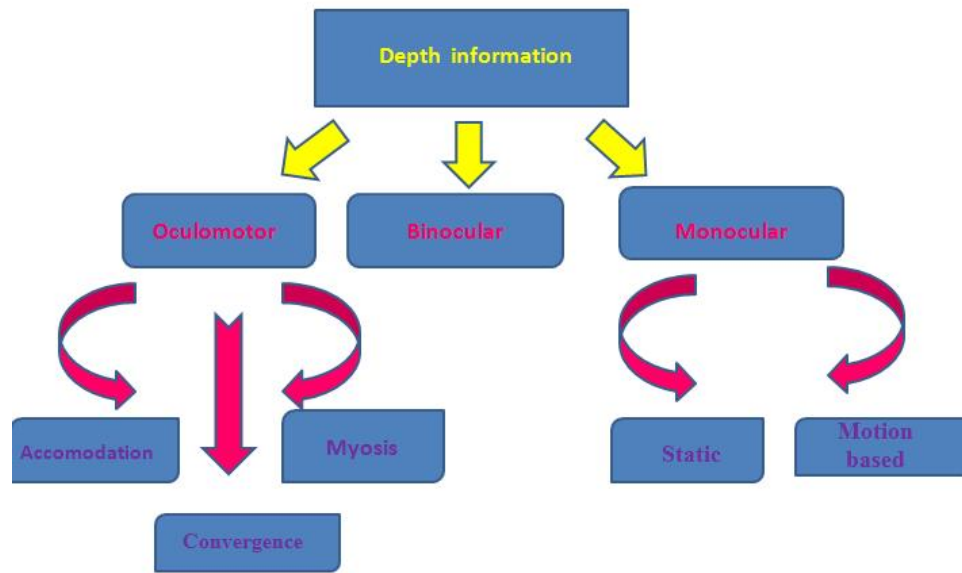


Figure 1.1.1. Depth cue categories.

Depth information is generated via monocular, binocular, and oculomotor cues.

Monocular cues provide a sense of relative distance and depth and can be further sub-divided as follows:

- a) Interposition cues are generated when objects overlap; the brain interprets the overlapped object lying furthest away;
- b) Linear perspective cues are determined when the smaller angle of objects further away makes them appear smaller than nearby objects [2];
- c) Aerial perspective cues are reliant on the relative color of the objects to indicate their distance from the observer [3], e.g., due to the scattering of the blue light in the atmosphere, distant objects are perceived with a greater intensity of blue;
- d) Light and shadow cues inform about depth; and

- e) Motion based cues occur when the observer is in motion, signaling that a closer object moves faster than an object lying at a greater distance from the observer [4].

Binocular (or stereopsis) cues facilitate depth perception by means of binocular retinal disparity caused from human physiology of having two eyes—each providing a slightly different view of the same scene. Brain interpretation of the dissimilar views renders a sense of the depth [3] [5].

Oculomotor cues can be subdivided into three types:

- a) Accommodation cues occur when the eye moves outward in an attempt to bring the image of a distant object into focus; this causes ciliary muscles to relax, which in turn adjusts lens curvature so that the brain interprets the applied tension as depth cues [3] [6].
- b) Convergence cues occur when the eye moves inward in an attempt to bring an image of a nearby object into focus, causing ciliary muscles to tighten and then adjust lens curvature [1]; and
- c) Myosis cues create a perception of size based on the perception of depth.

1.2 Various types of 3D displays

A number of display technologies have been proposed for visualizing a 3D scene. A review of basic technologies most commonly used is summarized below.

A schematic diagram of various displays is shown in Figure 1.2.1.

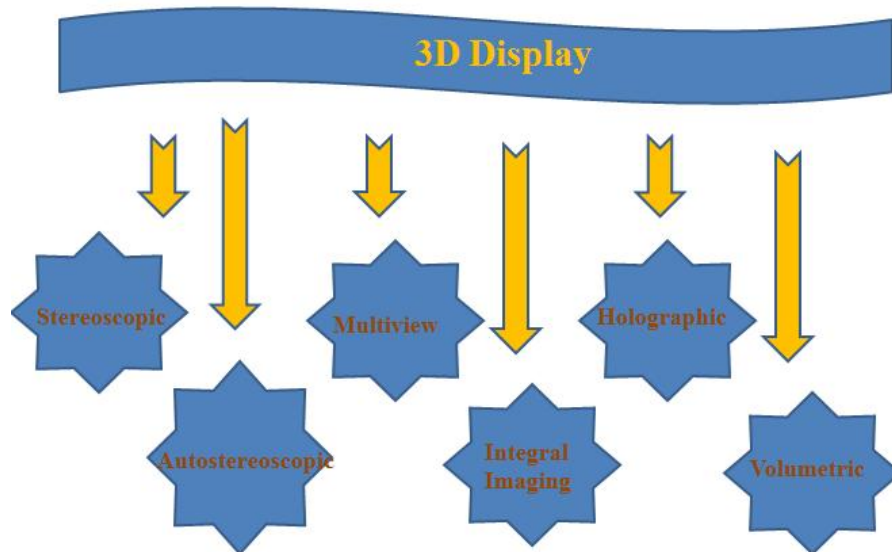


Figure 1.2.1. Schematic for 3D display types.

1.2.1 Stereoscopic display

Stereoscopy is based on the physiology of two eyes capturing two slightly different 2D images of a 3D scene at slightly different angles, and then simultaneously delivering each image to the corresponding eye [7] [8] [9]. This technique requires the viewer to wear special glasses. Various modes of separation techniques have been used by multiplexing methods, e.g., wavelength-division (anaglyph), time division, and polarization division, or combinations thereof.

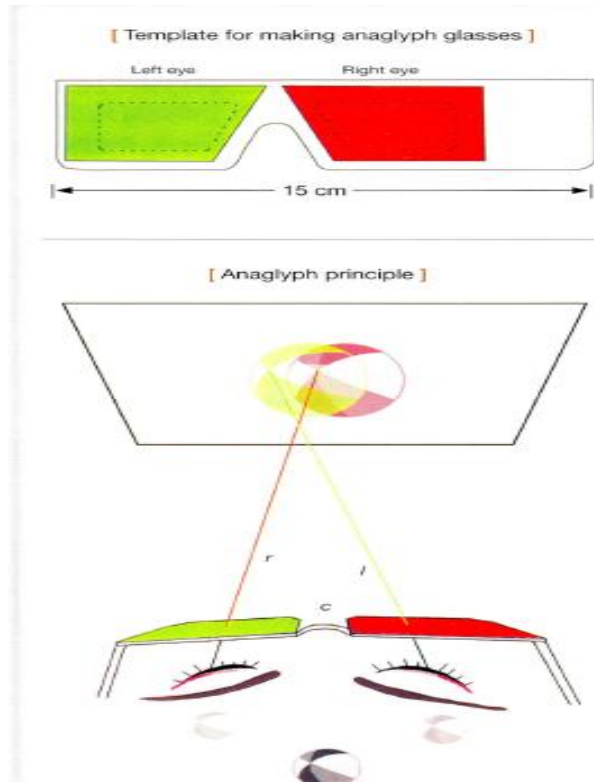


Figure 1.2.1.1. Anaglyph principle is an example of stereoscopic display [10].

1.2.2 Autostereoscopic display

Autostereoscopic displays vary from conventional stereoscopic displays in that they create a fixed viewing zone for each eye that does not require special eyewear [11] [12] [13] [14]. Two prevailing technologies include lenticular and parallax barrier, as shown in Figure 1.2.2.1.

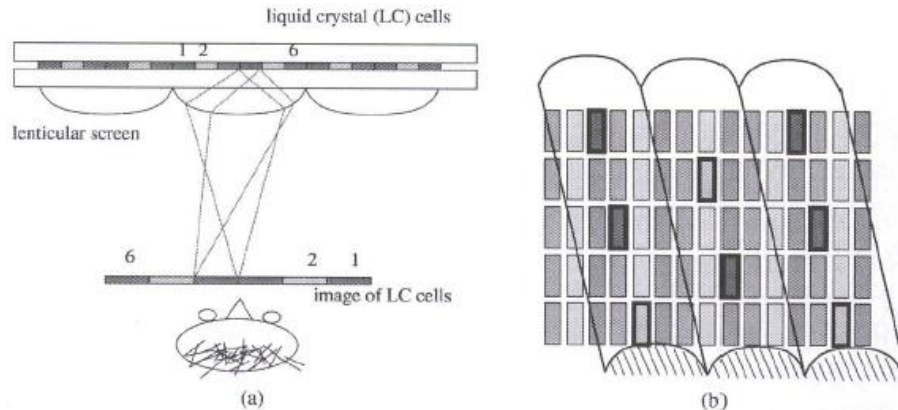


Figure 1.2.2.1. Type of Autostereoscopic Display (a) lenticular and (b) parallax barrier [15].

1.2.3 Multiview autostereoscopic

Multiview autostereoscopic display is an extension of two-view autostereoscopic technology. Like autostereoscopic display, each view propagates from the display within a narrow horizontal angle without vertical variation, allowing the viewer to change position only within a limited viewing area of a 3D scene. The advantage of this technique is that the observer can view the 3D scene while moving horizontally, although vertical motion remains a problem [16].

1.2.4 Integral imaging

Integral imaging display is an extension of lenticular multi-view display wherein the lenticular sheet is no longer a cylindrical lens array, but rather an array of very small spherical lenses. The display comprised from a large number of 2D views from a 3D scene separated both horizontally and vertically [17], as depicted in Figure 1.2.4.1.

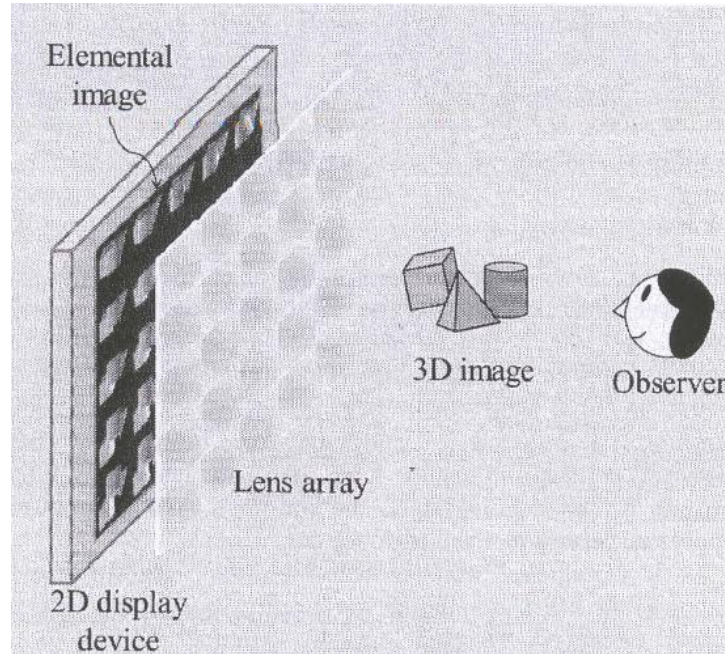


Figure 1.2.4.1. Integral imaging [17].

1.2.5 Holography

The holographic effect is achieved by recording the intensity and phase/directional information of light as an interference pattern between illumination of an object and a reference beam [18]. This is possible since interference occurs only with coherent light, as shown in Figure 1.2.5.1. Because laser light is coherent, it is used during recording.

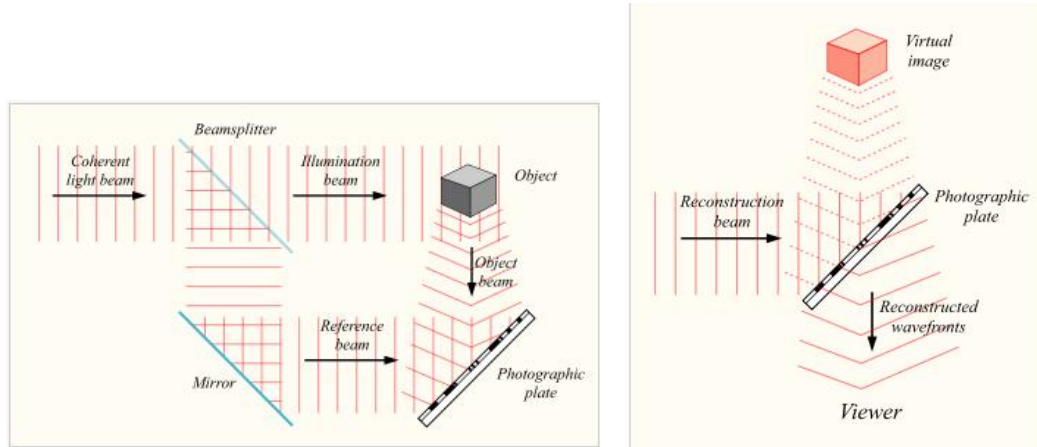


Figure 1.2.5.1. Recording and decoding the hologram [18].

1.2.6 Volumetric display

Volumetric display has several advantages. Not only does it provide a wide viewing zone, it also offers correct accommodation cues and full parallax images. However, occlusion cannot be implemented in this technology, as images are transparent rather than opaque. Volumetric display technologies can be divided into two categories: swept volumetric display and static volumetric display [19].

Swept volumetric display

In swept volumetric display, 2D slices of the 3D image are rotating and projected from different directions at a sufficient rate. If motion exceeds the human vision system tracking ability, the perceived image will appear to be 3D. For example, if a display of a pyramid is desired, a group of different sized triangles must be displayed on a rotating screen at sufficient speed [20] [21] [22]. An example of swept volume display is shown in Figure 1.2.6.1.

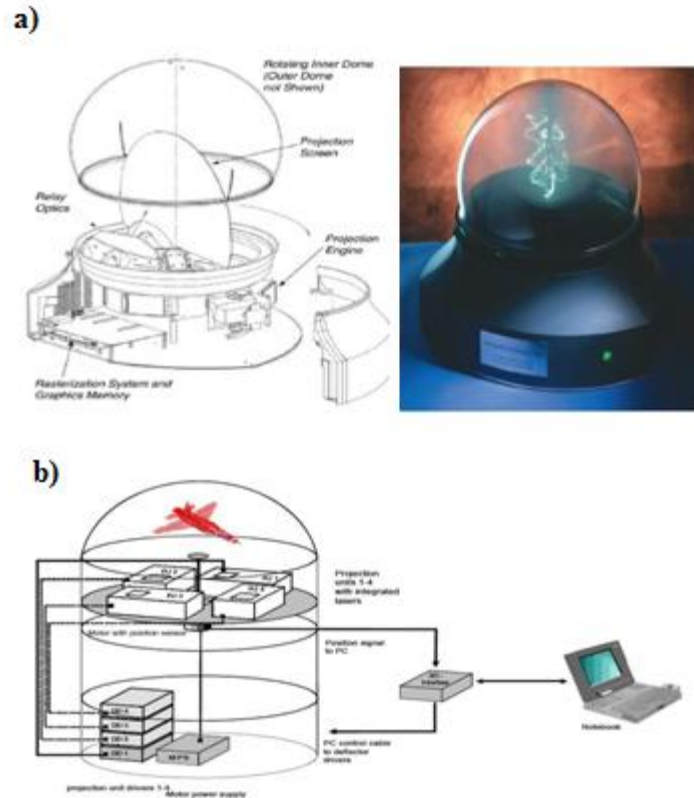


Figure 1.2.6.1. Swept volumetric display: a) Perspecta spatial 3D system [22] b) Felix 3D [23].

Static Volumetric display

Static volumetric display has the advantage of displaying the 3D image in a static volume without the adverse effects of moving mechanical parts. The CSpace[®] display serves as an example of such technology [24] [25]. An example of static volumetric display is provided in Figure 1.2.6.2.

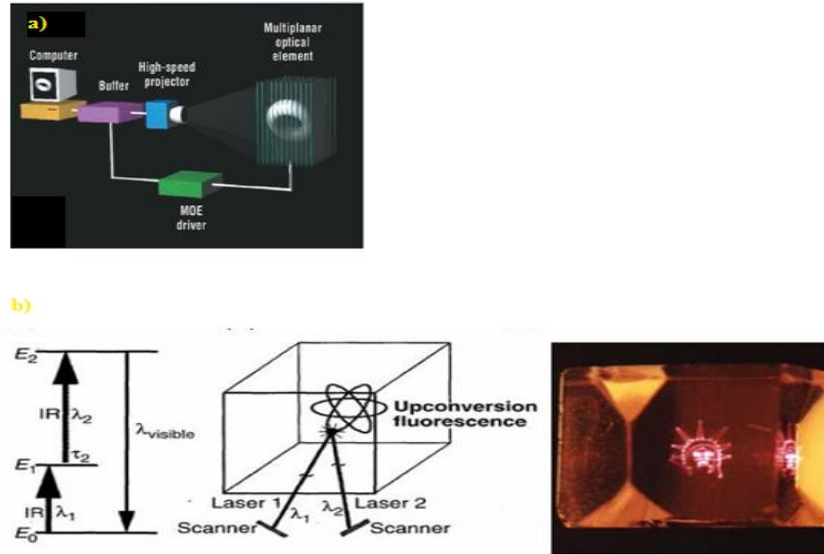


Figure 1.2.6.2. Static volumetric displays examples. a) DepthCube [24].
b) Elizabeth Downing volumetric display [25].

Figure 1.2.6.2.(b) shows a crystal image space of 1 cm^3 size. For all practical purposes, the size of this crystal is too small, especially if the purpose of the display is for specific commercial application. Growing large crystals is difficult and expensive, which affects the feasibility of producing 3D display for commercial purposes.

The motivation for the work undertaken for this dissertation is to overcome difficulties that researchers face when converting their crystal-based, static 3D display lab prototype into a commercialized 3D display. The image space that resulted from the author's experiments includes microcrystals dispersed in an index-matched host liquid. The microcrystals used in the proposed image space are simple to grow and cost effective. As a result, a 3D image space can be easily fabricated, up-scaled for large image display, and economically produced in large quantities.

1.3 Dissertation Outline

This dissertation is organized as follows:

Chapter 1 presents a brief introduction, including the motivation for and contributions of this work. Depth cues and human 3D perception are discussed. A background of current 3D displays, as well as their advantages and disadvantages in different field applications, is also described.

Chapter 2 presents a summary of the characteristic of CSpace[®] display.

Chapter 3 provides a complete description of up-conversion materials utilized for the research and development of this dissertation.

In Chapter 4 a method to fabricate a scalable medium for the CSpace[®] display is discussed. By grinding several rare-earth-doped fluoride bulk crystals into microcrystal powder, the medium can be dispersed in different refractive index liquids. Detailed experiments conducted on a number of host liquids are described. The process for preparing the microcrystal samples and for capturing SEM images, fluorescence strength, and the transmission measurement setup are also explained in detail.

Chapter 5 details a complete study and provides an analysis of green emission strength achieved from several different types of microcrystals when excited by two different infrared lasers, including 0.5% Er: KY₃F₁₀, 1%Er: NaYF₄ and 0.5% Er: LLF.

Chapter 6 examines different particle concentrations to demonstrate how this factor affects sample transparency and brightness.

Chapter 7 examines a collection of bulk crystals and details a comparison between bulk crystals and microcrystal.

Chapter 8 reviews and provides an analysis of results achieved and described in previous chapters. It also includes an example of the 3D volumetric image rendered inside the constructed prototype medium using CSpace[®] display.

Finally, Chapter 9 concludes the dissertation with a discussion of the contributions achieved and provides direction for further research.

Chapter 2

Cspace[®] display

Cspace[®] display is a static volumetric display funded by 3DIcon Corporation [26] and constructed at The University of Oklahoma. The prototype is targeted to create a 3D image that is viewable from all directions without the use of special glasses.

Cspace[®] display technology is comprised of a virtual moving-screen display containing a variety of particles suspended within a volumetric image space so that when excited by two different infrared lasers, the particles are illuminated to generate a 3D image. These particles include up-conversion materials that transform lower energy beams into higher energy, visible beams and function as light emitting phosphors. Two projection systems are required [27]. The first is a Digital Light Processing (DLP) spatial modulator in which a 2D array of micromirrors projects beams of specific wavelength and forms sequential slices of a 2D image along the length and width of the volumetric display. The second system—also a DLP spatial modulator—projects beams of specific wavelength and forms translational slices with a predetermined screen shape across the depth of the volumetric display, as shown in Figure 2.1.

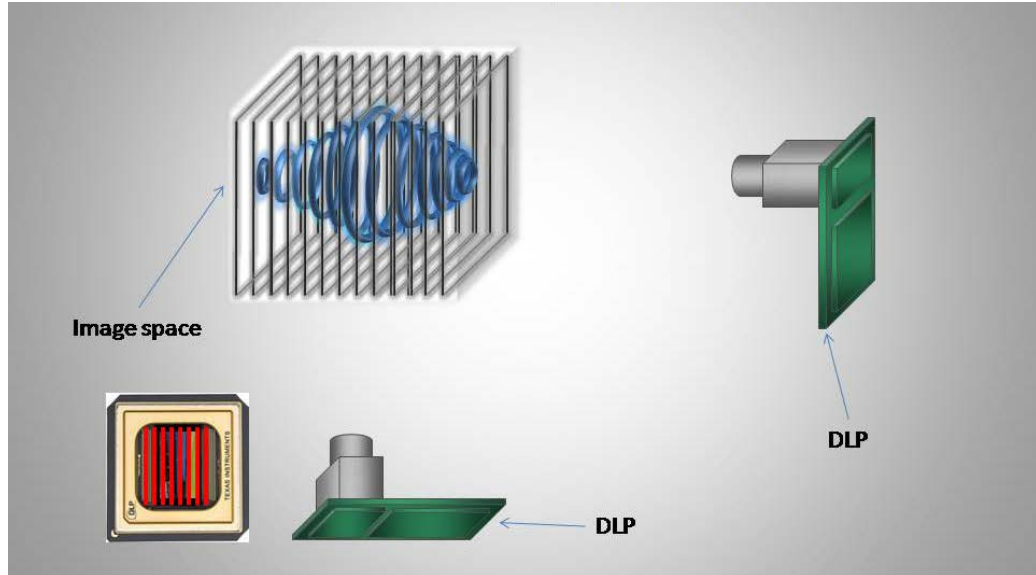


Figure 2.1. 3D volumetric display using two DLP projectors [27].

The DLP spatial light modulators can be positioned in several locations to provide different viewing zones. Figure 2.2 shows two DLP projectors angularly positioned to construct open 3D images that can be seen from any orientation.

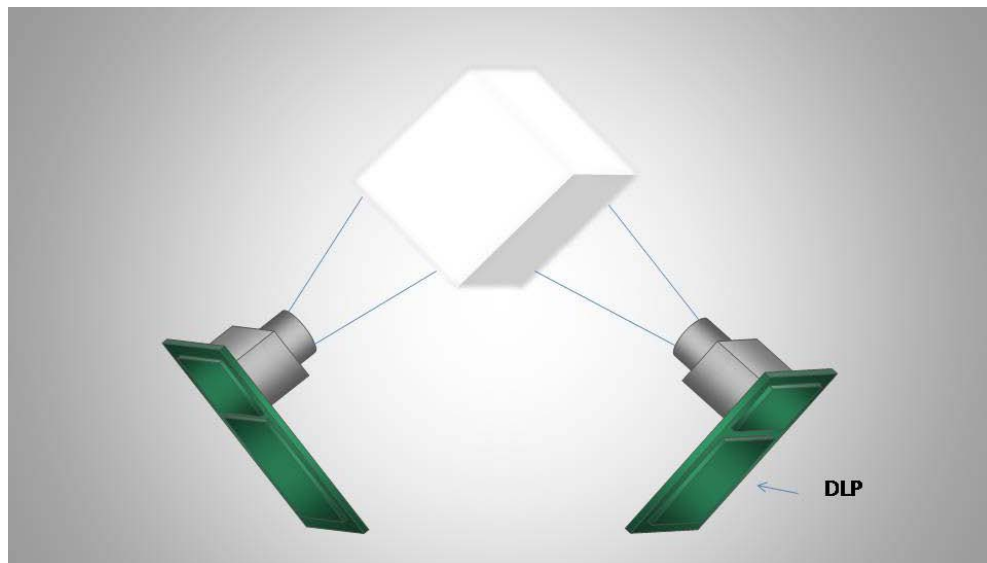


Figure 2.2. 3D volumetric Display where image space can be seen from all directions [27].

To produce the planar translational slice, all micro-mirrors (except those in the first column or row depending on the physical positioning of the projection system and volumetric display) that are associated with the second DLP projection system are set to off-state. Projection of the planar translational slice is synchronized with the 2D slices from the first DLP projection system. An approximately 90-degree intersection of the planar 2D translational slice with the 2D sequential slice energizes the particles at the intersection for a specified length of time and creates an illuminated 2D cross-section at a specified location within the 3D display.

Synchronizing operations of both projection systems enables the series of illuminated cross-sections of the 2D and planar translational slices to appear at a depth within the volumetric display. Repeating projections from the first and second projection systems throughout the entire volumetric display creates a 3D image.

Projecting three infrared wavelengths combined with the sequential 2D slices by the first projection system provides the means to generate red, green, and/or blue, along with a multitude of colors based on combinations of red, green, and/or blue, as shown in Figure 2.3.

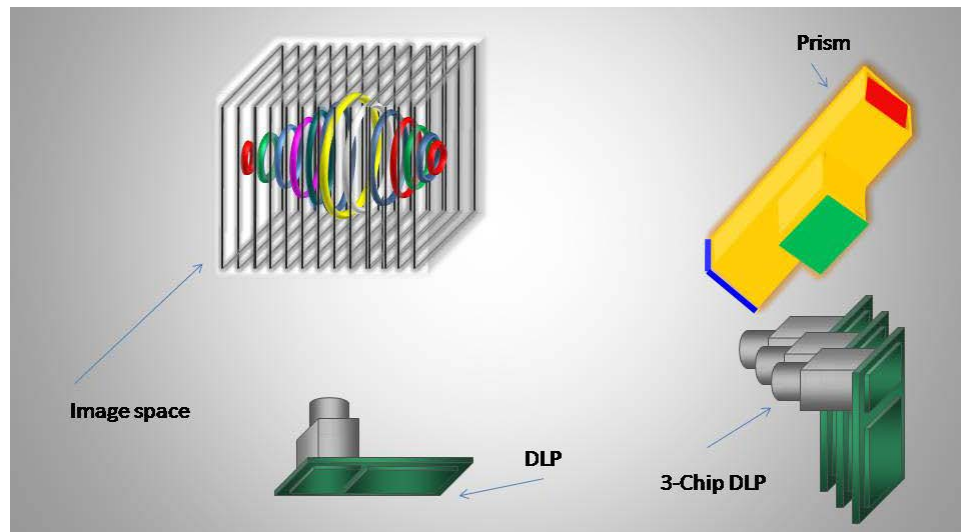


Figure 2.3. 3D Volumetric display using four DLP projectors [27].

As a result the 3D display constructs 3D images that are uniform in image space and viewable from practically any orientation. The display is fully static and capable of rendering high resolution, full-color 3D images [28].

Chapter 3

Physical Background of Materials

Several material types can be used as a display medium for CSpace[®] display, e.g., organic dye, gaseous material, and solid state. This dissertation looks in particular at solid-state material, especially rare-earth-doped fluoride crystals.

3.1 Photon conversion

3.1.1 Down-conversion

The down-conversion process is characterized as the conversion of one high-energy photon (, i.e., UV photon) into one photon with a lower energy (i.e., visible photon).

3.1.2 Quantum cutting

The principle of quantum cutting phosphors is based on emitting two visible photons (i.e., photon with low energy) for every UV photon (i.e., high energy photon) absorbed.

3.1.3 Up-conversion

Up-conversion is the process of converting two or more low-energy photons into one or more high-energy photons. This concept was introduced in 1959 by N. Bloembergen with his proposed infrared quantum counter device [29]. In his outline, he described how a rare-earth ion with multiple energy levels could simultaneously absorb two or more photons associated with transitions from the ground into an intermediate excited state, and then further excite the photons to a higher state, giving rise to visible luminescence. A general diagram for a simple three-level system is presented in Figure 3.1.3.1.

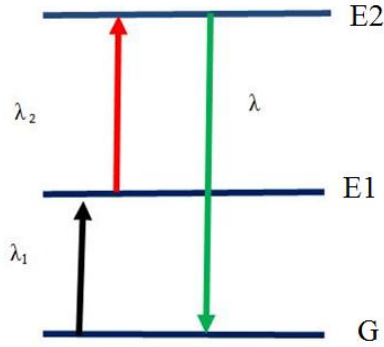


Figure 3.1.3.1. General diagram for a simple three-level system.

The figure above demonstrates how an ion that has been doped into the host material absorbs a photon from the first infrared laser beam at the wavelength λ_1 and is excited to an intermediate meta-stable state E_1 where it will stay for the time τ_1 . Before the ion has time to decay, it will absorb another pumped photon from the second infrared laser beam λ_2 and is excited to the second excited level E_2 , where it will stay for the time τ_2 . When the excited ion falls from E_2 to the ground level G , it will emit visible photon at the wavelength λ .

Previous research suggests that the sum of absorbed photon energies for up-conversion should be equal or greater than emitted photon energies, as shown in the following equation:

$$\sum E_{\text{emitted},n} = \sum E_{\text{absorbed},n} + E_{\text{loss}} \quad (1.1)$$

Up-conversion luminescence is attributed to three key processes: (1) excited state absorption (ESA); (2) energy transfer up-conversion (ETU); and (3) direct two-photon absorption (TPA) [2], as illustrated in Figure 3.1.3.2.

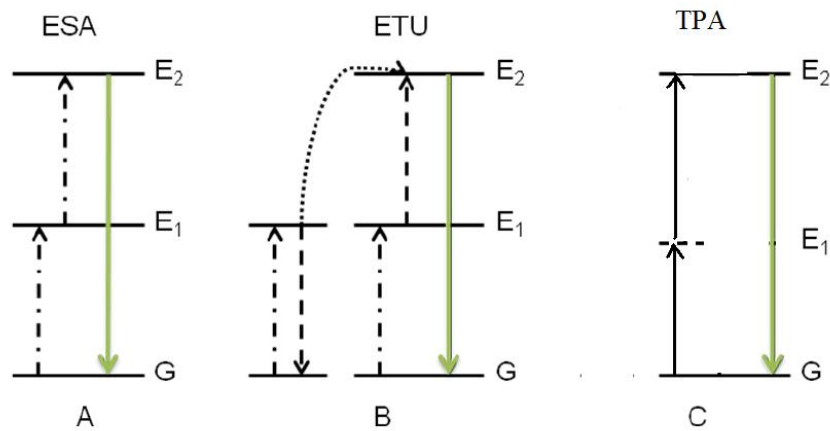


Figure 3.1.3.2. Various up-conversion mechanisms.

Excited state absorption (ESA)

ESA is comprised of a single ion process wherein a photon with energy of $h\nu_1$ “ h is the Plank’s constant, ν_1 is the corresponding frequency” is absorbed by an ion in a crystal matrix, transitioning it from the ground level (G) to a meta-stable intermediate level (E_1). The excited electron of E_1 may then return to either level G or absorb a photon of energy $h\nu_2$ that rises to a higher level (E_2) and results in an up-conversion emission that corresponds to the transition from level E_2 to G, as shown in the Figure 3.1.3.2.A. This then yields an emitted photon of energy $h\nu_3$, where ν_3 is larger than both ν_1 and ν_2 . However, it should be noted that the population in the process ESA is typically low. Three factors that determine the population at the meta-stable excited state are [30] [31]:

- (1) Excitation source power;
- (2) Intermediate level lifetime; and
- (3) Cross-section absorption of ions.

Energy transfer up conversion (ETU)

ETU is similar to ESA and based on the absorption of two photons to populate E_1 . However, in a typical ETU process, excitation is realized by an energy transfer between two ions wherein ion 1 acts as sensitizer and ion 2 as activator. Figure 3.1.3.2.B shows the schematic representation of the energy transfer. An example of sensitizer and activator is Er, Yb co-doped system, which is given in section 3.1.3.1.

Two types of energy transfer are considered, namely cross relaxation and cooperative sensitization. In cross relaxation, only the sensitizer ion absorbs the photon and is excited to E_1 , after which energy can be transferred to the activator to promote transition from G to E_1 . The sensitizer ion is relaxed to G. A second excitation of the activator enables the E_2 population. For cooperative sensitization, energy is accumulated by two excited ions, and then transferred to a third by the relaxation of the two ions. Notably, up-conversion efficiency of the ETU process is affected by dopant concentration, i.e., average distance between dopant ion neighbors.

Direct two-photon absorption (TPA)

The TPA process is a single ion process in which the simultaneous absorption of two photons takes place to excite the ion from G into E_2 via virtual intermediate excited level E_1 , which is indicated in Figure 3.1.3.2.C by the horizontal dashed line.

Azuel et al. [31] have shown that ESA and ETU are often significantly more efficient than TPA by relatively 10 orders of magnitude. Table 3.1.3.1 shows a comparison of three up-conversion processes and their corresponding efficiencies.

Process	Efficiency
Excited state absorption (ESA)	$\sim 10^{-5}$
Energy transfer up-conversion, cross relaxation	$\sim 10^{-3}$
Energy transfer up-conversion, cooperative sensitization	$\sim 10^{-6}$
Direct two photon absorption (TPA)	$\sim 10^{-13}$

Table 3.1.3.1. Comparison between the different up conversion processes regarding their efficiencies [9].

Up-conversion efficiency of these three processes varies substantially. ESA up-conversion luminescence is weaker when compared to ETU. Also, it only occurs in singly doped crystals. The ETU process is instantaneous and independent of excitation power. Likewise, it provides up-conversion emission in a magnitude two orders higher than ESA. Hence, based on ETU, a number of up-conversion materials comprised of more than one dopant ion have been investigated and developed.

Using single-doped crystal, up-conversion luminescence is primarily provided by ESA. Key parameters for efficient up-conversion material are the distance between two adjacent dopant ions and their absorption in a cross-section of ions. Increasing the dopant concentration above a certain level results in diminishing luminescence due to the cross-relaxation. Doping concentration should, therefore, be kept low. Moreover, most dopants have a low absorption cross-section, resulting in low ESA efficiency [30]. In fact, up-conversion efficiency of a single doped crystal is generally low. Another method used to increase up-conversion efficiency is co-doping with a second lanthanide ion, i.e., the sensitizer. By selecting a sensitizer with a moderate absorption cross-section in the NIR region, the ETU process between sensitizer and activator can be utilized.

3.1.3.1 Up-conversion mechanism in Er-Yb co-doped systems

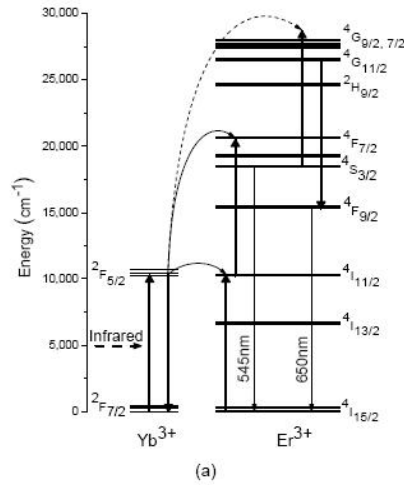


Figure 3.1.3.3. Up conversion mechanism in Er⁺³-Yb⁺³ co-doped systems [32].

The following describes the mechanism of infrared excited green emission in Er⁺³ [32], as shown in Figure 3.1.3.3 above.

- 1- Yb⁺³ ion absorbs a pump photon and is excited to level ²F_{5/2}. As energy is transferred from Yb⁺³ to Er⁺³; Er⁺³ is excited into level ⁴I_{11/2}.
- 2- A second excited Yb⁺³ ion excites an Er⁺³ ion so that Er⁺³ increases to level ⁴F_{7/2}, effectively relaxing via a non-radiative decay to level ⁴S_{3/2}. A green emission at 545nm occurs, given the transition from ⁴S_{3/2} to ⁴I_{15/2}.

Infrared excited red emission in Er⁺³ is achieved when ⁴F_{9/2} is transformed to ⁴I_{15/2} at 660 nm by way of one of three scenarios:

- a) Decay from level S_{3/2} to F_{9/2} through non-radiative decay;
- b) Er⁺³ ion excitation from level ⁴S_{3/2} to ²G_{7/2} via a third quantum from Yb⁺³ wherein Er⁺³ is relaxed into ²G_{11/2}, and then decays to level ⁴F_{9/2} via back transfer of energy to Yb⁺³; or

- c) Non-radiative decay occurs from ${}^4I_{11/2}$ to ${}^4I_{13/2}$ following the initial excitation so that Er^{+3} is excited to level ${}^4F_{9/2}$.

Sommerdijk [33] reported that mechanism (c) is most commonly found in fluoride crystals with low Yb^{+3} doping concentration due to relaxation of $I_{13/2}$ after initial up conversion steps. Mechanism (a) probability is extremely small in co-doped fluoride systems due to the high-energy gap between the two levels and the weak ion lattice interaction in fluoride lattices. Mechanism (b) offers a strong contribution and actually becomes stronger at higher rare-earth doping concentrations.

For efficient up-conversion visible emission, sufficient population in intermediate levels, e.g., ${}^4I_{11/2}$, is required. However, as Er^{+3} ions are excited into these levels energies can transfer back to Yb^{+3} ions, thus reducing the populations. This not only causes a decrease in the lifetime of ions at this level, but also represents depletion in overall transfer efficiency.

Er^{+3} in single-doped systems at approximately 800 nm has previously been studied [34]. The up-conversion mechanism transpires through two-step absorption from ${}^4I_{15/2}$ to ${}^4I_{9/2}$ and from ${}^4I_{13/2}$ to ${}^4S_{3/2}$. Co-doped systems with Yb^{+3} sensitization have proven more efficient than a single-doped system with Er^{+3} , as the Er^{+3} dopant level in single-doped systems must be low to prevent cross relaxation. In this way green output power remains low in single-doped systems, due to weak ground level absorption of the pump light [35].

3.1.3.2 Up-conversion mechanism in Tm³⁺-Yb³⁺ co-doped systems

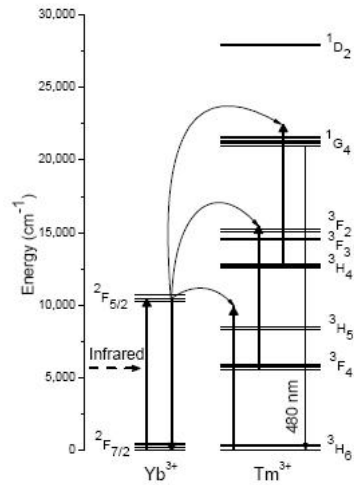


Figure 3.1.3.4. Up-conversion mechanism in Tm³⁺-Yb³⁺ co-doped systems [32].

For infrared excited blue emission in Tm³⁺, the Yb³⁺ ion absorbs a pump photon and is excited to level ²F_{5/2}, as shown in Figure 3.1.3.4 above. When energy transfers from Yb³⁺ to Tm³⁺, the result is excitation of the Tm³⁺ ion into level ³H₅. The Tm³⁺ ion is then relaxed into level ³F₄. The same Tm³⁺ ion is further excited from level ³F₄ into ³F₂ via a second excited Yb³⁺ ion, and then subsequently relaxed into level ³H₄. The ³⁺ion is excited once again from level ³H₄ to ¹G₄ via energy transfer from a third excited Yb³⁺ ion. When relaxing from level ¹G₄ to the ground level, blue emission is emitted at 480 nm, and red is emitted at 650 nm after relaxing into level ³F₄.

Once Tm³⁺ ions are excited to an intermediate level, e.g., ³F₄, energies can revert to the Yb³⁺ ions, leading to a decline in population at intermediate levels. The resultant energy transfer is related to the temperature. When temperatures are low, the back-transfer process decreases.

Chapter 4

Scalable Medium for CSpace[®] display

Efficient up-conversion emitters are necessary for the operation of CSpace[®] 3D display. In previous work, we reviewed up-conversion in rare-earth, co-doped fluoride bulk crystals that convert laser light from near infrared to visible light [39]. Limitations of extreme difficulty, expense, and time associated with growing a large, single crystal have resulted in an increasing need for replacement of bulk crystals by either nanocrystals or microcrystals.

4.1 Crystal size

4.1.1 Nanocrystal

Nanocrystal material size is relative to that of nanometers. Researchers investigating 3D displays in Singapore have developed NaYF₄ nanocrystals and dispersed them in transparent silicone displays. Using this method, an infrared laser light is utilized to generate a 3D image by scanning the silicon with invisible light, which allows the nanocrystals to emit light. The group also reports finding a method to control crystal growth and to adjust crystal size and structure [20]. The disadvantage of utilizing nanocrystals is that up-conversion efficiency decreases when the size of the phosphor is decreased to nano size. For this reason, a nanocrystal medium is not a good candidate for replacing the CSpace[®] display volume.

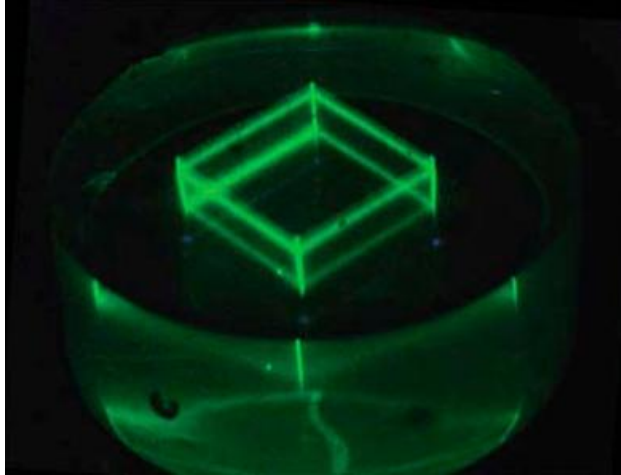


Figure 4.1.1.1. 3D image in silicone [40].

4.1.2 Microcrystal

To avoid complications associated with growing a large bulk crystal doped with rare-earth ions, small crystals can be grown at little cost, and later ground into a powder using a mortar and pestle. The powder can be placed in an index-matched host, e.g., liquid, oil, or polymer. Using this method, a scalable medium can be produced that when compare with a bulk crystal medium is less time consuming to prepare, more cost effective, and also lighter in weight. Additionally, different crystal powders can be mixed and placed in a host material to form a single medium. For example, Er: NaYF₄ and Pr: NaYF₄ can be mixed to form a colored, single medium by selecting different wavelengths. Among the various types of up-conversion crystals, a 1% Er: NaYF₄, 0.5% Er: KYF₁₀, and 0.5% Er:LLF were chosen as candidates for this study [39] [41].

4.1.3 Bulk crystal

Co-doped fluoride bulk crystals were used as a model. 1% Er: NaYF₄, 0.5%Er: KYF₁₀ and 0.5%Er: LLF were procured from AC Materials. The crystal structure of KY₃F₁₀ is suitable to the volumetric display application. It has an isotropic and cubic crystal structure that leads to a single refractive index throughout the crystal. Grinding this type of crystal into microcrystals and uniformly distributing them in an index-matched host material can be a simple procedure, especially when compared that of birefringent materials.

4.2 Experimental setup

4.2.1 Sample preparation procedure

Samples were prepared using the following procedure.

AC Materials provided 1% Er: NaYF₄, 0.5%Er: KYF₁₀ and 0.5%Er: LLF bulk crystals. Bulk crystals were broken down into microcrystal powders. Particles were dispersed in different index-matching liquids whose refractive index varied with a range between 1.45 and 1.49.

4.2.1.1 Preparation of 10% wt microcrystals with different refractive index liquid

First, an empty cuvette was weighed using a portable milligram scale. The cuvette was weighed again after filling it with the desired refractive index liquid. The difference between the two weights was calculated to determine refractive index liquid weight. Next, microcrystal powder particles equaling 10% of the refractive liquid weight were added to the liquid. Up-conversion microcrystal particles caused difficulties, as the particle size was unable to be uniformly dispersible in the liquid. Therefore, a stirring bar with a magnetic stirrer [42] was employed to form a homogenous solution at room

temperature. A number of different index-matched samples were created to determine the ideal condition. Microcrystals provided by Cargille Laboratories were utilized in various refractive index liquids, e.g., 1.45, 1.456, 1.46, 1.464, 1.468, 1.47, 1.474, 1.476, 1.48, 1.484, and 1.49 [43]. Samples with various weight percentages, e.g., 10%, 20%, 30%, were used. Structural and optical characterization was used for each sample studied.

4.2.2 Structural characterization

To characterize various dispersed microcrystals, scanning electron microscope (SEM) images were utilized. A high magnification power and high resolving capacity, made this method most valuable for structural characterization.

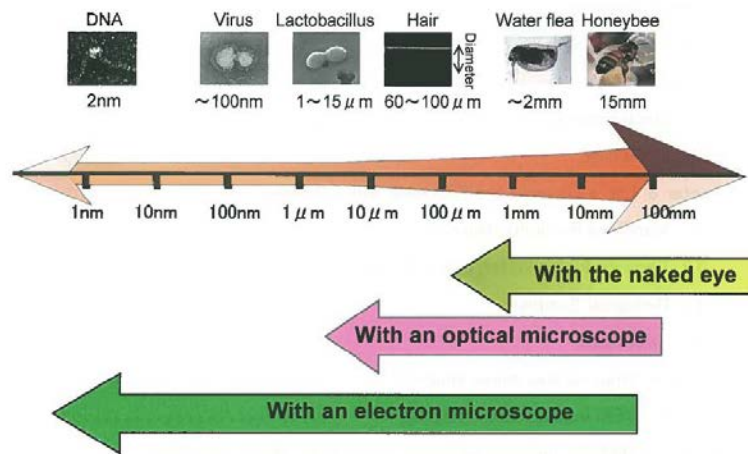


Figure 4.2.2.1. SEM Microscope resolution.

An SEM has a much higher magnification than an optical microscope. It employs an electron beam to create an image, as demonstrated in Figure 4.2.2.1, so that resolution reaches nearly atomic level.

SEM is an imaging technique in which a beam of high-energy electrons is focused to release a diversity of signals at the specimen surface. Signals resulting from interactions between electron and sample are used to display information about texture, chemical composition, and crystalline structure. SEM surface scans produce electrons and allow them to bounce or scatter so that an imaging device can collect scattered electrons and generate a high-resolution, 3D image that has accurate representation and can be viewed on a TV screen.

4.2.3 Optical characterization

Optical characterization includes measuring the scattering and green emission strength. All samples in this research were generated within a period of one week from the time of dispersion.

4.2.3.1 Transmission or Scattering

Transmission was measured to determine the amount of scattering that results when the infrared light passes through the sample. The experimental setup employed to measure transmission included the following components:

1. An infrared laser diode operating at 850nm was used because absorption at this wavelength is nearly zero at low power. Zero absorption is required to measure scattering. The laser was connected to a current driver and a temperature controller. The current driver provided the required regulated current and voltage to the laser, while the temperature controller measured the laser temperature and operated a thermo electric cooler (TEC) to cool the laser temperature when needed.

2. An optical fiber with 400 μ m core diameter and 0.22 Numerical Aperture (NA) was utilized.
3. Optical fiber output was placed at the focal point of the input beam collimator lens. The collimator device focuses the diverging light emitted from the fiber output toward its projecting direction. Hence, the output is a collimated beam with a minor divergence so that beam radius does not change within a moderate propagation distance [45]. The radius remains nearly constant at approximately 3mm.
4. In this set of experiments, the beam expander was installed counter to the typical way. In this way, the beam expander was used as a condenser. Hence, the input was a collimated beam with a radius 3mm, and the output was a collimated beam with 1mm radius, i.e., the diameter for the collimated input beam was decreased to a narrower collimated output beam when we put the beam expander in the opposite direction.
5. The 50:50 beam splitter cube is composed of two right-angled prisms coated with dielectric, which is capable of reflecting and transmitting 50% of the incident beam.
6. The photodetector is a device that measures light power and is connected to the optical power meter.
7. The power meter is an optical power and energy meter. Fluorescence was detected in the visible spectral range with a detector connected to a power meter, as shown in Figure 4.2.3.1.1.

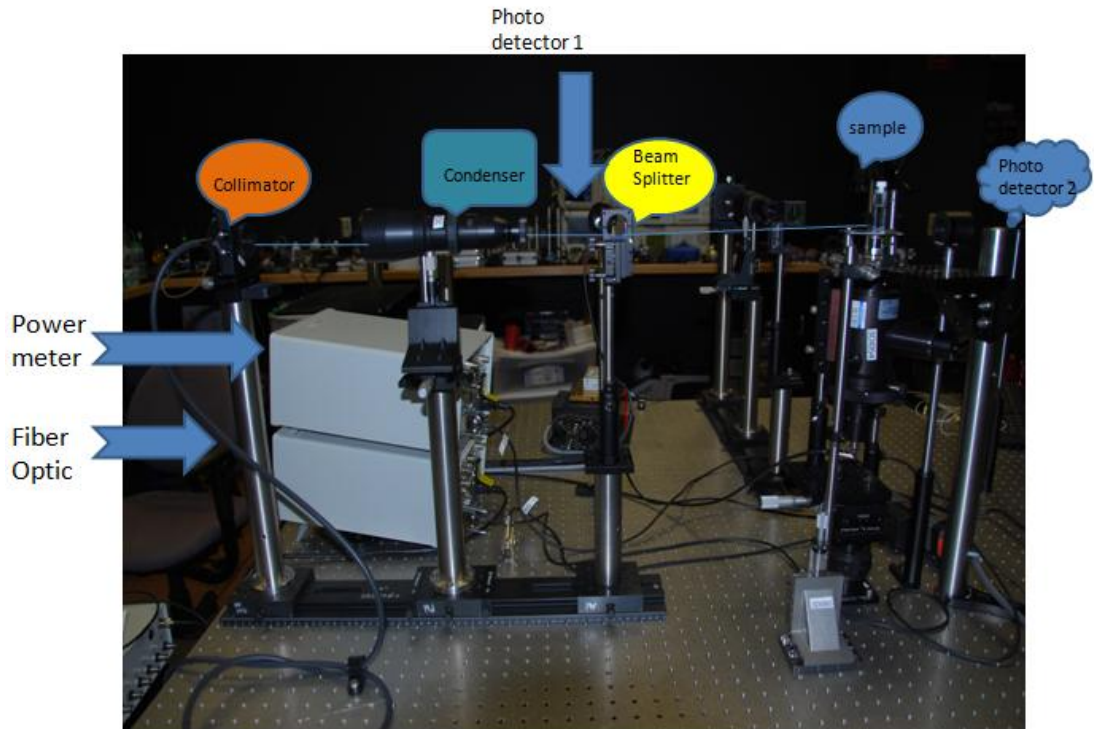


Figure 4.2.3.1.1. Scattering setup schematic.

Using the scattering setup described above, photodetector 1 measured the optical power of the 850 nm laser before entering the sample. Photodetector 2 measured the optical power after the laser emerged from the sample. The division between these two measurements is the transmission.

4.2.3.2 Green emission strength

Two infrared laser pumps were intersected inside the samples. The first infrared laser beam at 850 nm was incident from the left side of Figure 4.2.3.2.1, and the second infrared laser beam at 1532 nm was incident perpendicular to the direction of the page. A green voxel was generated inside the sample, and its intensity was measured during a period of approximately 20 seconds due to the fact that green emission strength differs depending on the stirring bar. The 20-second period served as the average intensity.

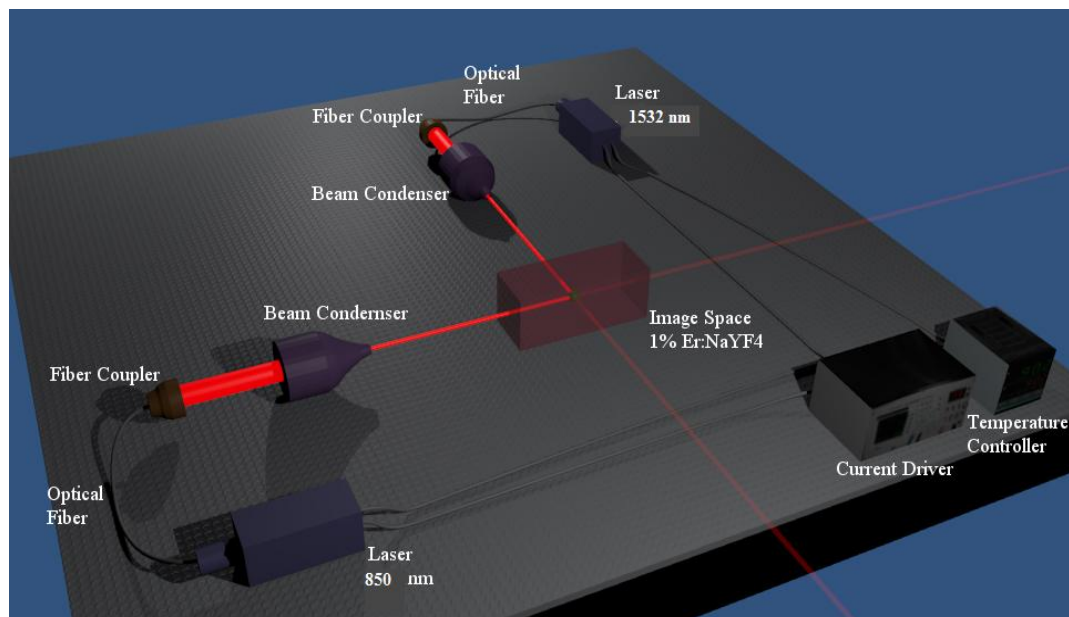


Figure 4.2.3.2.1. Measurement setup for green emission intensity.

One side of the green emission experimental setup is comprised of the following components:

1. Infrared laser at 850nm.
2. Optical fiber with 400 μm core diameter and 0.22 NA.
3. Beam collimator.
4. Beam condenser.
5. 50:50 beam splitter cube.
6. Photodetector; and
7. Power meter

The other side uses the same components, except that 850nm is increased to 1532nm wavelength.

A cuvette filled with the material under study was placed at the intersection of the two infrared laser beams. At the point of intersection within the material, a green

emitted voxel became visible and a solid projection angle of the light was collected using a telescope lens that directed the light into an optical fiber. The light was transmitted through the optical fiber to a digital signal processing radiometer, as shown in Figure 4.2.3.2.2.

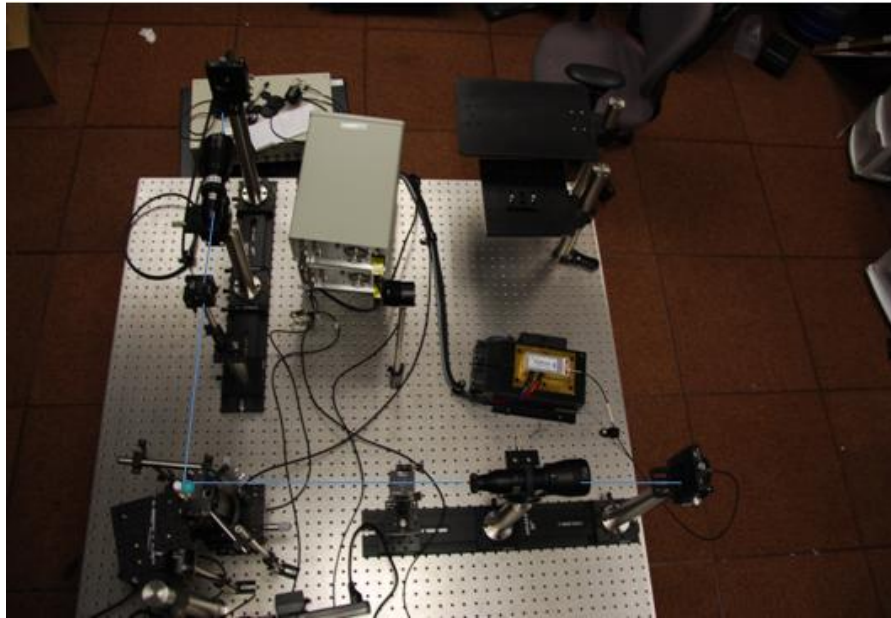


Figure 4.2.3.2.2. Green emission strength setup measurement.

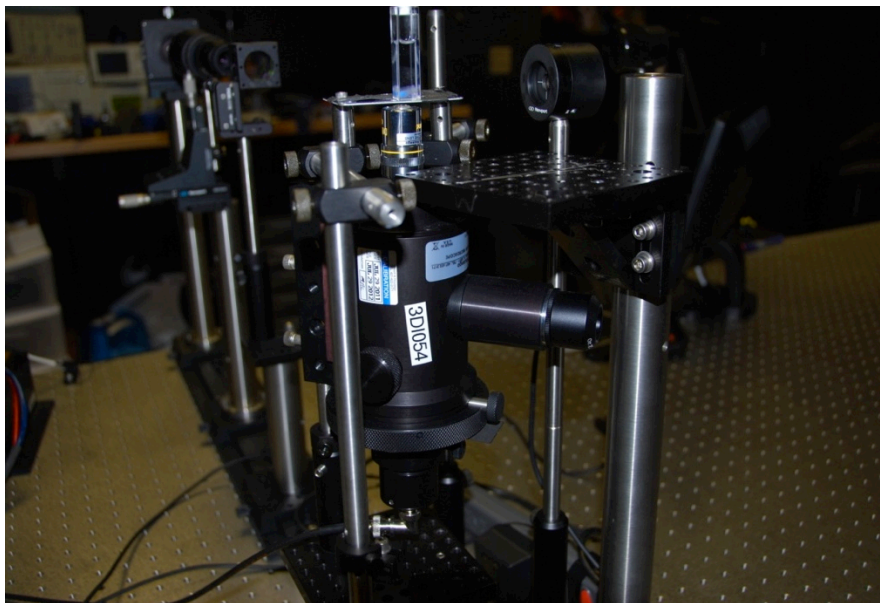


Figure 4.2.3.2.3. Telescope measuring the green emission voxel inside the placed sample.

Figure 4.2.3.2.3 shows the telescope capturing the green emission at specific location inside the cuvette. As explained before, the captured green emission was transported to the radiometer through an attached optical fiber. These experimental setups were utilized to measure transmission and green emission strength of several different microcrystal powders dispersed in different refractive index host liquids. The experiments and their results are explained in detail in the next chapter.

Chapter 5

Microcrystal Testing

Samples for each microcrystal material were prepared using the preparation procedure described in Chapter 4.

5.1 1% Er: NaYF₄ 10 wt% microcrystals with different refractive index

5.1.1 SEM Measurement

The low- and high-resolution SEM images of 1% Er: NaYF₄ microcrystals increasing in order of magnification are shown in Figure 5.1.1.1.

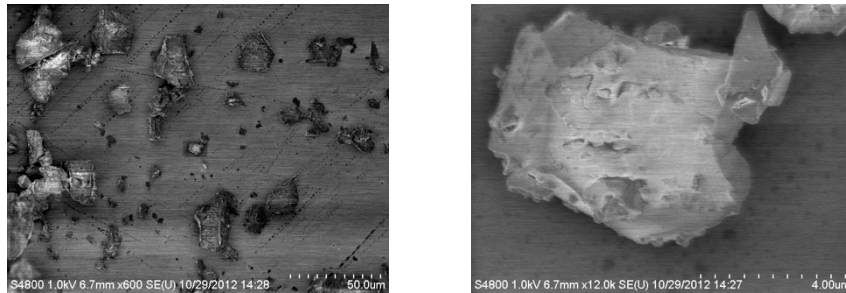


Figure 5.1.1.1. a) low resolution SEM images of 1% Er: NaYF₄ with 50 µm scale bar, B) high resolution SEM image with 4 µm scale bars.

Particle size was in the range of 2-28µm, as shown in the figure above. Notably, the particles have different shapes. When the particles were mechanically stressed using a mortar and pestle, some were found to have a structure that caused light to scatter. Because most particles have such a structure, the quality of the 3D display medium will be degraded.

5.1.2 Transmission measurements that demonstrate the amount of scattering

To determine transparency, the letters OU were written on a piece of paper and placed behind samples measuring 2mm in depth. See Figure 5.1.2.1.

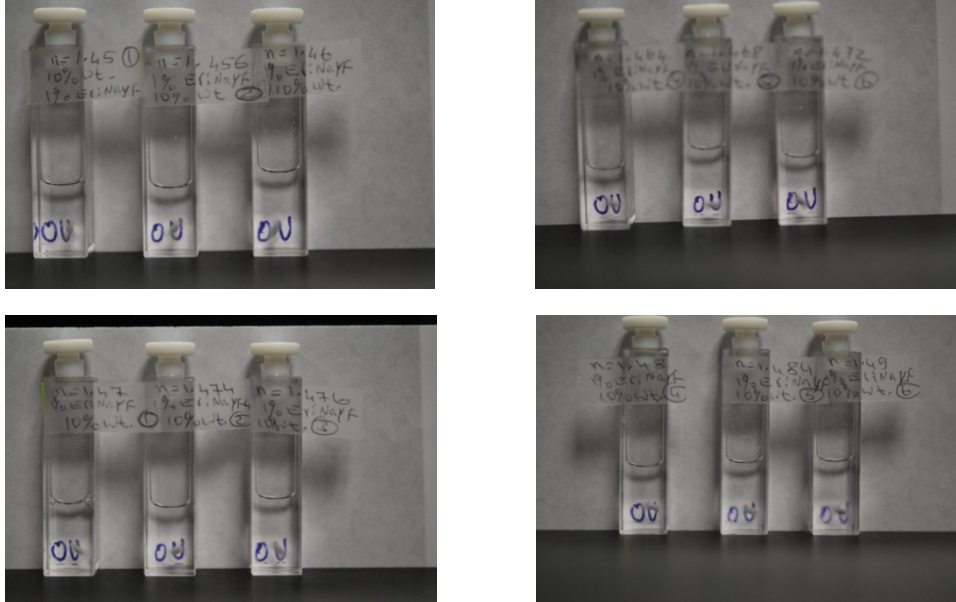


Figure 5.1.2.1. 2-28 μ m 1%Er: NaYF₄10% wt dispersed in 1.45,1.456,1.46 refractive index liquids, b) 1%Er: NaYF₄10% wt dispersed in 1.464,1.468,1.472, c) 1%Er: NaYF₄10% wt dispersed in 1.47,1.474, 1.476, d) 1%Er: NaYF₄10% wt dispersed in 1.48,1.484,1.49.

While it may not be apparent to the reader from the photograph, it is clear when viewed in person that Figure 5.1.2.1 demonstrated the sample 2-28 μ m size 1%Er:NaYF₄10% wt dispersed in a liquid with a 1.468 refractive index has superior visible transparency.

The refractive index of 1%Er: NaYF₄ microcrystals should match that of the liquid. When they do the sample will have less scattering and be more transparent. If not, the results will be to the contrary.

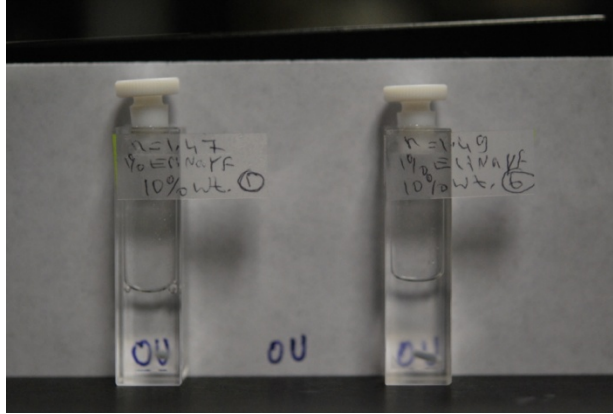


Figure 5.1.2.2. Comparison between 2-28 μ m size 1%Er: NaYF₄10% wt particles dispersed in 1.47 and 1.49 index matching liquid.

Figure 5.1.2.2 shows that the sample with the 1.47 index matching liquid is more transparent than the 1.49 index matching liquid sample.

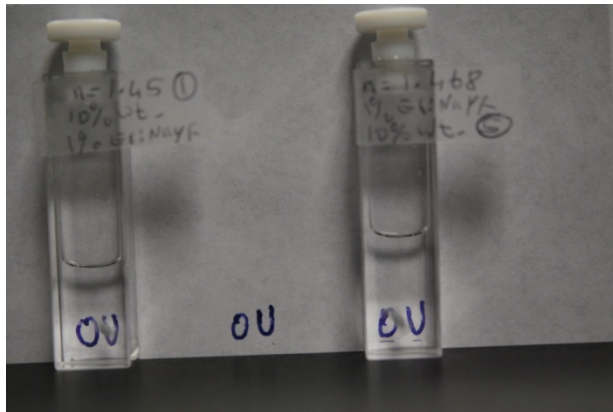


Figure 5.1.2.3. Comparison between 2-28 μ m size 1%Er: NaYF₄ 10% wt particles dispersed in 1.45 and 1.468 index matching liquid.

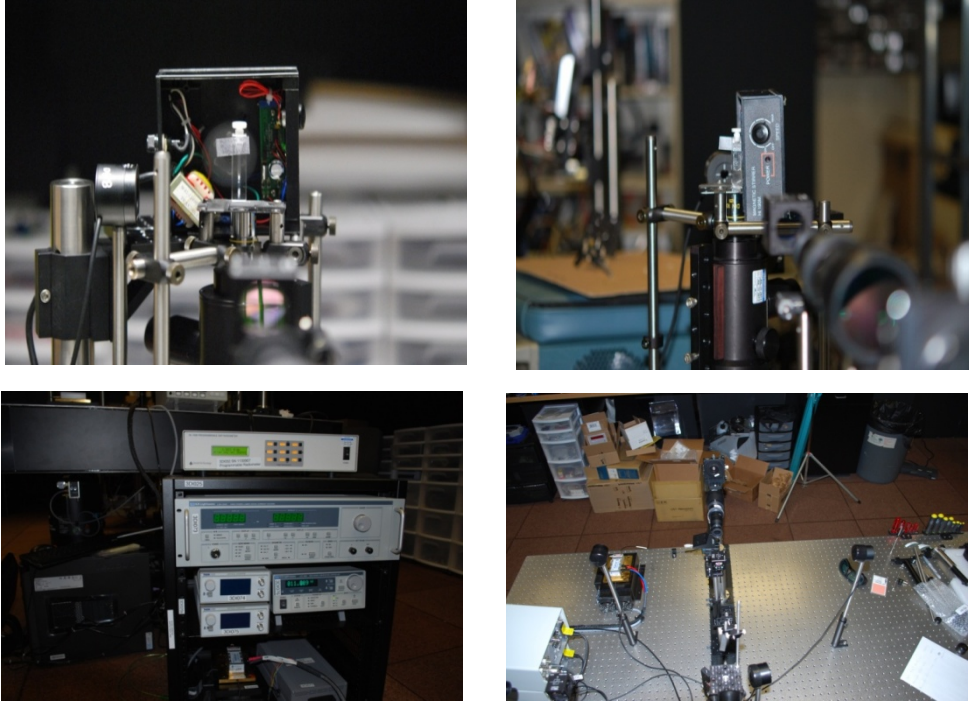


Figure 5.1.2.4. Transmission measurement setup.

Results of the transmission measurement for the dispersed 1%Er: NaYF₄ microcrystal powder in 1.48 refractive index liquid are pictured in Figure 5.1.2.5. The right image in the figure shows the applied current necessary to generate approximately 40 mw of optical power; the left image shows the captured optical power after the laser passes through the sample.

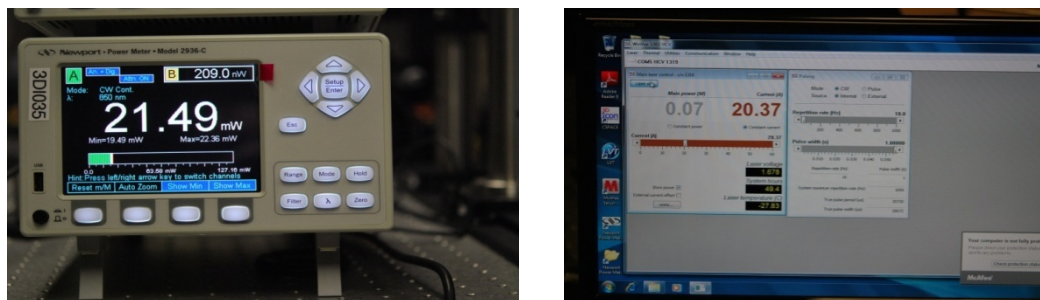


Figure 5.1.2.5. Transmission setup for the sample 1%Er: NaYF₄ dispersed in a 1.48 refractive index liquid.

Additional experiments tested various samples with different refractive index liquids. Figure 5.1.2.6 demonstrates the curve of transmission for dispersion of 1%Er: NaYF₄ in different refractive index liquids.

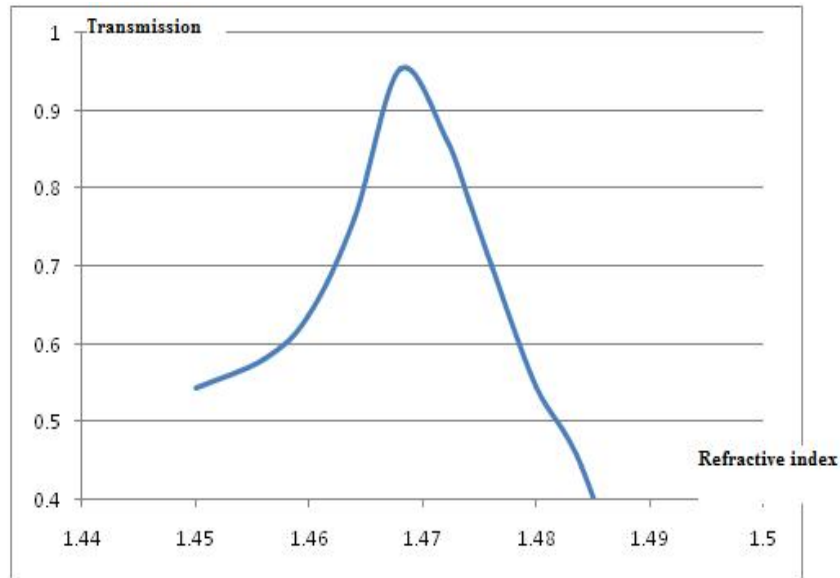


Figure 5.1.2.6. Transmission measurements for 1%Er: NaYF₄ in different refractive index liquid samples.

Transmission strength was measured for the 1%Er: NaYF₄ sample using different refractive index liquids. Results indicated that when compared with other samples, 1%Er: NaYF₄ microcrystals dispersed in an index matched liquid of 1.468 had the least overall scattering.

5.1.3 Green emission strength measurements

Using the measurement setup described in Chapter 4, the green emission strength of 1%Er: NaYF₄ 10 wt% microcrystals was dispersed in different refractive index liquids, e.g., 1.45, 1.456, 1.46, 1.464, 1.468, 1.47, 1.474, 1.476, 1.48, 1.484, and 1.49, and measured, as shown in the figures below.

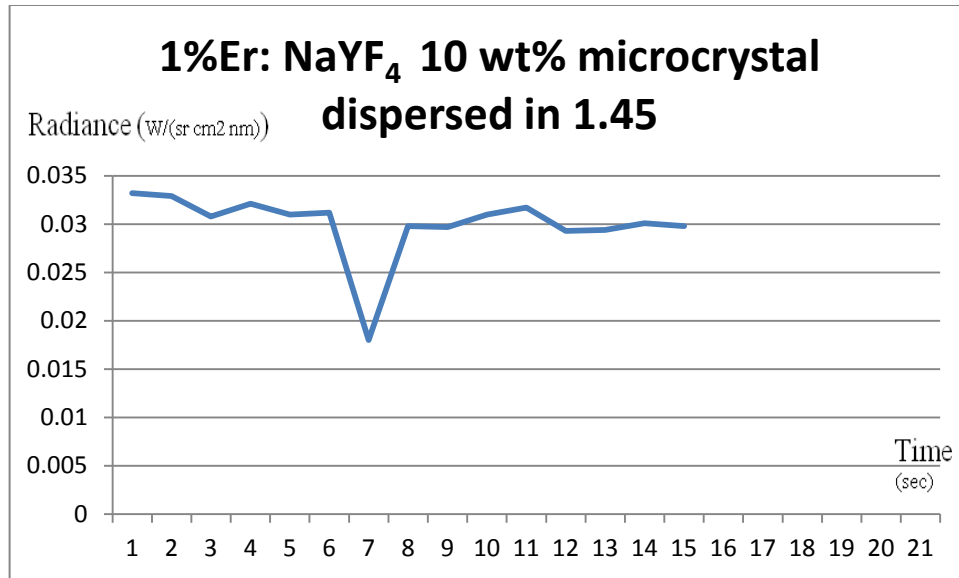


Figure 5.1.3.1. Green emission strength for the sample 1%Er: NaYF₄ 10 wt% microcrystals dispersed in 1.45 refractive index liquid.

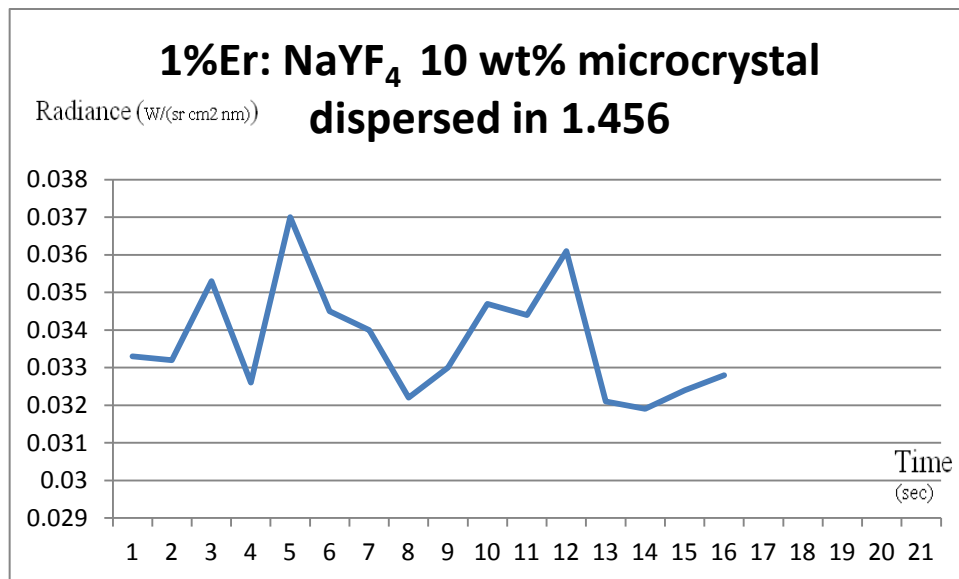


Figure 5.1.3.2. Green emission strength for the sample 1%Er: NaYF₄ 10 wt% microcrystals dispersed in 1.456 refractive index liquid.

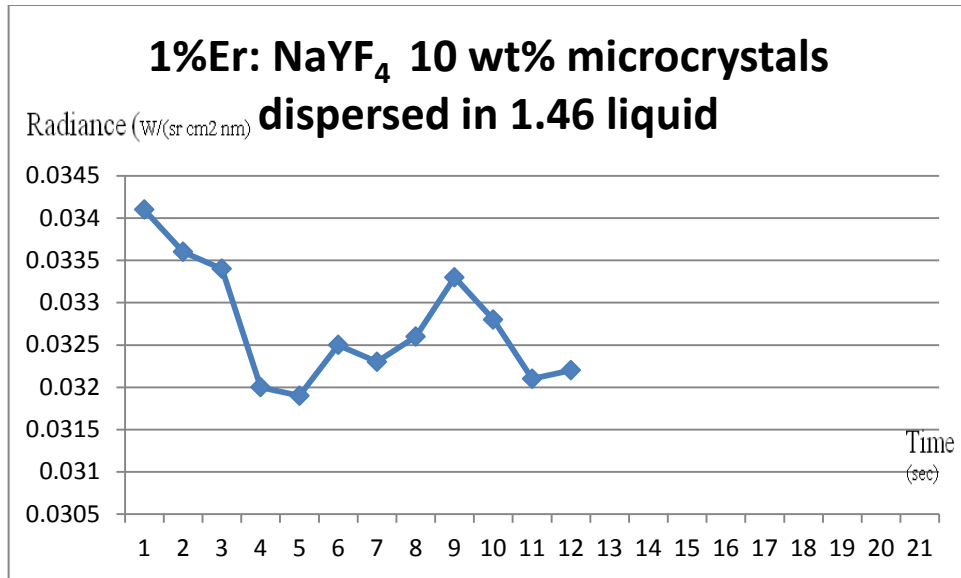


Figure 5.1.3.3. Green emission strength for the sample 1%Er: NaYF₄ 10 wt% microcrystals dispersed in 1.46 refractive index liquid.

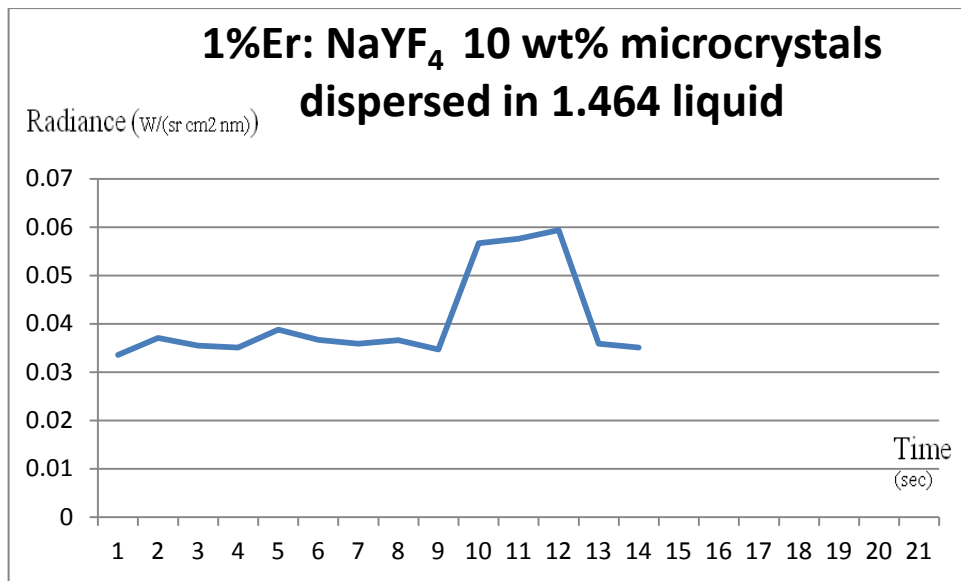


Figure 5.1.3.4. Green emission strength for the sample 1%Er: NaYF₄ 10 wt% microcrystals dispersed in 1.464 refractive index liquid.

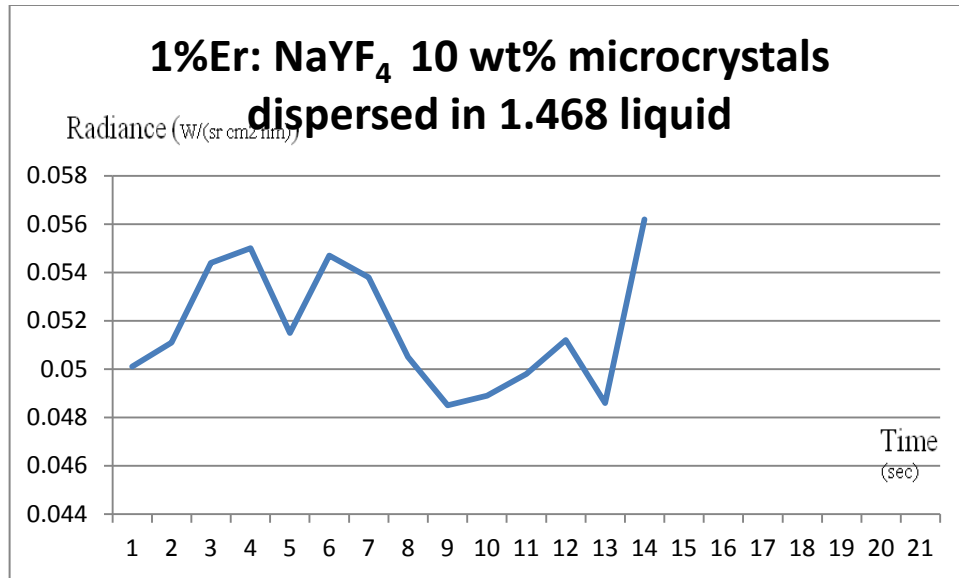


Figure 5.1.3.5. Green emission strength for the sample 1%Er: NaYF₄ 10 wt% microcrystals dispersed in 1.468 refractive index liquid.

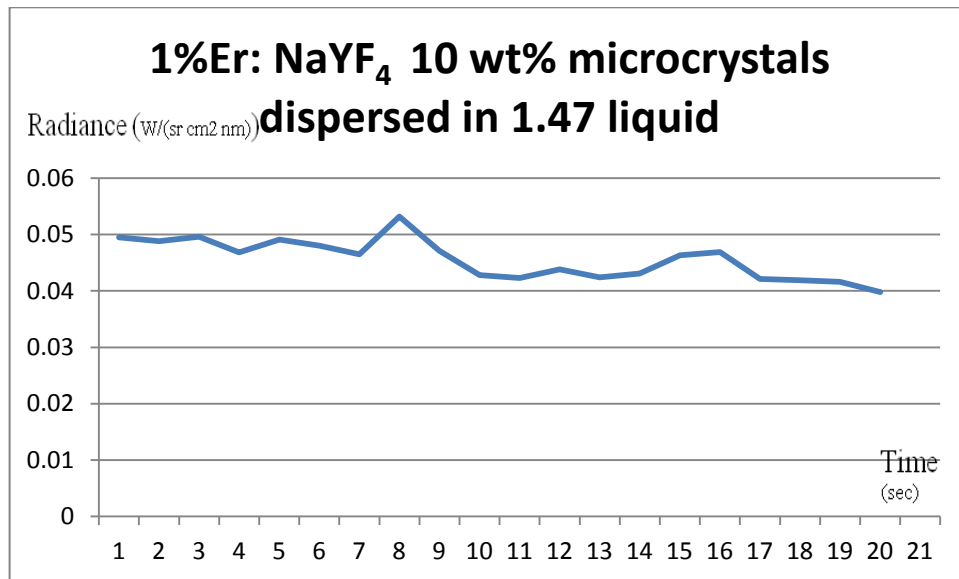


Figure 5.1.3.6. Green emission strength for the sample 1%Er: NaYF₄ 10 wt% microcrystals dispersed in 1.47 refractive index liquid.

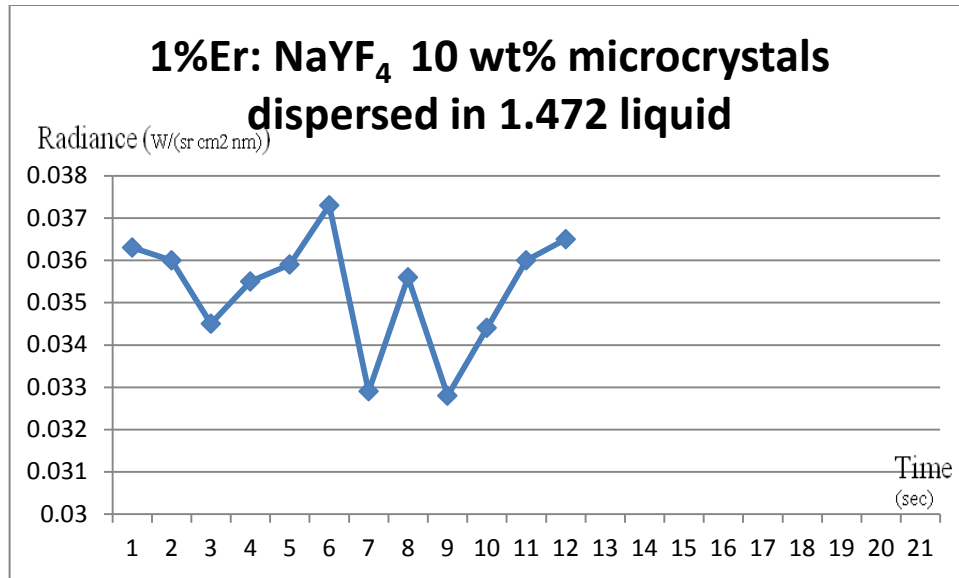


Figure 5.1.3.7. Green emission strength for the sample 1%Er: NaYF₄ 10 wt% microcrystals dispersed in 1.472 refractive index liquid.

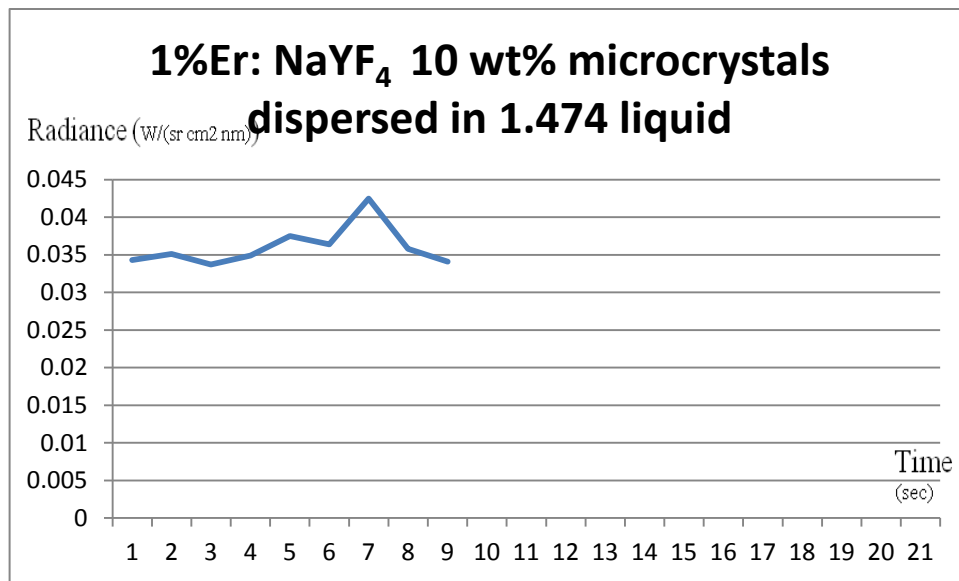


Figure 5.1.3.8. Green emission strength for the sample 1%Er: NaYF₄ 10 wt% microcrystals dispersed in 1.474 refractive index liquid.

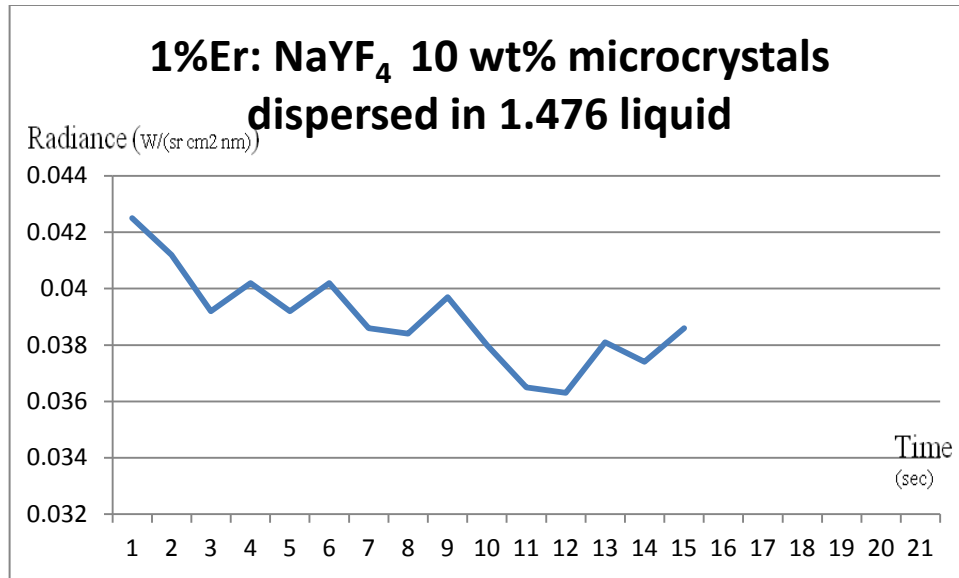


Figure 5.1.3.9. Green emission strength for the sample 1%Er: NaYF₄ 10 wt% microcrystals dispersed in 1.476 refractive index liquid.

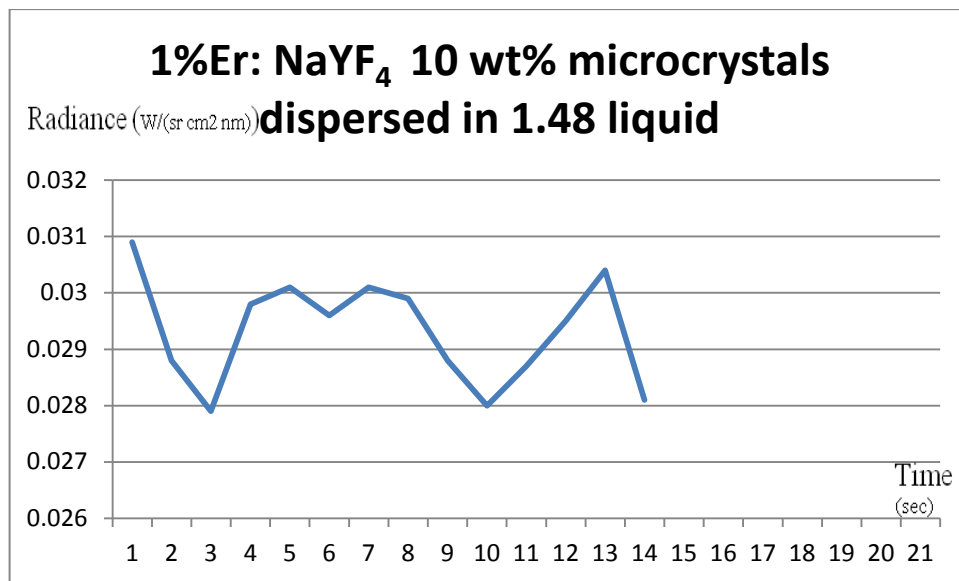


Figure 5.1.3.10. Green emission strength for the sample 1%Er: NaYF₄ 10 wt% microcrystals dispersed in 1.48 refractive index liquid.

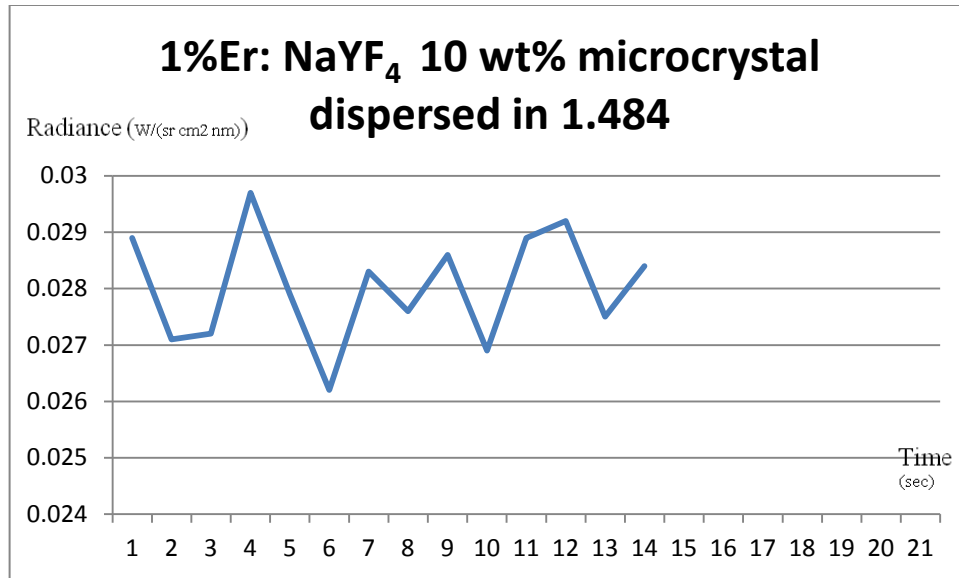


Figure 5.1.3.11. Green emission strength for the sample 1%Er: NaYF₄ 10 wt% microcrystals dispersed in 1.484 refractive index liquid.

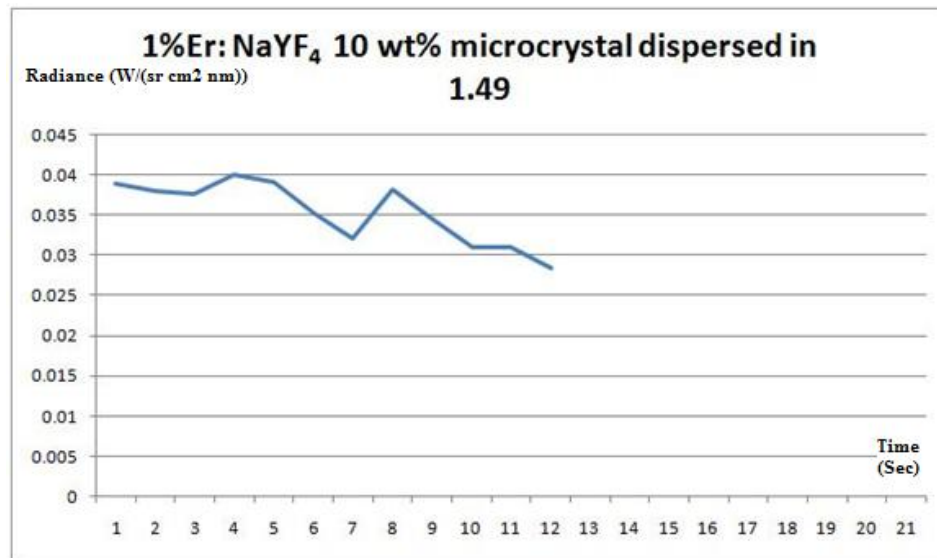


Figure 5.1.3.12. Green emission strength for the sample 1%Er: NaYF₄ 10 wt% microcrystals dispersed in 1.49 refractive index liquid.

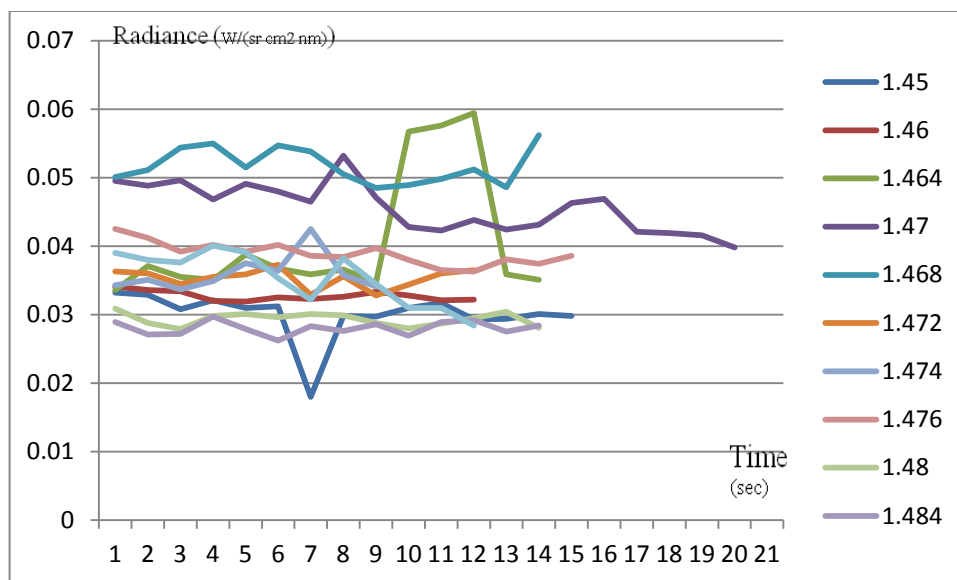


Figure 5.1.3.13. Green emission strength for samples of 1%Er: NaYF₄ 10 wt% microcrystals dispersed in different refractive index liquids.

Material type	Average green emission strength
1%Er: NaYF ₄ 10 wt% microcrystal dispersed in 1.45	0.03
1%Er: NaYF ₄ 10 wt% microcrystal dispersed in 1.456	0.033
1%Er: NaYF ₄ 10 wt% microcrystal dispersed in 1.46	0.0327
1%Er: NaYF ₄ 10 wt% microcrystal dispersed in 1.464	0.04
1%Er: NaYF ₄ 10 wt% microcrystal dispersed in 1.468	0.0517
1%Er: NaYF ₄ 10 wt% microcrystal dispersed in 1.47	0.0455
1%Er: NaYF ₄ 10 wt% microcrystal dispersed in 1.472	0.0353
1%Er: NaYF ₄ 10 wt% microcrystal dispersed in 1.474	0.036
1%Er: NaYF ₄ 10 wt% microcrystal dispersed in 1.476	0.0389
1%Er: NaYF ₄ 10 wt% microcrystal dispersed in 1.48	0.029
1%Er: NaYF ₄ 10 wt% microcrystal dispersed in 1.484	0.028
1%Er: NaYF ₄ 10 wt% microcrystal dispersed in 1.49	0.0353

Table 5.1.3.1. The average green emission strength for the sample 1%Er: NaYF₄ 10 wt% microcrystal dispersed in different refractive index liquid.

Figure 5.1.3.13 and Table 5.1.3.1 demonstrate that the 1%Er: NaYF₄ 10 wt% dispersed in 1.468 refractive index liquid offers the best green emission strength among other samples tested, confirming transmission or scattering results. The measured transmission in Figure 5.1.2.6 shows that the 1%Er: NaYF₄ 10 wt% sample in a liquid with a refractive index of 1.468 has the lowest scattering among other samples.

5.2 0.5% Er: KY₃F₁₀ 10 wt% microcrystals with different refractive index liquids

5.2.1 SEM Measurement

SEM images of 0.5% Er: KY₃F₁₀ 10 wt% microcrystals were obtained. Figure 5.2.1.1 shows a series of low and high magnification SEM images.

The high magnification image shows that the microcrystals have a significant size distribution. The mean size of the microcrystals was found to be 2μm to 30μm.

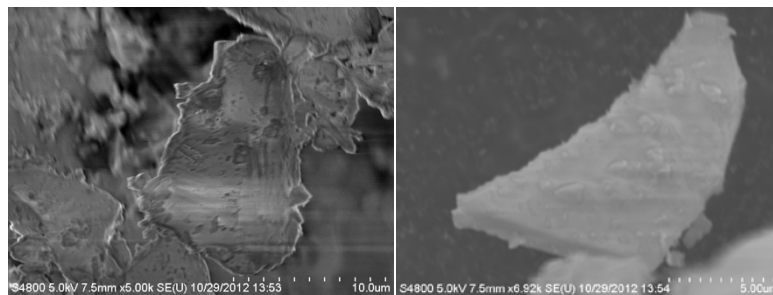


Figure 5.2.1.1. SEM measurement for 0.5% Er: KY₃F₁₀ 10 wt%.

5.2.2 Transmission measurements that demonstrate the amount of scattering

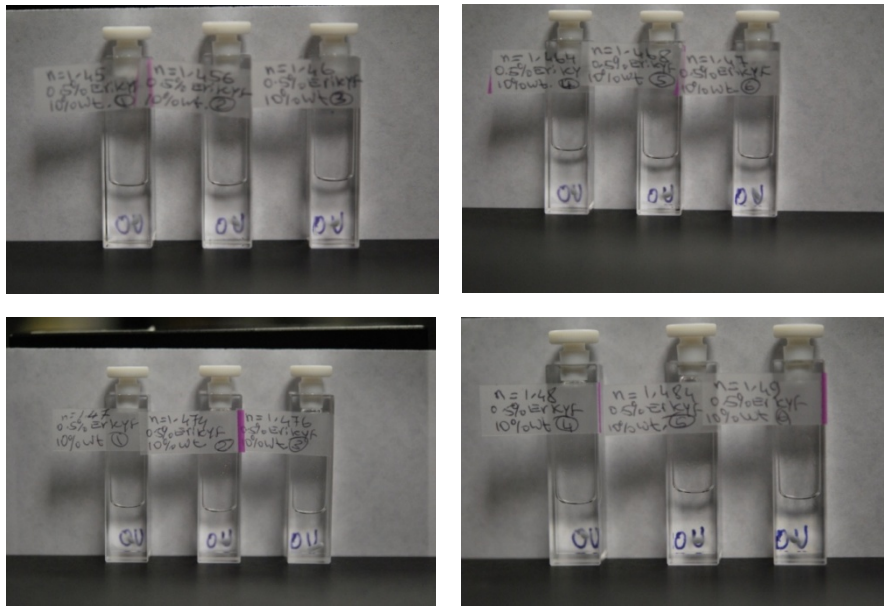


Figure 5.2.1.2. a) 0.5% Er: KY₃F₁₀ 10 wt% dispersed in 1.45,1.456,1.46 refractive index liquids
b) 0.5% Er: KY₃F₁₀ 10 wt% dispersed in 1.464,1.468,1.47, c) 0.5% Er: KY₃F₁₀ 10 wt% dispersed
in 1.47,1.474, 1.476,, d) 0.5% Er: KY₃F₁₀ 10 wt% dispersed in 1.48,1.484,1.49.

While perhaps not apparent to the reader in the reproduced photograph above, the sample dispersed in 1.49 refractive index liquid demonstrated the best visibility and transparency.

A comparison was made between the 0.5% Er: KY₃F₁₀10 wt% microcrystals dispersed in 1.49 liquid and those dispersed in 1.47 liquid, as shown in Figure 5.2.1.3. Notably, the sample dispersed in 1.49 liquid demonstrated better transparency than one dispersed in 1.47.

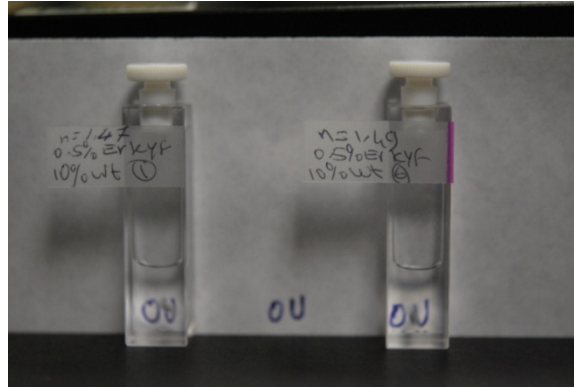


Figure 5.2.1.3. Comparison between the sample 0.5% Er: KY₃F₁₀ 10 wt% dispersed in 1.47 and 1.49 refractive index liquid.

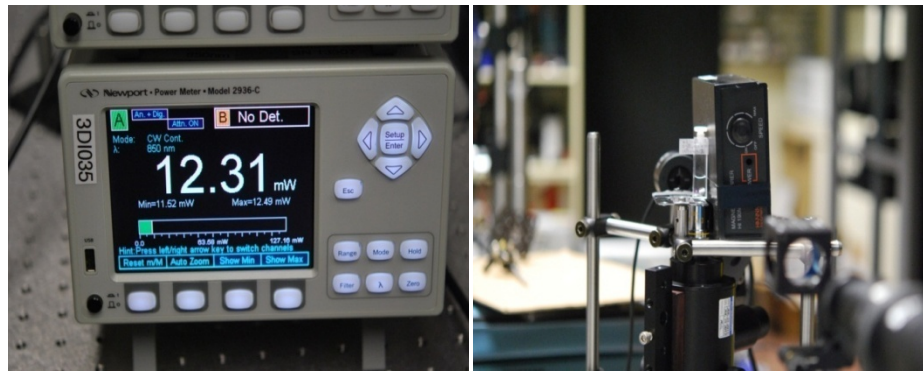


Figure 5.2.1.4. Transmission measurement for the sample 0.5% Er: KY₃F₁₀ 10 wt% dispersed in 1.46 refractive index liquid.

Many samples were formulated by mixing 0.5% Er: KY₃F₁₀ 10 wt% with various refractive index liquids, such as 0.5% Er: KY₃F₁₀ 10 wt% dispersed in 1.46, as shown in Figure 5.2.1.4. The samples were measured, and the result is indicated in the curve in Figure 5.2.1.5 below.

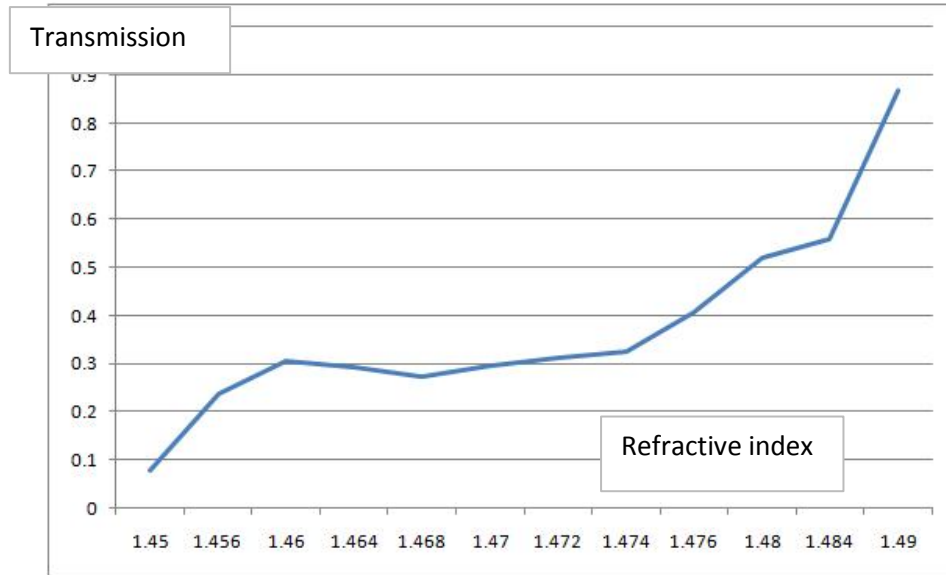


Figure 5.2.1.5. Transmission measurement for 0.5% Er: KY₃F₁₀ 10 wt%: in different refractive index liquids.

The curve in Figure 5.2.1.5 illustrates that 0.5% Er: KY₃F₁₀ 10 wt% microcrystals dispersed in the 1.49 index matching liquid offered superior results. This indicates that the refractive index of the sample 0.5% Er: KY₃F₁₀ is 1.49.

5.2.3 Green emission strength measurements

Using the green emission measurement setup described in Chapter 4, the green emission strength of 0.5%Er: KY₃F₁₀ 10 wt% microcrystals dispersed in different refractive index liquids, e.g., 1.45, 1.456, 1.46, 1.464, 1.468, 1.47, 1.474, 1.476, 1.48, 1.484, and 1.49, was measured, as shown in the figures below.

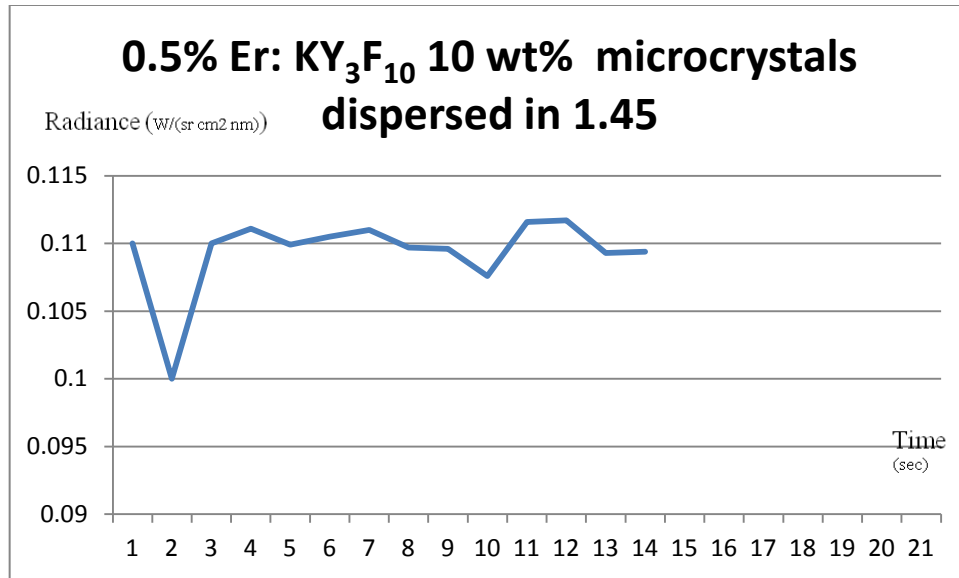


Figure 5.2.3.1. Green emission strength for 0.5% Er: KY₃F₁₀ 10 wt% dispersed in 1.45 refractive index liquid.

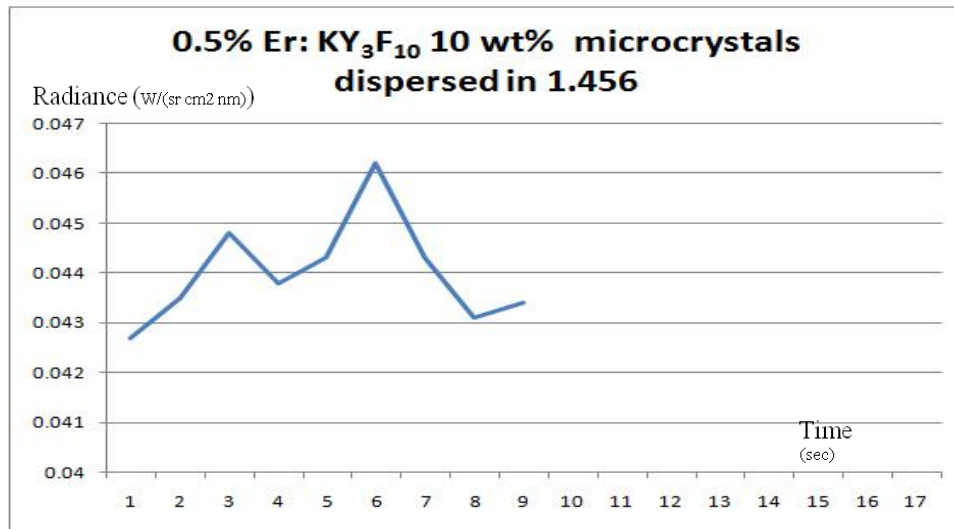


Figure 5.2.3.2. Green emission strength for 0.5% Er: KY₃F₁₀ 10 wt% dispersed in 1.456 refractive index liquid.

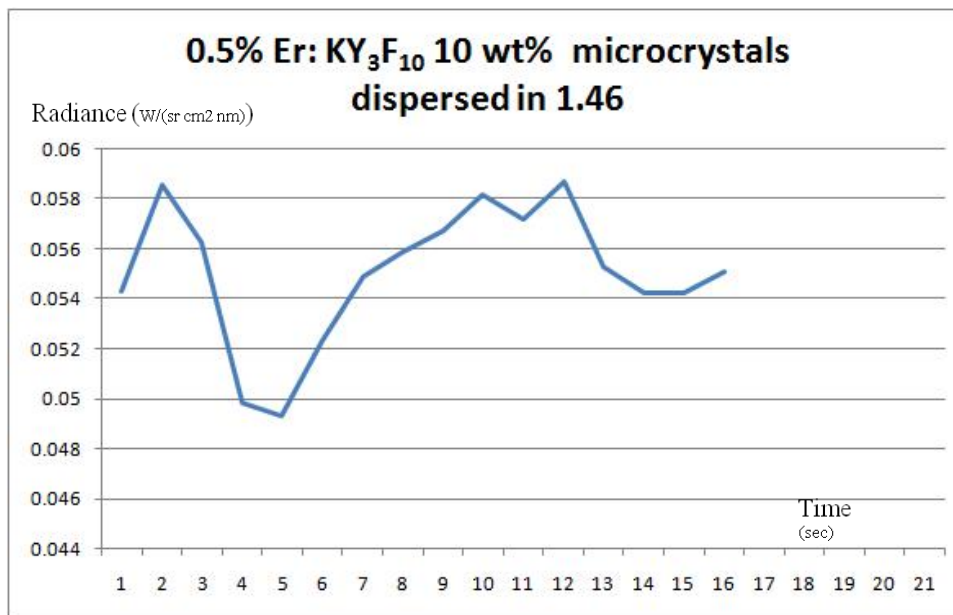


Figure 5.2.3.3. Green emission strength for 0.5% Er: KY₃F₁₀ 10 wt% dispersed in 1.46 refractive index liquid.

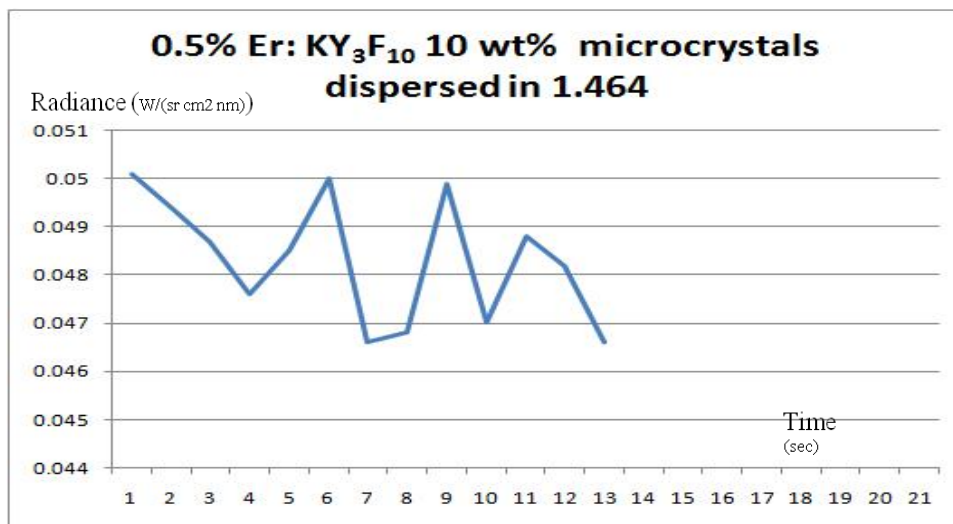


Figure 5.2.3.4. Green emission strength for 0.5% Er: KY₃F₁₀ 10 wt% dispersed in 1.464 refractive index liquid.

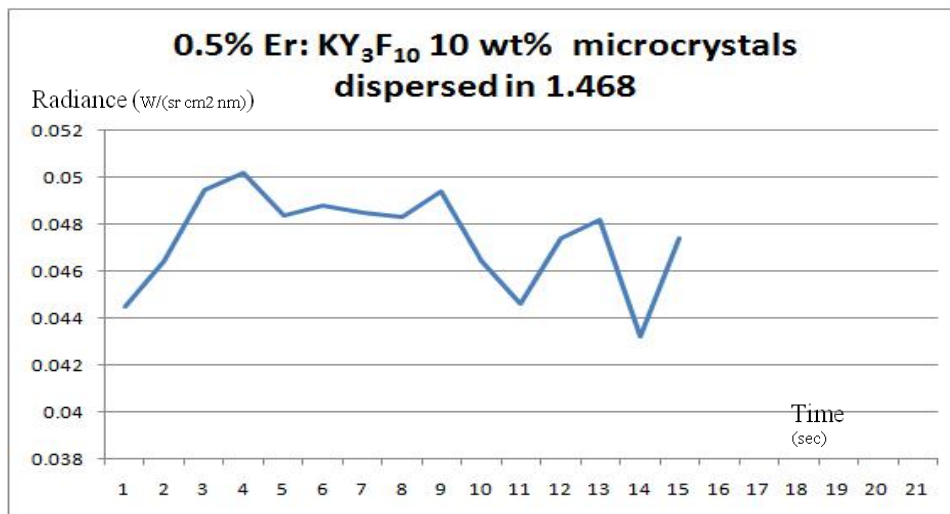


Figure 5.2.3.5. Green emission strength for 0.5% Er: KY₃F₁₀ 10 wt% dispersed in 1.468 refractive index liquid.

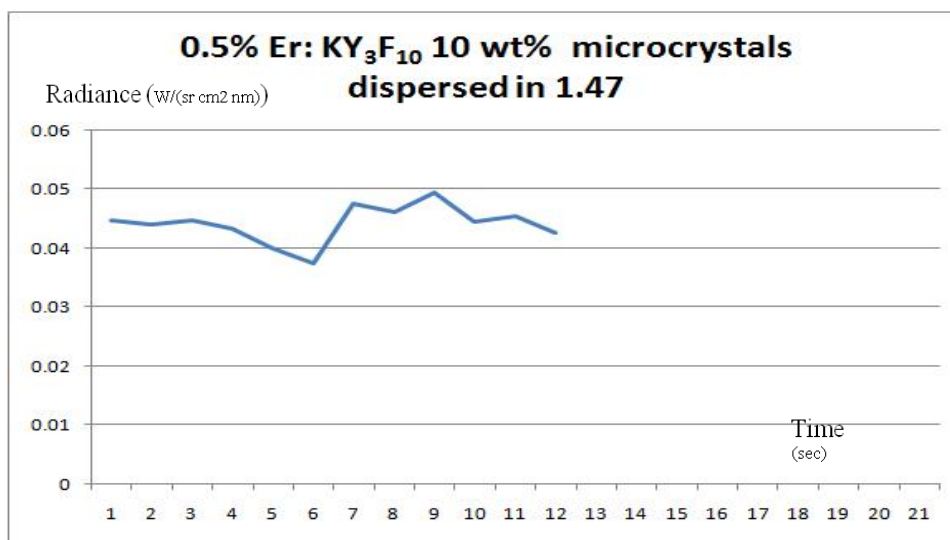


Figure 5.2.3.6. Green emission strength for 0.5% Er: KY₃F₁₀ 10 wt% dispersed in 1.47 refractive index liquid.

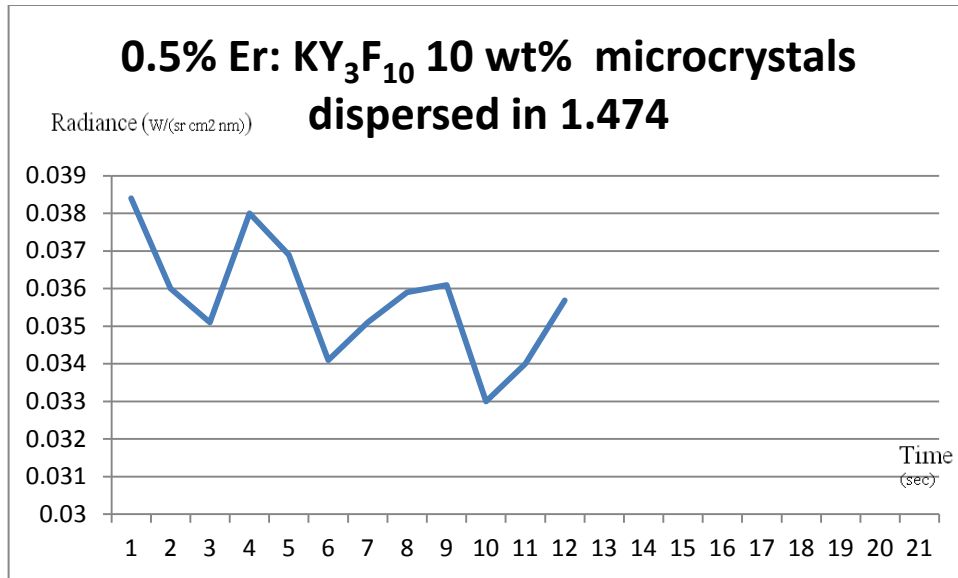


Figure 5.2.3.7. Green emission strength for 0.5% Er: KY₃F₁₀ 10 wt% dispersed in 1.474 refractive index liquid.

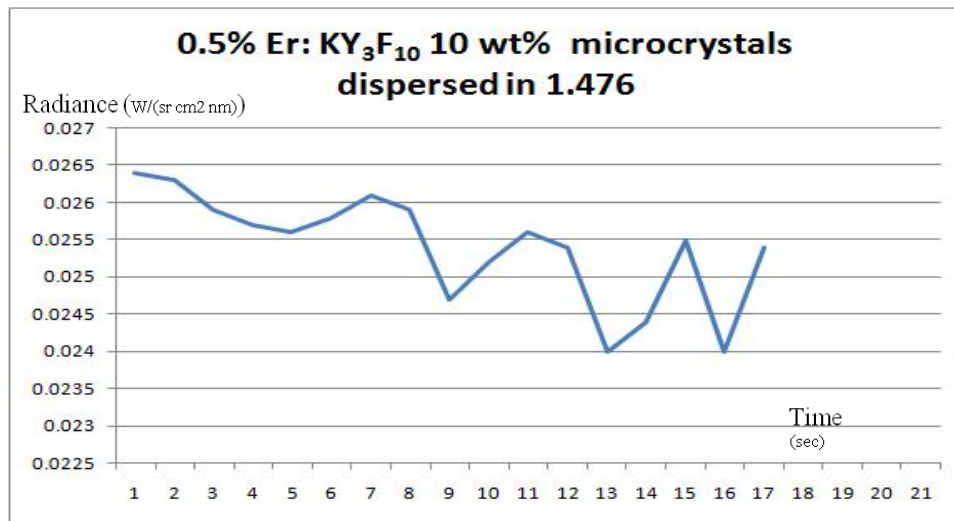


Figure 5.2.3.8. Green emission strength for 0.5% Er: KY₃F₁₀ 10 wt% dispersed in 1.476 refractive index liquid.

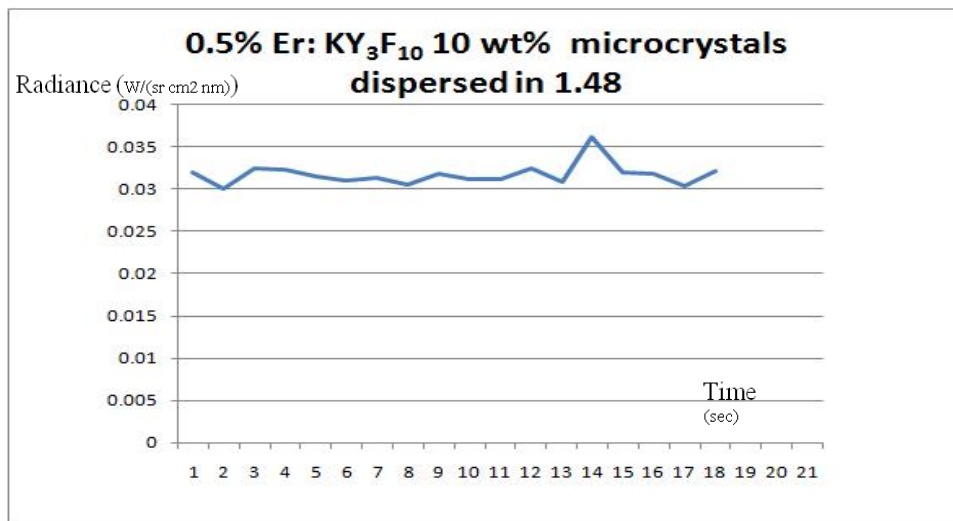


Figure 5.2.3.9. Green emission strength for 0.5% Er: KY₃F₁₀ 10 wt% dispersed in 1.48 refractive index liquid.

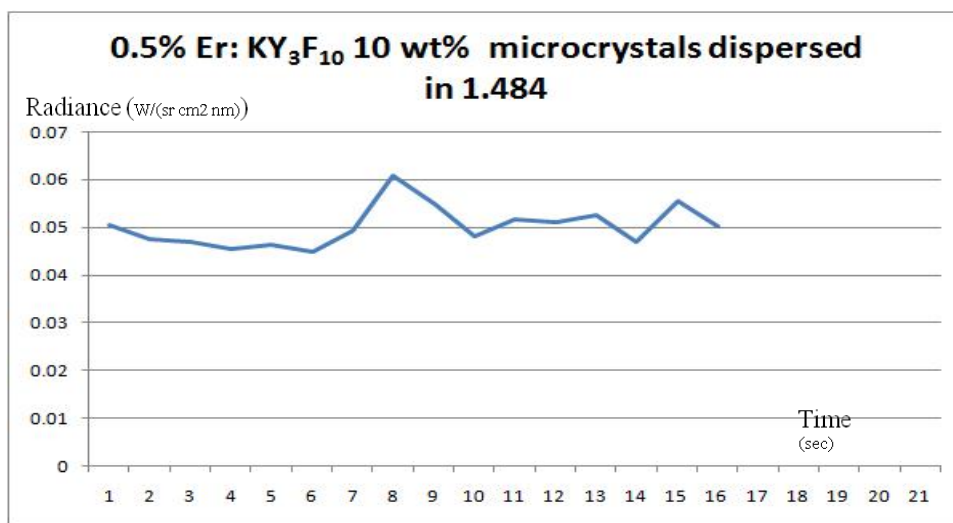


Figure 5.2.3.10. Green emission strength for 0.5% Er: KY₃F₁₀ 10 wt% dispersed in 1.484 refractive index liquid.

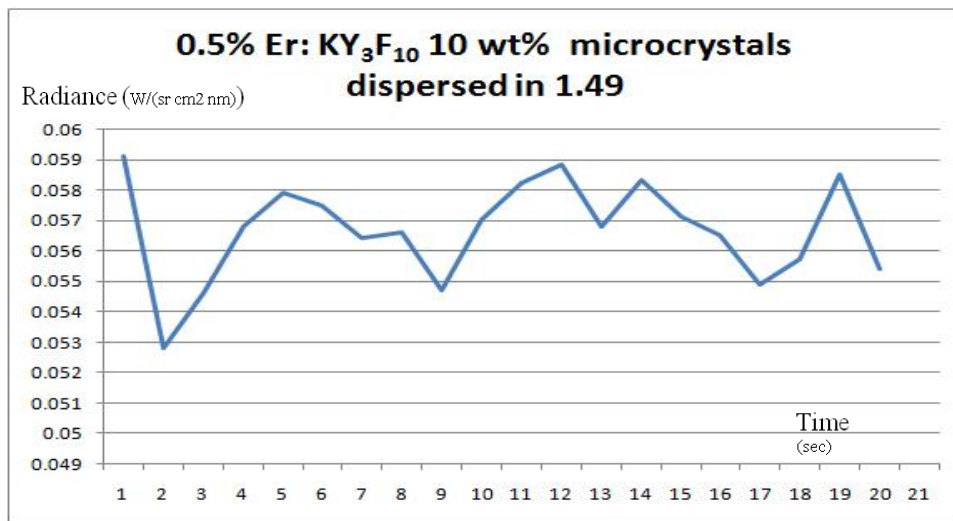


Figure 5.2.3.11. Green emission strength for 0.5% Er: KY₃F₁₀ 10 wt% dispersed in 1.49 refractive index liquid.

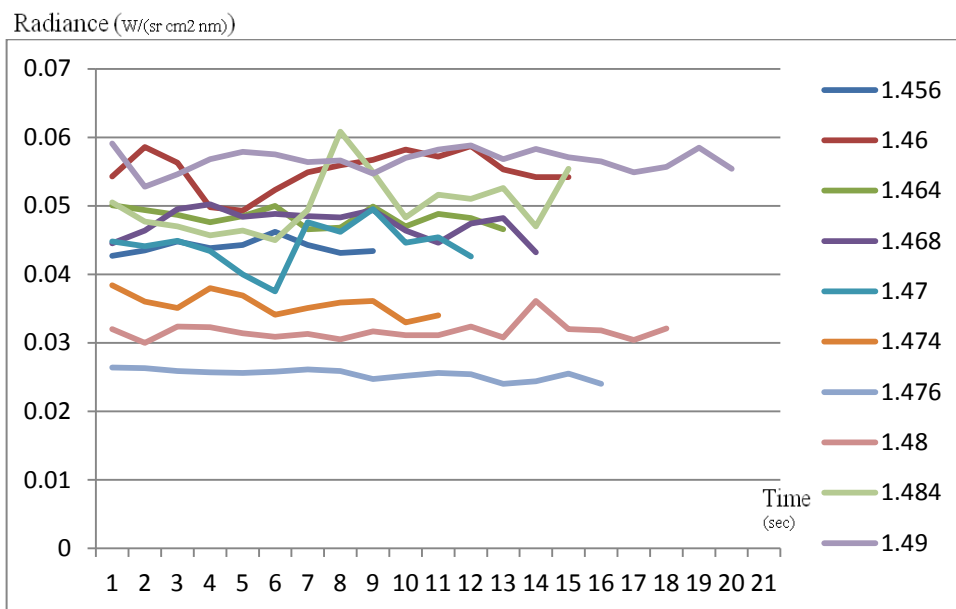


Figure 5.2.3.12. Green emission strength measurement for the sample 0.5% Er: KY₃F₁₀ 10 wt% dispersed in different refractive index liquids.

Sample	Average green emission strength
0.5% Er: KY ₃ F ₁₀ 10 wt% dispersed in 1.45	0.1093
0.5% Er: KY ₃ F ₁₀ 10 wt% dispersed in 1.456	0.044
0.5% Er: KY ₃ F ₁₀ 10 wt% dispersed in 1.46	0.055
0.5% Er: KY ₃ F ₁₀ 10 wt% dispersed in 1.464	0.0483
0.5% Er: KY ₃ F ₁₀ 10 wt% dispersed in 1.468	0.0474
0.5% Er: KY ₃ F ₁₀ 10 wt% dispersed in 1.47	0.0442
0.5% Er: KY ₃ F ₁₀ 10 wt% dispersed in 1.474	0.0356
0.5% Er: KY ₃ F ₁₀ 10 wt% dispersed in 1.476	0.025
0.5% Er: KY ₃ F ₁₀ 10 wt% dispersed in 1.48	0.0316
0.5% Er: KY ₃ F ₁₀ 10 wt% dispersed in 1.484	0.0502
0.5% Er: KY ₃ F ₁₀ 10 wt% dispersed in 1.49	0.056

Table 5.2.3.1: Average green emission measurements for the sample 0.5% Er: KY₃F₁₀ 10 wt% dispersed in different refractive index liquid.

After comparing the average green emission strength measurements for the 0.5% Er: KY₃F₁₀ 10 wt% sample dispersed in different refractive index liquids, the highest value was for the sample dispersed in 1.45 and 1.49. The average green emission for the sample dispersed in 1.45 was 0.109, and the sample dispersed in 1.49 was 0.056. For the sample dispersed in 1.45, the particles clearly failed to index match with those of the liquid, meaning that the particles remained in the bottom of the cuvette even though a stirring bar was employed. Concentrations were higher in the bottom than in the overall cuvette, leading to higher green emission strength. Given these results, it can be concluded that the sample dispersed in 1.49 refractive index liquid demonstrated the best overall green emission strength.

5.3 0.5% Er: LLF 10 wt% microcrystal with different refractive index liquids

5.3.1 SEM measurement

The image in Figure 5.3.1 is highly magnified.

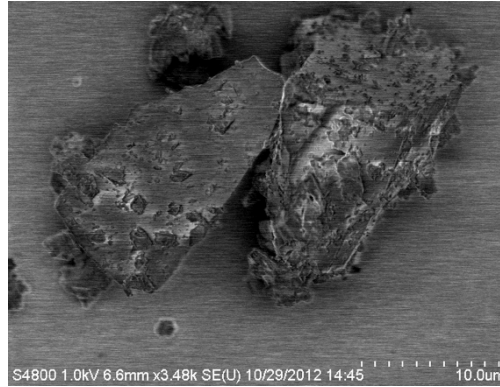


Figure 5.3.1.1. High magnification SEM images for the sample 0.5% Er: LLF10wt%.

Results obtained from the SEM measurement show that the sizes of the 0.5% Er: LLF 10 wt% microcrystals were between 15 and 20 μm .

5.3.2 Transmission measurements that demonstrate the amount of scattering

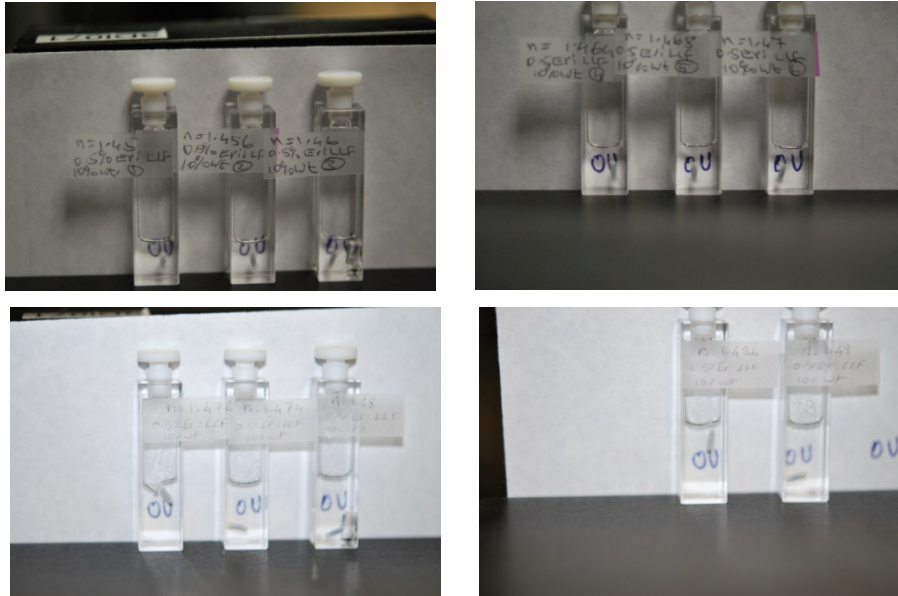


Figure 5.3.2.1. a) 0.5% Er: LLF10 wt% dispersed in 1.45,1.456,1.46 refractive index liquids, b) 0.5% Er: LLF 10 wt% dispersed in 1.464,1.468,1.47, c) 0.5% Er: LLF 10 wt% dispersed in 1.47,1.474, 1.48,, d) 0.5% Er: LLF 10 wt% dispersed in 1.484,1.49.

Figure 5.3.2.1 shows that the sample 0.5% Er: LLF10 wt% dispersed in 1.472 had the best clarity when compared with the other samples.

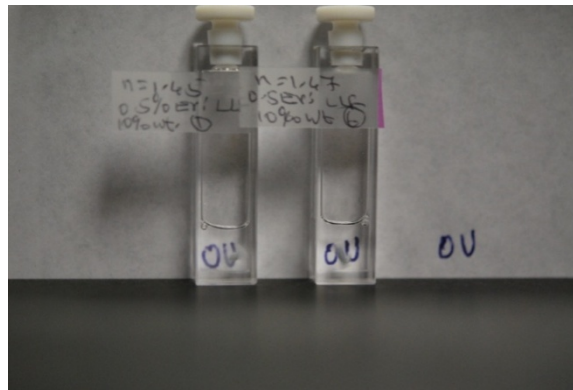


Figure 5.3.2.2. Comparison for the 0.5% Er: LLF10 wt% sample dispersed in 1.45 and 1.47 refractive index liquid.

The 0.5% Er: LLF10 wt% sample dispersed in 1.45 exhibited scattering due to non- transparency. In contrast, the sample dispersed in 1.47 was optically transparent, as shown in Figure 5.3.2.2.



Figure 5.3.2.3. Measurement setup for the transmission test for the sample 0.5% Er: LLF10 wt% dispersed in 1.45.

Using the experiment setup described in Chapter 4, 0.5% Er: LLF10 wt% dispersed in different refractive index liquids was tested. Results are shown in Figure 5.3.2.4. One particular tested sample is shown in Figure 5.3.2.3.

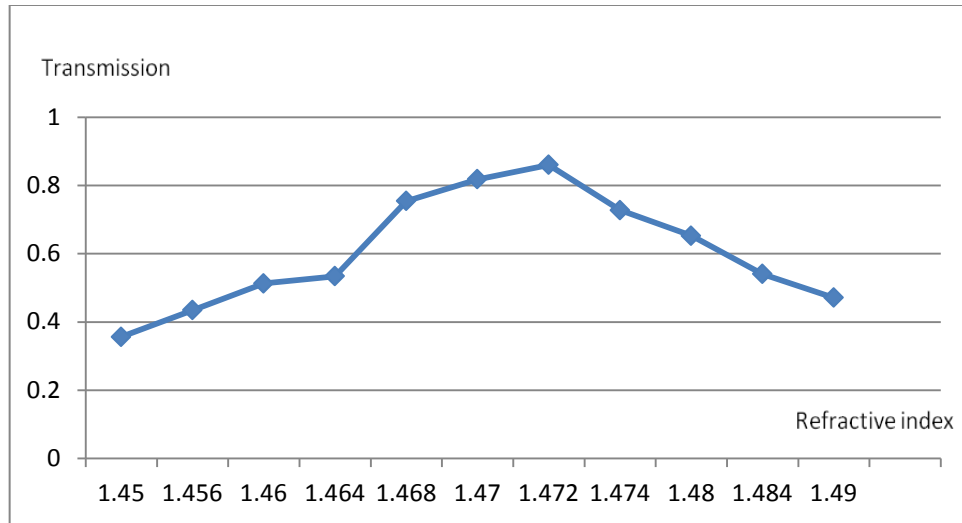


Figure 5.3.2.4. Transmission measurements for 0.5% Er: LLF 10 wt% dispersed in different refractive index liquids.

From the curve in the figure above, one can see that the 0.5% Er: LLF 10 wt% sample dispersed in 1.472 liquid showed the best results.

5.3.3 Green emission strength measurement

The green emission strength for 0.5% Er: LLF10 wt% samples dispersed in different refractive index liquids was measured using the experiment setup mentioned in Chapter 4.

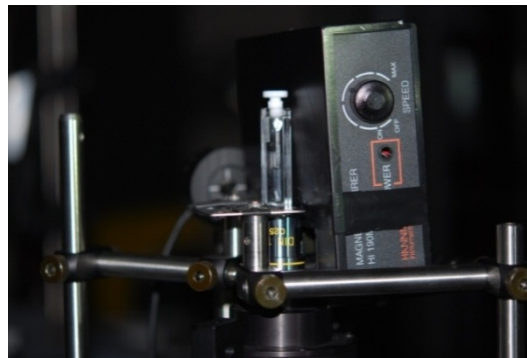


Figure 5.3.3.1. The sample 0.5% Er: LLF 10 wt% dispersed in 1.45 under measurement.

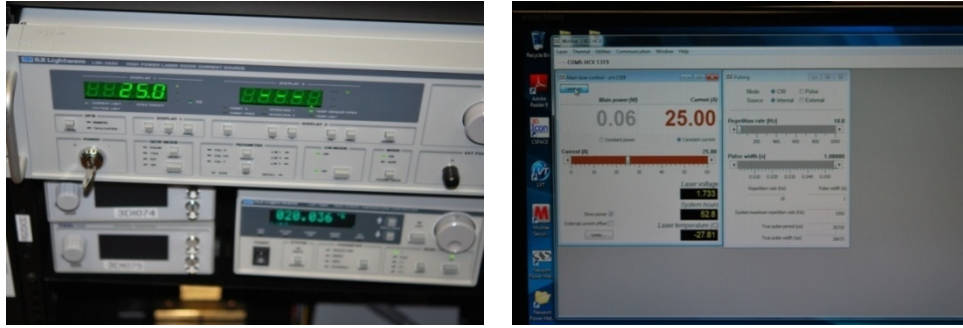


Figure 5.3.3.2: Measurement green emission setup for 0.5% Er: LLF 10 wt% samples.

Figure 5.3.2.1 shows the sample 0.5% Er: LLF 10 wt% microcrystals dispersed in the 1.45 index matched liquid. The measured green emission strength is shown in Figure 5.3.2.2.

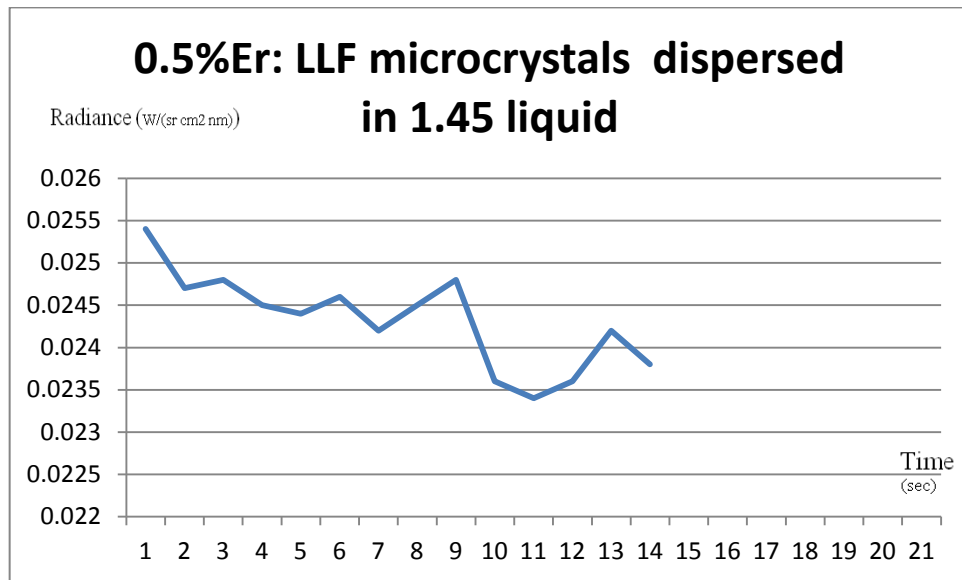


Figure 5.3.2.2. Green emission strength for 0.5% Er: LLF 10 wt% dispersed in 1.45 refractive index liquid.

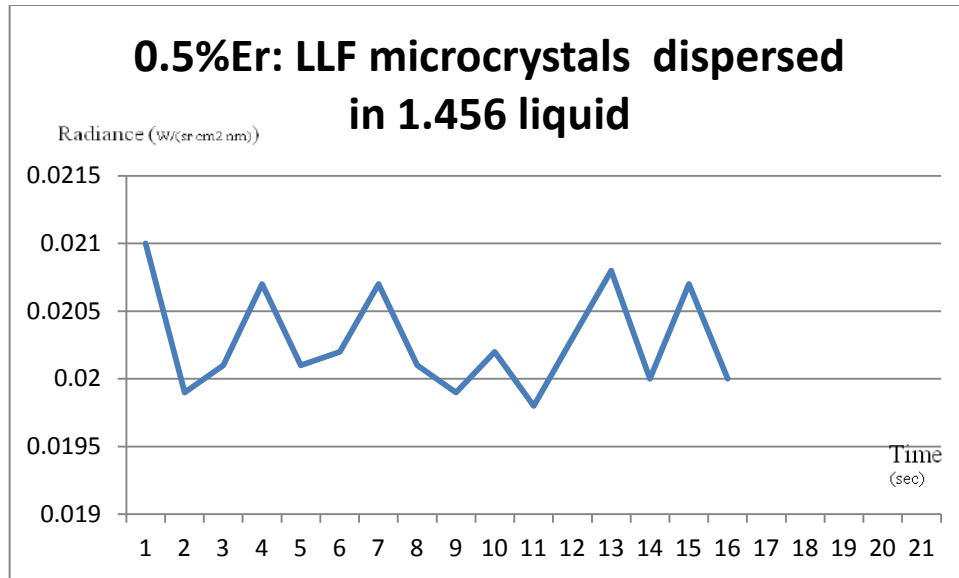


Figure 5.3.2.3. Green emission strength for 0.5% Er: LLF 10 wt% dispersed in 1.456 refractive index liquid.

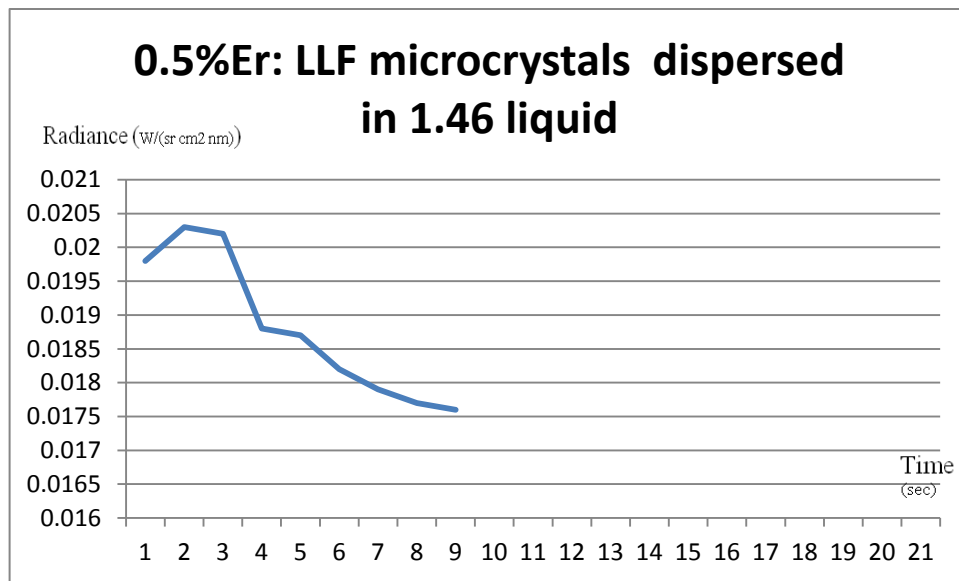


Figure 5.3.2.4. Green emission strength for 0.5% Er: LLF 10 wt% dispersed in 1.46 refractive index liquid.

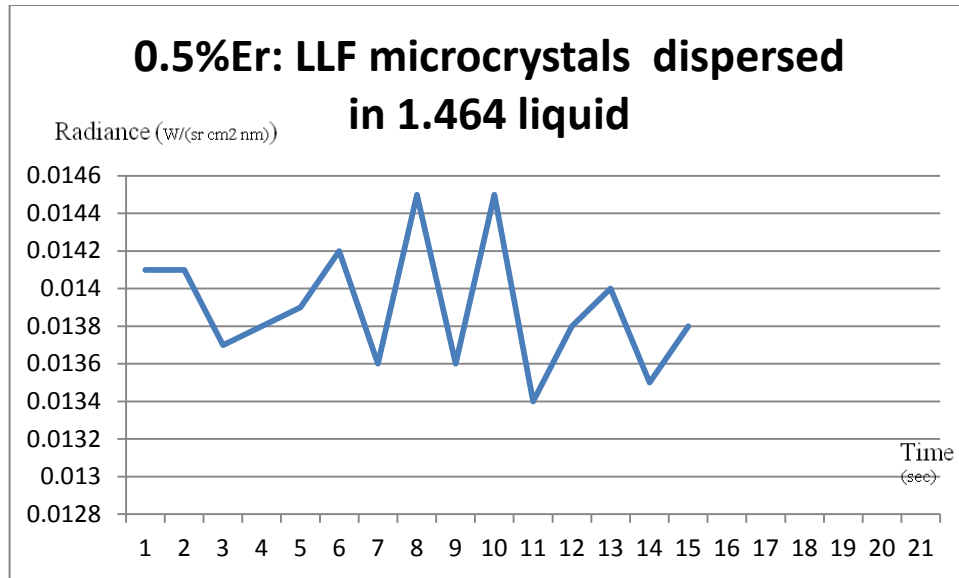


Figure 5.3.2.5. Green emission strength for 0.5% Er: LLF 10 wt% dispersed in 1.464 refractive index liquid.

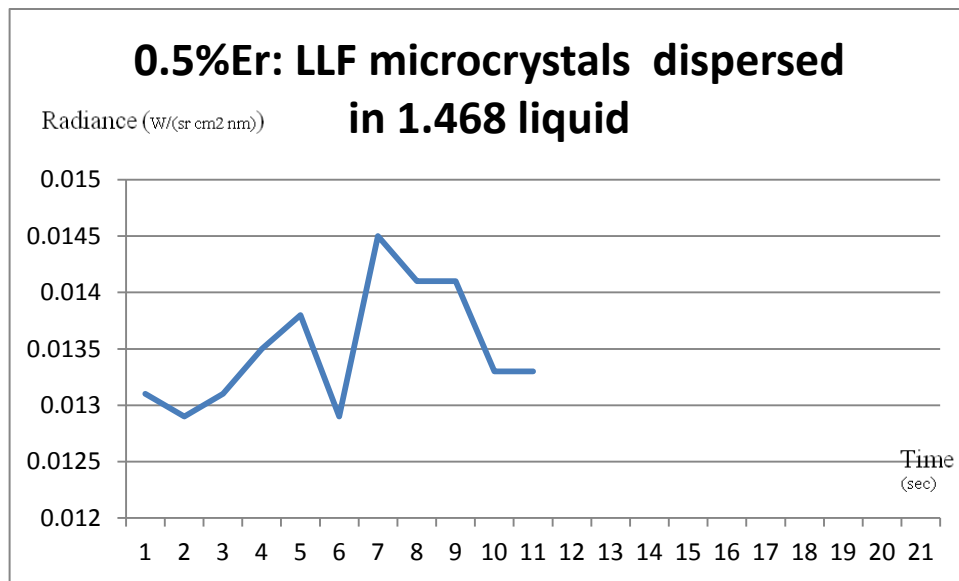


Figure 5.3.2.6. Green emission strength for 0.5% Er: LLF 10 wt% dispersed in 1.468 refractive index liquid.

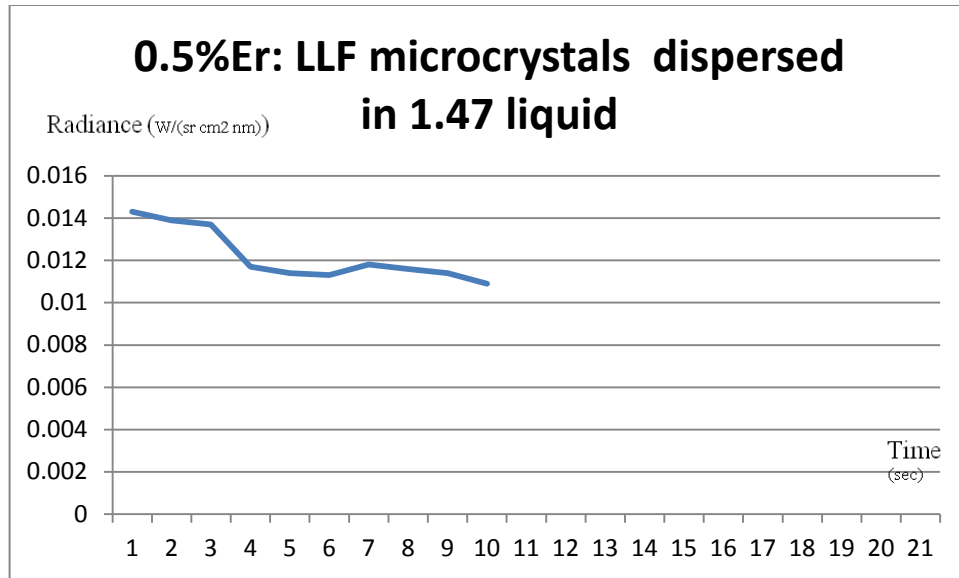


Figure 5.3.2.7. Green emission strength for 0.5% Er: LLF 10 wt% dispersed in 1.467 refractive index liquid.

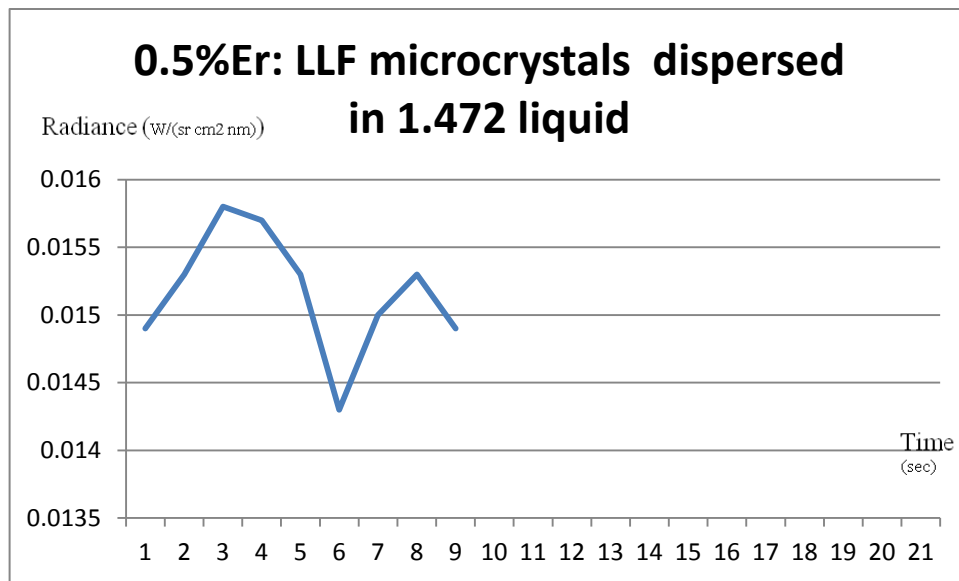


Figure 5.3.2.8. Green emission strength for 0.5% Er: LLF 10 wt% dispersed in 1.472 refractive index liquid.

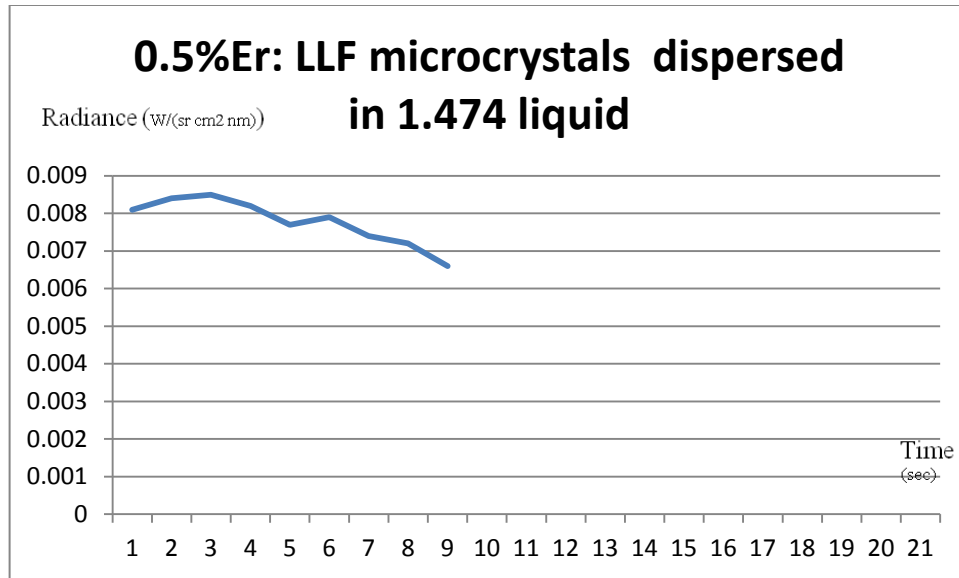


Figure 5.3.2.9. Green emission strength for 0.5% Er: LLF 10 wt% dispersed in 1.474 refractive index liquid.

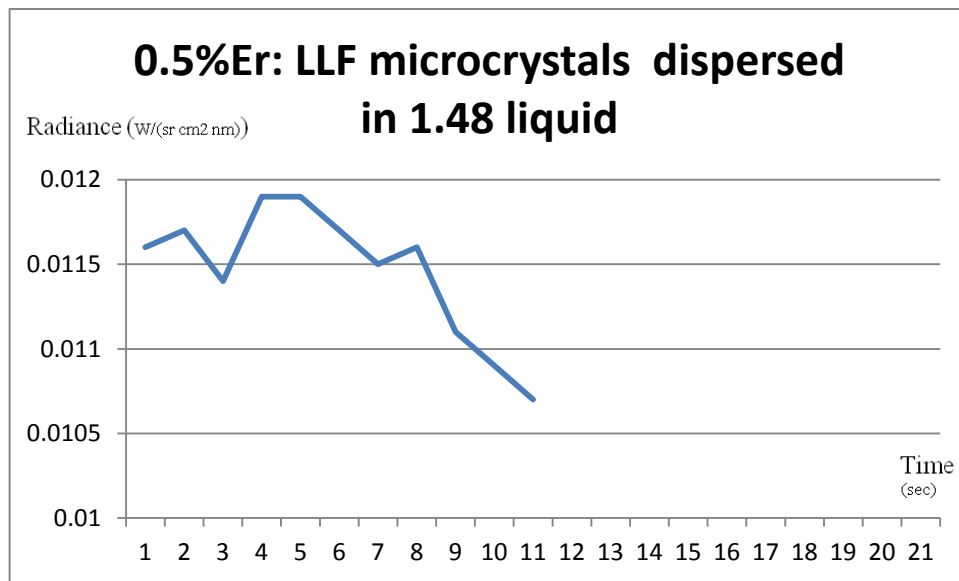


Figure 5.3.2.10. Green emission strength for 0.5% Er: LLF 10 wt% dispersed in 1.48 refractive index liquid.

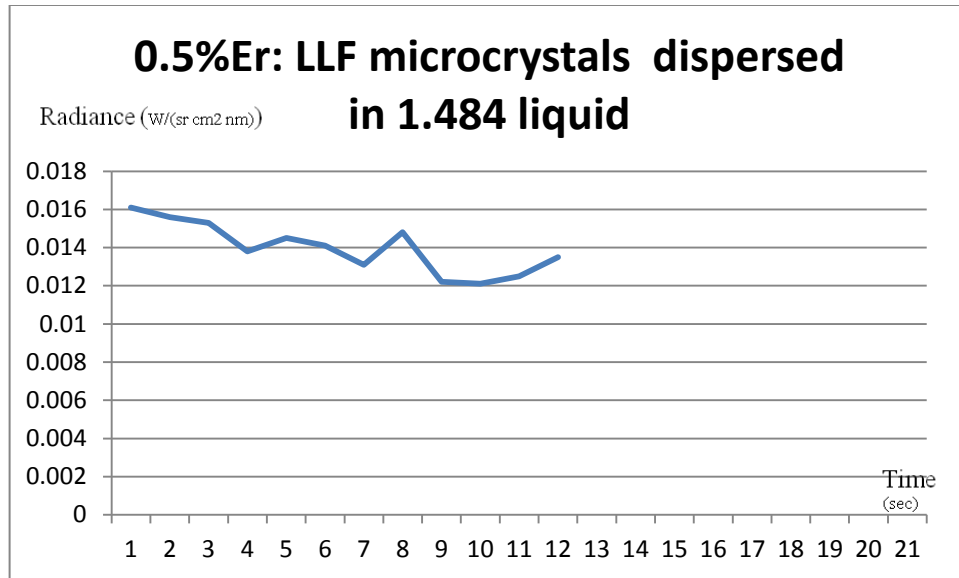


Figure 5.3.2.11. Green emission strength for 0.5% Er: LLF 10 wt% dispersed in 1.484 refractive index liquid.

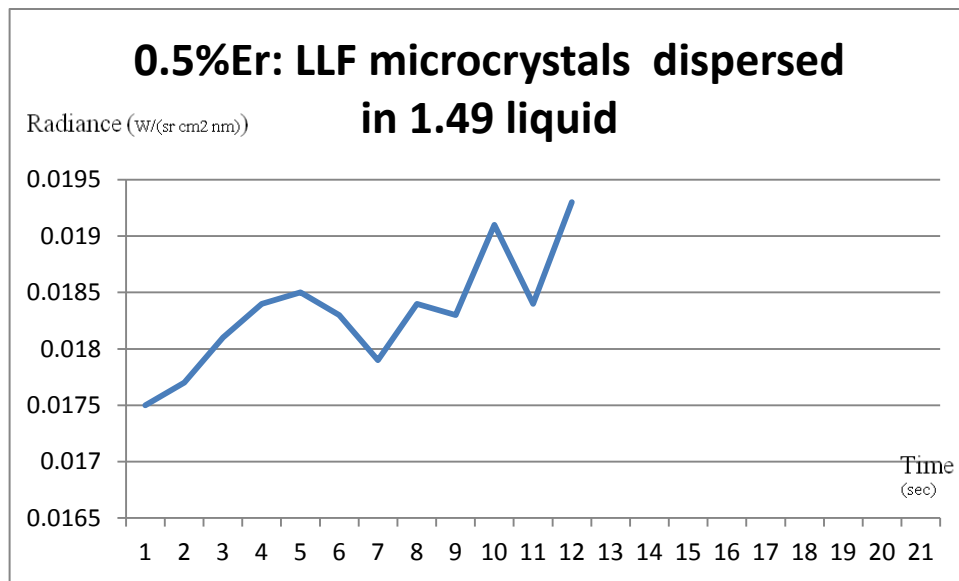


Figure 5.3.2.12. Green emission strength for 0.5% Er: LLF 10 wt% dispersed in 1.49 refractive index liquid.

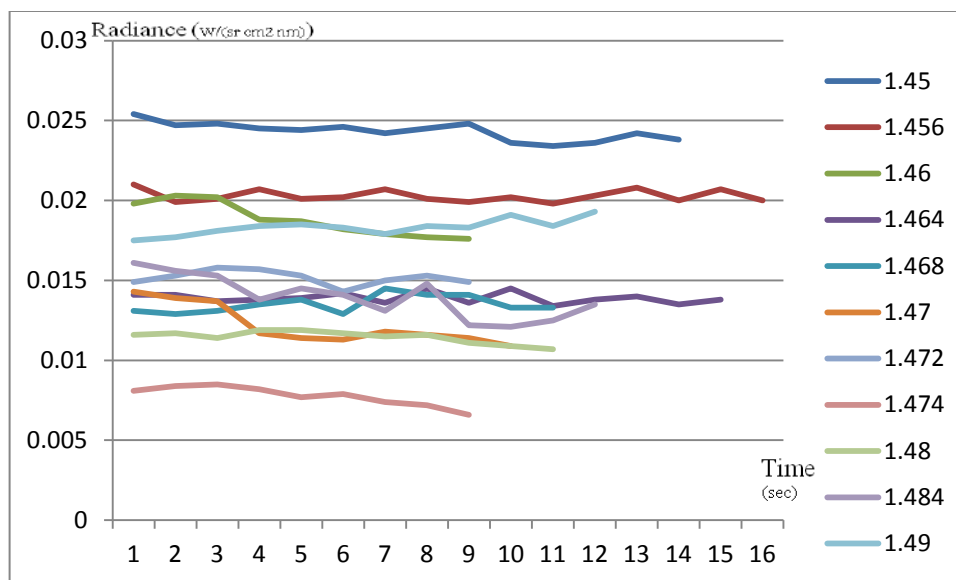


Figure 5.3.2.13. Green emission measurement for the 0.5% Er: LLF 10 wt% microcrystals dispersed in collection of different refractive index liquids.

Sample	Average green emission strength
0.5% Er: LLF 10 wt% dispersed in 1.45	0.024
0.5% Er: LLF 10 wt% dispersed in 1.456	0.0202
0.5% Er: LLF 10 wt% dispersed in 1.46	0.0188
0.5% Er: LLF 10 wt% dispersed in 1.464	0.0139
0.5% Er: LLF 10 wt% dispersed in 1.468	0.0135
0.5% Er: LLF 10 wt% dispersed in 1.47	0.0122
0.5% Er: LLF 10 wt% dispersed in 1.472	0.0151
0.5% Er: LLF 10 wt% dispersed in 1.474	0.0077
0.5% Er: LLF 10 wt% dispersed in 1.48	0.01145
0.5% Er: LLF 10 wt% dispersed in 1.484	0.0139
0.5% Er: LLF 10 wt% dispersed in 1.49	0.0183

Table 5.3.2.1. Average green emission strength for the microcrystal 0.5% Er: LLF 10 wt% dispersed in different refractive index liquids.

Figure 5.3.2.13 and Table 5.3.2.1 show that the 0.5% Er: LLF 10 wt% sample dispersed in 1.45, 1.456, 1.46, and 1.472 refractive index liquids showed superior green

emission strength. At the time the transmission measurements were taken the samples clearly showed that the 0.5% Er: LLF 10 wt% microcrystals dispersed in 1.45, 1.456, and 1.46 remained on the bottom of the cuvette. Hence, the refractive index of the former was mismatched with the 1.45, 1.456, 1.46 liquids. When eliminating these three liquids from consideration, the 0.5% Er: LLF 10 wt % sample dispersed in 1.472 was selected, because the microcrystals were well dispersed.

The 0.5% Er: LLF 10 wt % sample dispersed in 1.472 liquid had a low green emission strength when compared with 0.5% Er: KY₃F₁₀ 10 wt% dispersed in 1.49 liquid and 1%Er: NaYF₄ 10 wt% dispersed in 1.468 liquid. Hence, the 0.5% Er: LLF material was the least efficient at converting the infrared light energy into green light energy. As a result, no further studies were performed on this material. Only the samples with the highest emission from well-dispersed particles, namely 1% Er:NaYF₄ in 1.468 and 0.5% Er:KY₃F₁₀ in 1.49, were selected for further studies.

Chapter 6

Different particle concentrations

Other important factors influence the transparency and brightness of the microcrystal samples. One of these is the microcrystal concentration of the sample. Different concentrations were examined to investigate how this factor can affect sample transparency and brightness.

Based on measurements discussed in Chapter 5, superior results were found for 0.5% Er: KY₃F₁₀ 10 wt% dispersed in 1.49 liquid and 1%Er: NaYF₄ 10 wt% dispersed in 1.468 liquid. Hence, concentrations of 20%wt and 30%wt for both samples were investigated.

6.1 Medium 1%Er: NaYF₄ 20wt% dispersed in 1.468 liquid

A new sample with the same particle size as that tested in Chapter 5, but with a 20% higher particle concentration, was investigated. Results are described below. The same preparation procedure described in Chapter 4 was followed. Increasing the particle concentration will determine if particle concentration will affect scattering, green emission strength, and transparency.

6.1.1 Transmission measurement

The setup for the transmission measurement for the 1%Er: NaYF₄ 20 wt% sample dispersed in 1.468 liquid is shown below in Figure 6.1.1.1.

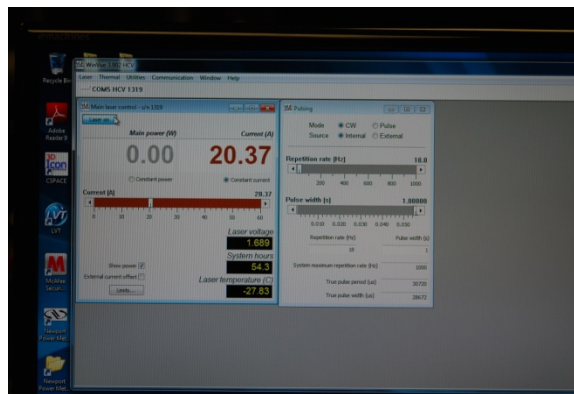


Figure 6.1.1.1. Transmission measurement setup- the generated optical power measured and the required current to generate this optical power.

The result of the transmission measurement for the 1%Er: NaYF₄ 20 wt% sample dispersed in 1.468 liquid is shown in Figure 6.1.1.2. Notably, power meter results decreased, as explained below.

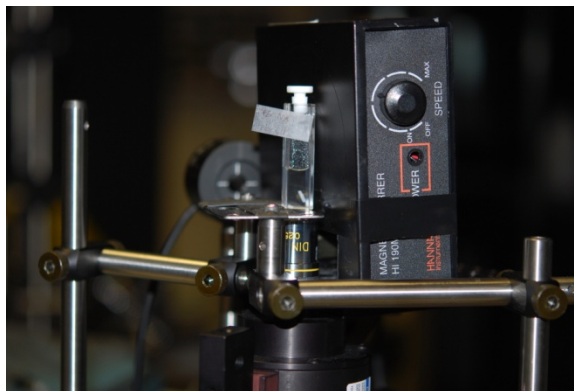
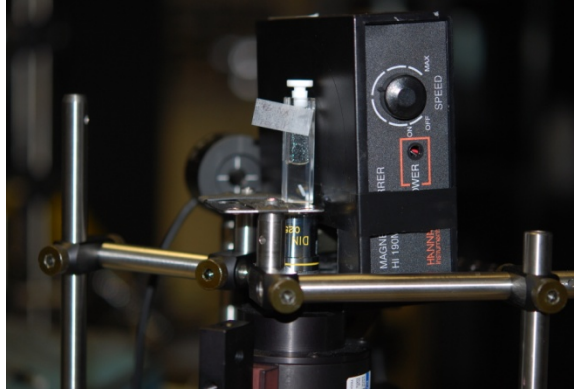


Figure 6.1.1.2: Transmission result for the sample 1%Er: NaYF₄ 20 wt% dispersed in 1.468.

The measured transmission for the 1%Er: NaYF₄ 20 wt% sample dispersed in 1.468 liquid was 0.837, which was lower when compared to the 1%Er: NaYF₄ 10 wt% sample dispersed in 1.468 liquid that yielded 0.952. This test indicated that increasing the concentration increases scattering due to an increased number of particles.

6.1.2 Green emission measurement

Green emission measurement strength was examined for the 1%Er: NaYF₄ 20 wt% sample dispersed in 1.468 liquid.

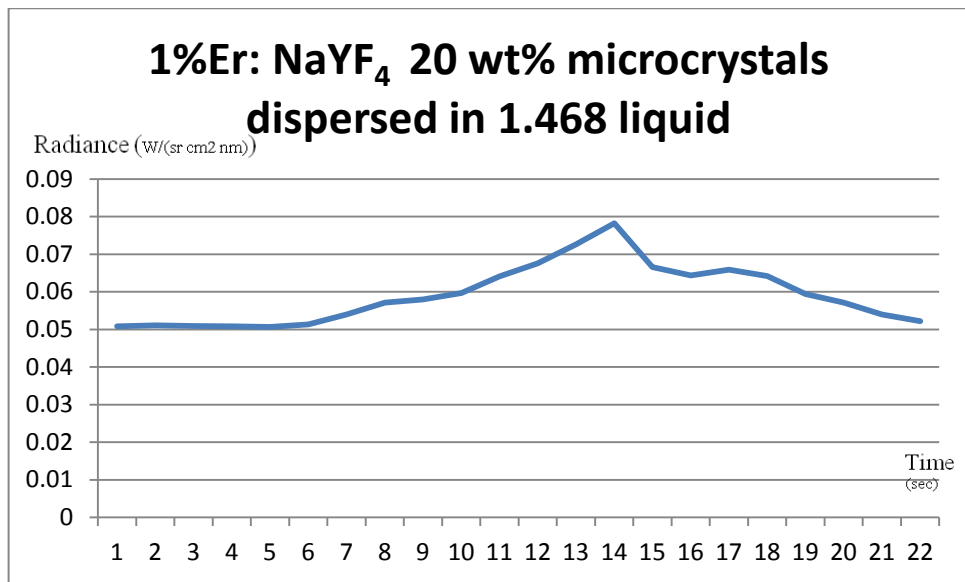


Figure 6.1.2.1. Green emission strength for 1%Er: NaYF₄ 20 wt% dispersed in 1.468 liquid.

Green emission strength average for 1%Er: NaYF₄ 20 wt% dispersed in 1.468 was 0.059123.

6.2 Medium 1%Er: NaYF₄ 30 wt% dispersed in 1.468 liquid

To determine the consequence of increasing the concentration, a sample as described in Chapter 4 was prepared. The weight percentage of particles added was increased from 10% to 30%.

6.2.1 Transmission measurement

A transmission test for the 1%Er: NaYF₄ 30 wt% sample dispersed in 1.468 liquid is shown below in Figure 6.2.1.1.



Figure 6.2.1.1. Scattering measurement for the sample 1%Er: NaYF₄ 30 wt% dispersed in 1.468.

Increasing the concentration resulted in lower transmission. Transmission for the 1%Er: NaYF₄ 30 wt% sample dispersed in 1.468 liquid was 0.62, which was lower than 1%Er: NaYF₄ 10 wt% dispersed in 1.468 liquid and 1%Er: NaYF₄ 20 wt% dispersed in 1.468 liquid. Thus, increasing the particles increases scattering and decreases transmission.

6.2.2 Green emission strength measurement

The green emission strength for the 1%Er: NaYF₄ 30 wt% sample dispersed in 1.468 liquid was also measured. The average green emission strength measured 0.0706, as shown below in Figure 6.2.2.1.

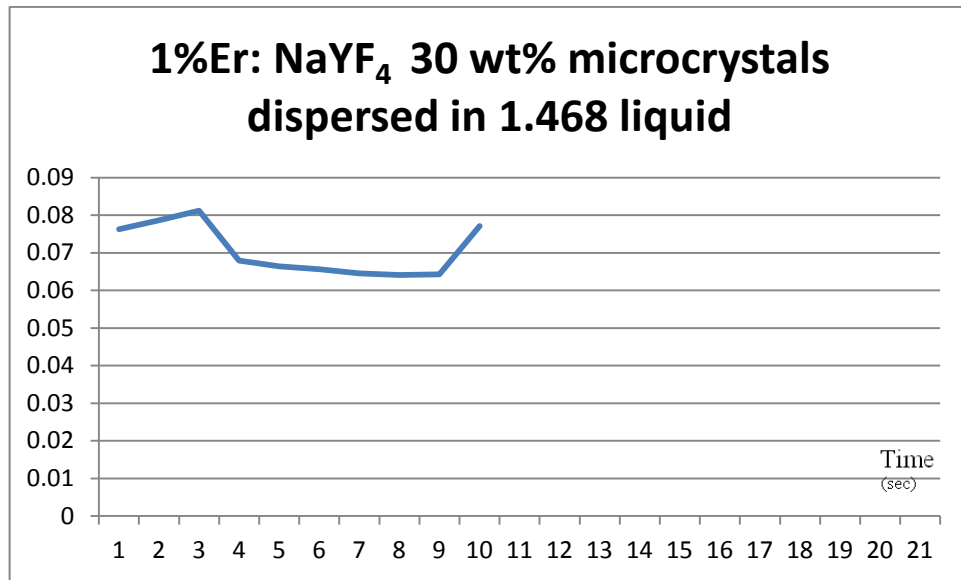


Figure 6.2.2.1. Green emission strength for 1%Er: NaYF₄ 30 wt% dispersed in 1.468.

It can be concluded, then, that the brightness of a voxel depends directly on the density of the active material. However, more NaYF₄ particles imply more scattering. To determine the degree of concentration of crystallites, several properties must be considered, including display medium size and desired voxel brightness.

6.3 Medium 0.5% Er: KY₃F₁₀ 20 wt% dispersed in 1.49 liquid

6.3.1 Transmission measurement

The transmission measurement for the 0.5% Er: KY₃F₁₀ 20 wt% sample dispersed in 1.49 liquid is shown below in Figure 6.3.1.1.

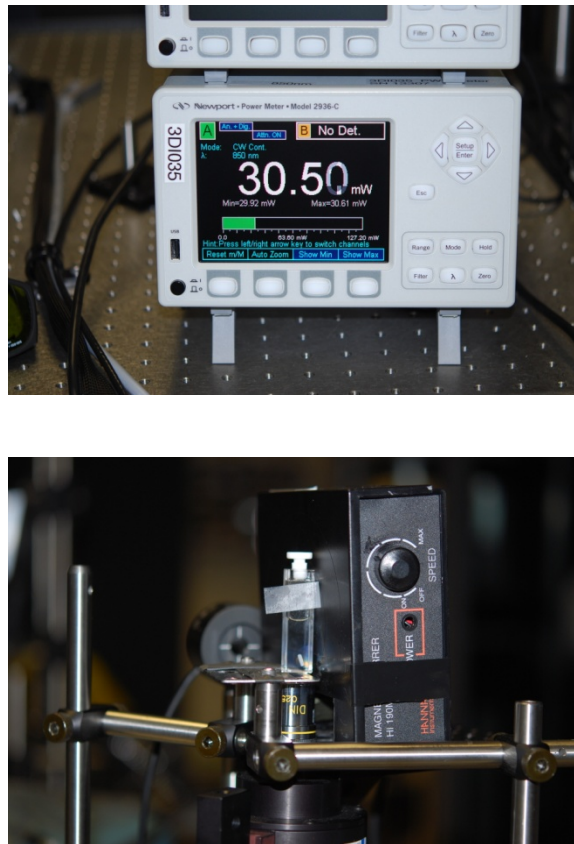


Figure 6.3.1.1. Transmission measurement for the 0.5% Er: KY₃F₁₀ 20 wt% sample dispersed in 1.49 liquid.

Transmission of the 0.5% Er: KY₃F₁₀ 20 wt% sample dispersed in 1.49 liquid was 0.761. This figure was less than 0.877 for the transmission of the 0.5% Er: KY₃F₁₀ 10 wt% sample dispersed in 1.49 liquid, meaning that transmission decreased and scattering increased.

6.3.2 Green emission strength measurement

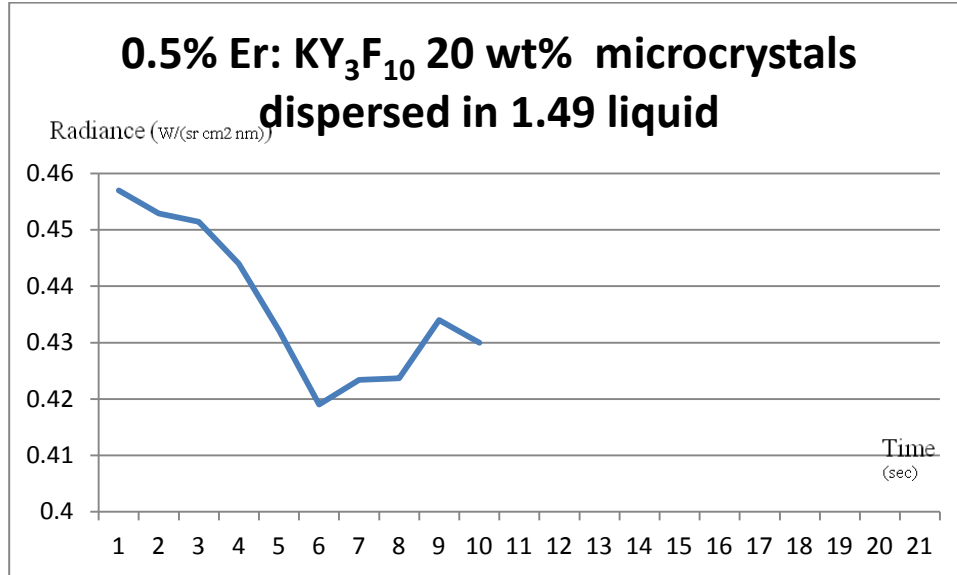


Figure 6.3.2.1. Green emission strength for 0.5% Er: KY₃F₁₀ 20 wt% dispersed in 1.49.

The average strength for the green emission for the 0.5% Er: KY₃F₁₀20 wt% sample dispersed in 1.49 liquid was 0.437, which increased dramatically from 0.05668 for 0.5% Er: KY₃F₁₀10 wt% dispersed in 1.49 liquid.

6.4 Medium 0.5% Er: KY₃F₁₀30 wt% dispersed in 1.49 liquid

6.4.1 Transmission measurement

The transmission measurement for 0.5% Er: KY₃F₁₀30 wt% is shown below in Figure 6.4.1.1.

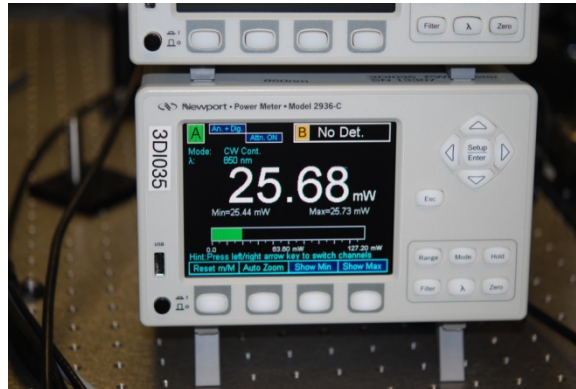


Figure 6.4.1.1. Transmission measurement for the sample 0.5% Er: KY₃F₁₀ 30 wt% dispersed in 1.49.

The transmission of the 0.5% Er: KY₃F₁₀30 wt% sample dispersed in 1.49 liquid was 0.6411, which was less than that of both 10% and 20% concentrations. Hence, increasing particle concentration decreases transmission.

6.4.2 Green emission strength measurement

Figure 6.4.2.1 shows that when measured during a time period of 60 seconds, the average green emission strength for the 0.5% Er: KY₃F₁₀30 wt% sample dispersed in 1.49 liquid was 0.5989.

Figure 6.4.2.1 shows the green emission strength for this same sample during a time period of 20 seconds.

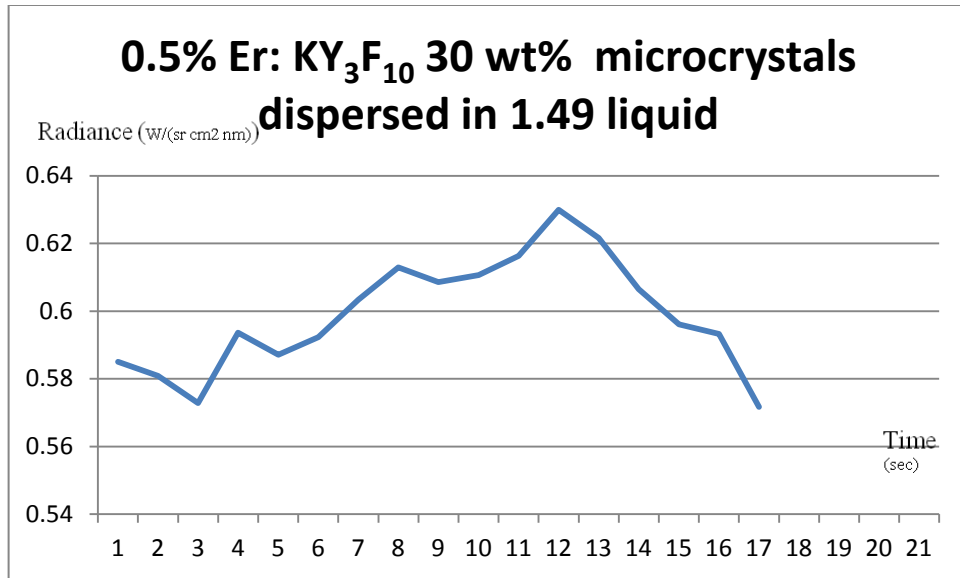


Figure 6.4.2.1. Green emission strength measurement for 0.5% Er: KY₃F₁₀ 30 wt% dispersed in 1.49.

6.5 Transparency

6.5.1 Medium 1%Er: NaYF₄ dispersed in 1.468 liquid

To determine the degree of transparency, a comparison was made among the same microcrystal particles using different concentrations.

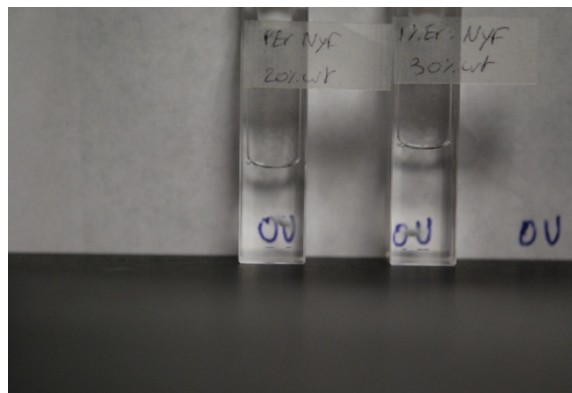


Figure 6.5.1.1. Comparison between 1%Er: NaYF₄ 20 wt% and 30% Wt dispersed in 1.468.

The samples used in Figure 6.5.1.1 had 20% wt and 30% wt concentration of particles. Looking at the letters OU in the picture above, one can see that the 30%

concentration was more opaque. Thus, increasing particle concentration increases scattering and decreases transparency.

6.5.2 Medium 0.5% Er: KY₃F₁₀ dispersed in 1.49 liquid

The 0.5% Er: KY₃F₁₀ sample dispersed in 1.49 liquid was tested with concentrations of 20% and 30%.

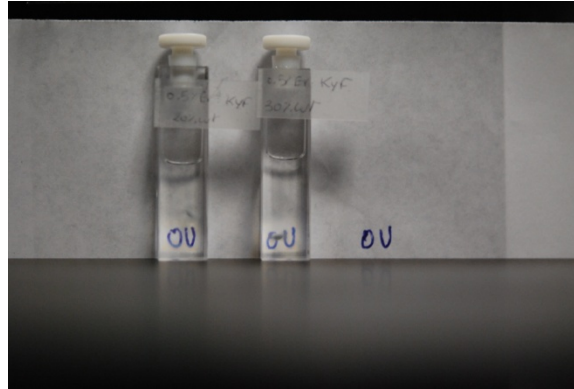


Figure 6.5.2.1. Comparison between 0.5% Er: KY₃F₁₀ 30wt% and 20% dispersed in 1.49 liquid.

The picture above shows that increasing the particle concentration of 0.5% Er: KY₃F₁₀ increases opacity.

Due to difficulties in achieving a scatter-free microcrystal medium, a tradeoff between the degree of transparency and the green emission strength must be identified. Hence, if the desired application is for a large size display, then the concentration should be lower than that for a smaller display to sustain a certain degree of transparency. This will aid the viewer in seeing the image, even if it is not as bright.

Chapter 7

Bulk crystals

Another experiment was conducted wherein a laser was projected through a collection of bulk crystals. The green voxel that appeared from the sample was measured using the green emission measurement protocol described in Chapter 4.

7.1 Bulk Crystal 1%Er:NaYF₄

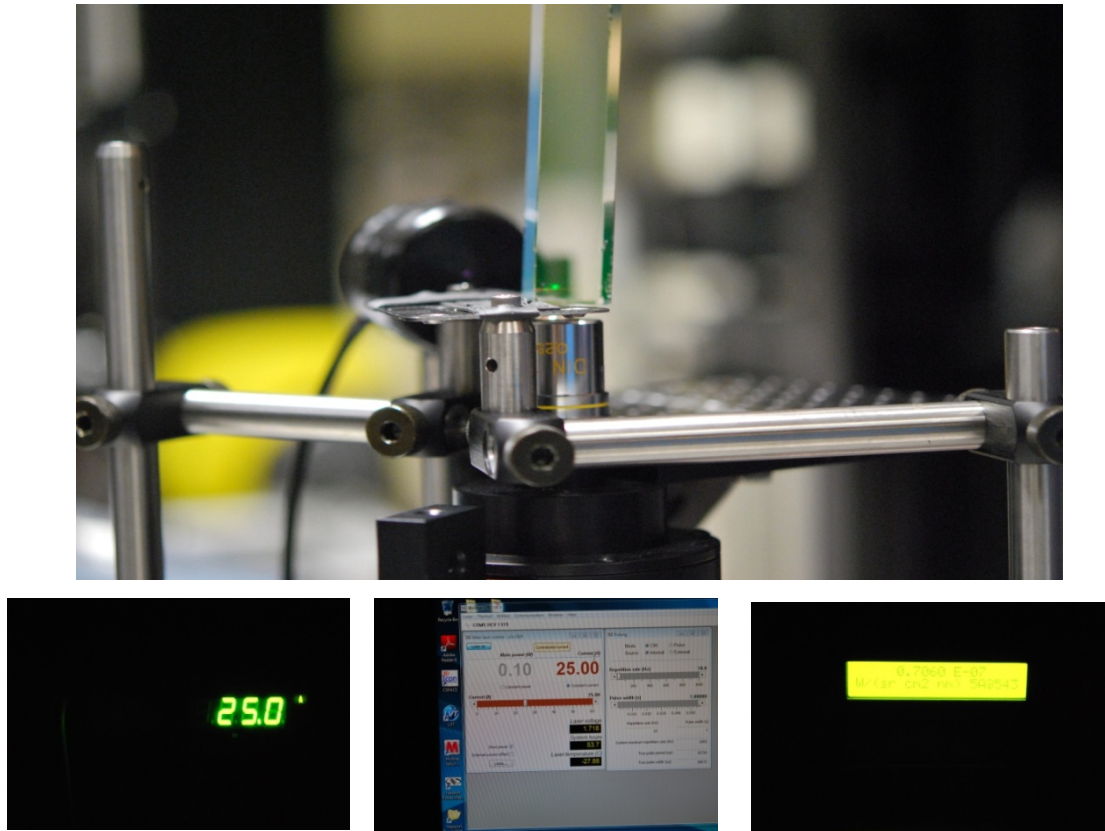


Figure 7.1.1. 1%Er: NaYF₄ bulk crystal- 25 Amperes were applied on each laser source to generate the required optical powers from both lasers of 850 nm and 1532 nm.

As shown above in Figure 7.1.1, the green emission strength for the bulk crystal 1%Er: NaYF₄ was 0.7073.

7.2 Bulk Crystal 2%Er: NaYF₄

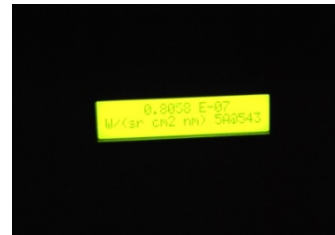
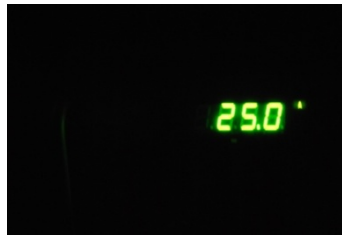
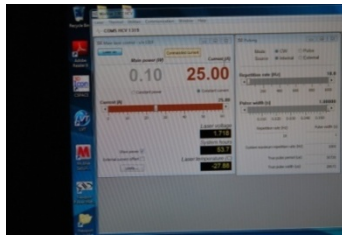
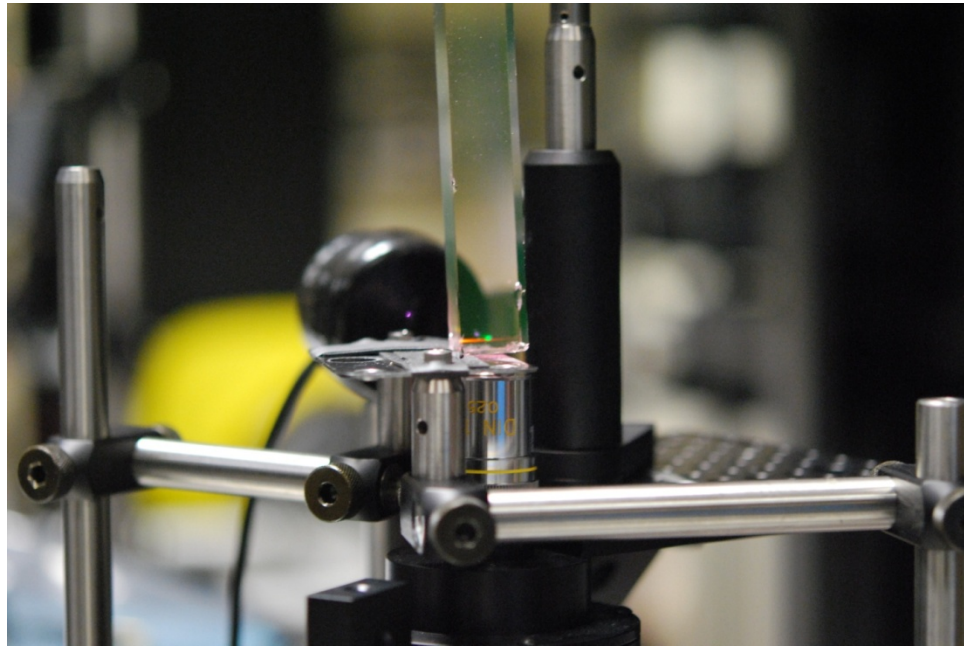


Figure 7.2.1. 2%Er: NaYF₄ bulk crystal.

Figure 7.2.1 demonstrates that the green emission strength for the bulk crystal 2%Er:NaYF₄ was 0.8065.

7.3 Bulk Crystal 0.5% Er:KY₃F₁₀:

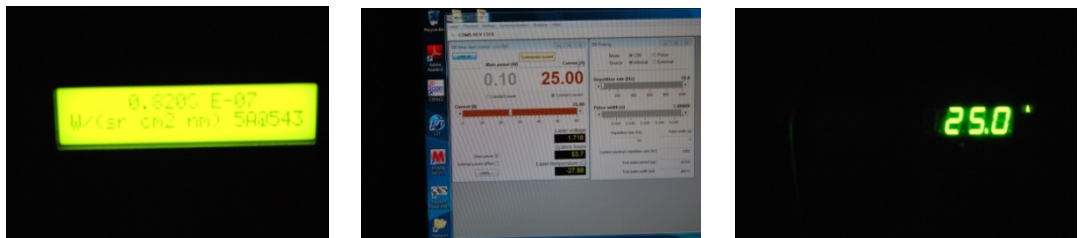
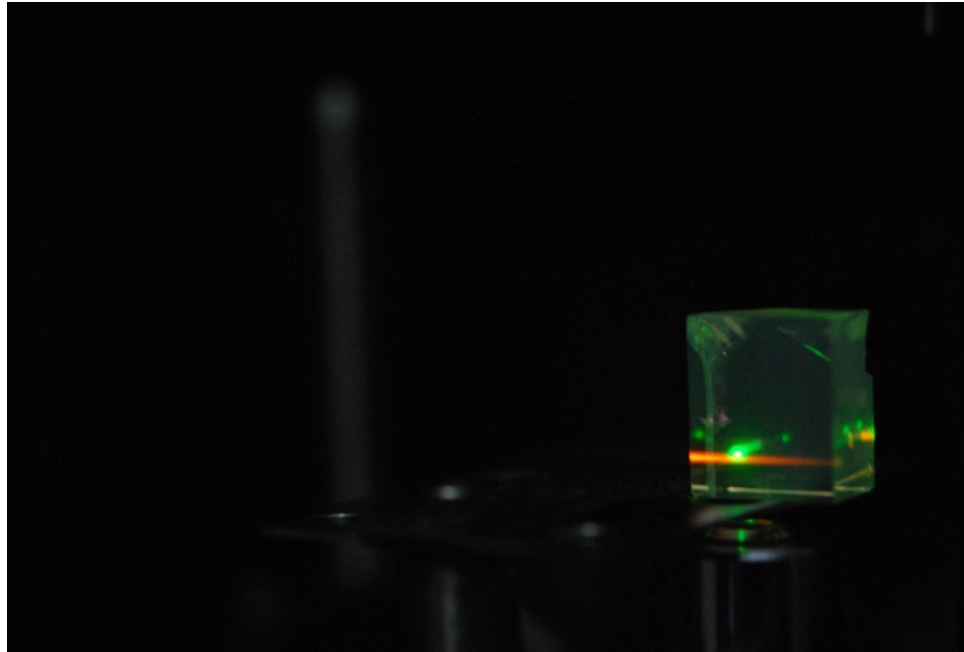


Figure 7.3.1. 0.5% Er: KY₃F₁₀bulk crystal.

Figure 7.3.1 shows that green emission strength for the bulk crystal 0.5% Er: KY₃F₁₀ was 0.8203.

7.4 Bulk Crystal 0.5% Er: YLF:



Figure 7.4.1. 0.5% Er: YLF bulk crystal.

Figure 7.4.1 demonstrates that the green emission strength for the bulk crystal 0.5% Er: YLF was 0.0411.

7.5 Data analysis

The bulk crystals under study are listed below.

1%Er: NaYF₄17x17x100 mm³

2%Er: NaYF₄17x17x100 mm³

0.5% Er: KY₃F₁₀10x10x10 mm³

0.5% Er: YLF 17x17x70 mm³

Green emission measurements for the studied samples are enumerated in the following table.

Sample	1%Er: NaYF ₄	2%Er: NaYF ₄	0.5% Er: KY ₃ F ₁₀	0.5% Er: YLF
Green emission strength	0.7073	0.8065	0.8203	0.0411

Table 7.5.1. Green emission measurements for the studied bulk crystal.

Results show that the crystal 0.5% Er: KY₃F₁₀, delivered the optimal green emission strength measurement, and 0.5% Er: YLF delivered the worst.

Although the 0.5% Er: KY₃F₁₀ bulk crystal was found to be the most promising medium for the CSpace[®] 3D display, growing the crystal is an expensive, time-consuming process. Hence, instead of struggling to grow a large crystal of 0.5% Er: KY₃F₁₀, it is preferable to grow small crystals of 0.5% Er: KY₃F₁₀, and then grind them into a powder before placing them in an index matched host. After preparing 0.5% Er: KY₃F₁₀ microcrystal powder and dispersing it in various refractive index liquids with varying amounts of particle concentrations, the 0.5% Er: KY₃F₁₀ microcrystal 30% wt sample dispersed in 1.49 liquid was found to be optimal.

Sample	bulk	10% wt	20% wt	30% wt
0.5%Er:KY ₃ F ₁₀	0.8203	0.056	0.437	0.5989

Table 7.5.2. Green emission for the sample 0.5% Er: KY₃F₁₀

Table 7.5.2 shows that the best results were found using bulk crystal. In order to obtain a scalable medium, 30% of 0.5% Er: KY₃F₁₀ dispersed in 1.49 oil is optimal. Table 7.5.2 also confirms that the percentage of weight from the bulk crystal is not linearly related to the percentage of the green emission strength, i.e., there is no linear relation between the percentile of the weight and the brightness.

Chapter 8

Review of results and analysis, and 3D Image constructed using the CSpace[®] display

As explained in previous chapters, a number of preliminary experiments and measurements were conducted to evaluate the green emission strength and scattering of several bulk crystals and microcrystal candidates. For microcrystals, cuvettes were prepared wherein each cuvette contained oil with a specific refractive index of the following: 1.45, 1.456, 1.46, 1.468, 1.47, 1.472, 1.474, 1.476, 1.478, 1.48, 1.484 and 1.49.

A 10% weight concentration of microcrystal powder of 1%Er: NaYF₄, which equaled 10% of the liquid weight, was added to each sample. The same preparation was used for 0.5% Er: KY₃F₁₀ and 0.5% Er: YLF, as well. Using a magnetic bar and stirrer, microcrystals were uniformly distributed within the liquid throughout the time period the medium was measured. Results show that the 1%Er:NaYF₄ microcrystal sample dispersed in 1.468 proved superior when compared with microcrystal powder of 1%Er: NaYF₄ dispersed in 1.45, 1.456, 1.46, 1.47, 1.472, 1.474, 1.476, 1.478, 1.48, 1.484, and 1.49 refractive index liquids. Also, the sample 0.5% Er:KY₃F₁₀ microcrystal dispersed in 1.49 liquid was the best selection when compared with the microcrystal powder of 0.5% Er: KY₃F₁₀ dispersed in 1.45, 1.456, 1.46, 1.468, 1.47, 1.472, 1.474, 1.476, 1.478, 1.48, and 1.484 refractive index liquid. Various concentrations of 20% wt and 30% wt of 1%Er:NaYF₄ and 0.5% Er: KY₃F₁₀ microcrystal powders were prepared. Optical characterization, including green emission strength and scattering, were conducted as well. Results showed that increasing the concentration of microcrystal powder for 1%Er:NaYF₄ dispersed in 1.468 liquid from 10% wt to 20% wt, and then also at 30%

wt, increased green emission strength from 0.0517 to 0.0591 to 0.07, respectively. Increasing the concentration for the 0.5% Er: KY₃F₁₀ microcrystal sample dispersed in 1.49 liquid from 10% to 20% wt, and then to 30% wt, also increased green emission strength from 0.056 to 0.437 to 0.5989, respectively. Notably, the intensity of the emission significantly depended on the concentration of the particles. Results proved that increasing the particle concentration of the sample 0.5% Er:KY₃F₁₀10% wt microcrystal dispersed in 1.49 liquid to 20% wt increased green emission strength from 0.056 to 0.437.

In spite of comparing green emission of the microcrystal samples and the bulk crystal candidates, similar measurements for the bulk crystal 0.5% Er:KY₃F₁₀, 1%Er:NaYF₄, and 2%Er:NaYF₄ were carried out. The results are shown below in the Table 8.1.

Sample candidate	Bulk crystal	Microcrystal powder 10% wt	Microcrystal powder 20% wt	Microcrystal powder 30% wt
1%Er: NaYF ₄	0.7073	0.0517	0.05912	0.0706
0.5% Er: KY ₃ F ₁₀	0.8203	0.056	0.437	0.5989
LLF	0.0411			

Table 8.1. Green emission measurements for the studied samples.

Several observations are apparent. First, the intensity of the emission significantly depends on the concentration of particles, and, therefore, it is imperative to

highly increase the concentration of particles. However, increasing the particle concentration decreases transparency. If increasing particle concentration exceeds a certain level, a large amount of scattering will occur, which in turn decreases brightness. Hence, increasing the particle concentration should be to a level wherein both transparency and brightness of the sample is acceptable.

Second, there is no linear relation between the percentage of particle concentration on the microcrystal and the emission strength of the voxel. The green emission strength for the bulk crystal 0.5% Er:KY₃F₁₀ was 0.8203, but the sample with a 20% wt of the microcrystal had a green emission strength of 0.43. Hence, the effect of the weight of the particle concentrations on the microcrystal samples relative to green emission strength is not a linear process.

In spite of scattering measurements, results proved that increasing particle concentration increases scattering and decreases transmission. Since it is impossible to achieve a scalable medium that is exceptionally bright and scatter-free, a tradeoff between brightness and scattering is necessary. To determine the level of concentration, several specifications need to be considered, such as the display medium size and the voxel brightness desired.

This investigation found that 0.5% Er: KY₃F₁₀30% wt microcrystal powder dispersed in 1.49 liquid offered an acceptable level of both transparency and brightness. With this sample, a scalable medium was achieved, and a 3D image was rendered using CSpace[®] display.

8.1 Volumetric 3D image inside special image space constructed using CSpace[®] display

The CSpace[®] display used for the current investigation and its operating principles are described in Chapter 2. An image was created inside the image space using the two-step two-frequency up-conversion (TSTF-UC) method. The image space used for the current work was a Fluorometer cell (cuvette) [47] of size of 12.5 mm x 42mm x 48 mm. The interior size of the cuvette was 10 mm x 40 mm x 45mm filled with 30% microcrystal of 0.5%Er: KY₃F₁₀ dispersed within oil that has refractive index of 1.49. The image space is shown in Figure 8.1.1.

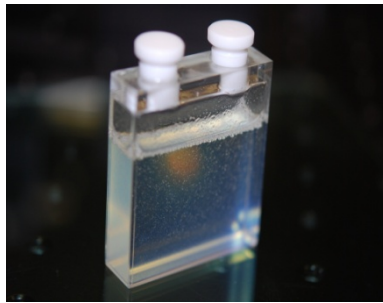


Figure 8.1.1. Scalable medium for CSpace[®] display.

To create an image like the gear shown in Figure 8.1.2, the CSpace[®] display will slice the gear into six slices.



Figure 8.1.2. The desired image “gear” [48].

Clearly, for this particular image, all six slices are similar to each other, as shown in Figure 8.1.3.

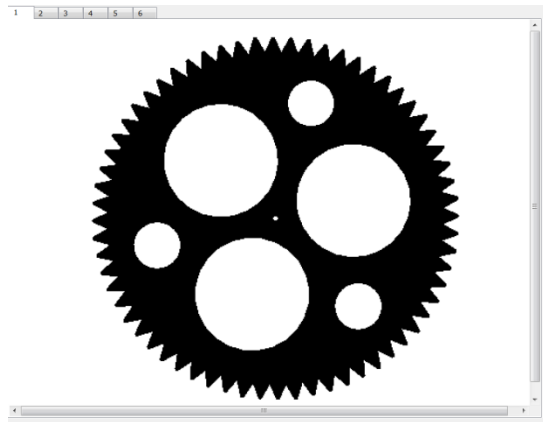


Figure 8.1.3. Six slices for the gear image.

The construction of these six slices within the 2D screen is shown in Figure 8.1.4.

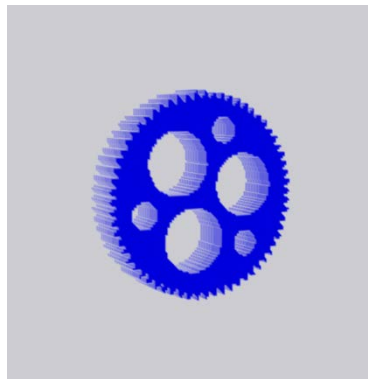


Figure 8.1.4. The gear with depth of 6 slices.

To render this image using the CSpace[®] display, mirrors in both DMDs were selected such that the beams were both present only at specific points. Typically, one line of mirrors in the addressing system is activated, effectively illuminating one slice of the image space. Each sphere in the slice corresponds to one mirror in the DMD of the

imaging system. By selecting and activating the appropriate mirrors in the imaging system DMD, only those spheres needed to create the image are illuminated by the 850 nm light, and only these voxels emit green light to make the image visible to the observer.

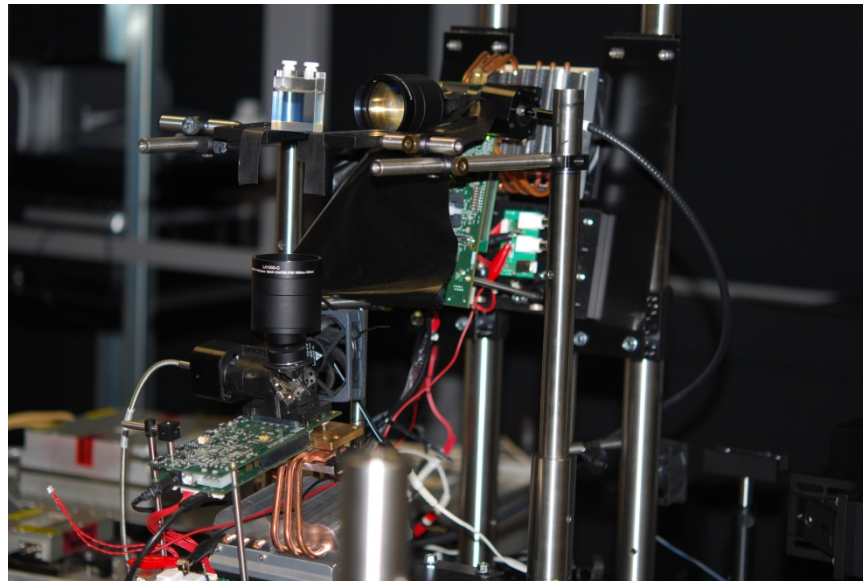


Figure 8.1.5. The scalable medium placed in the CSpace[®] display.

A fully 3D image was rendered by illuminating successive slices in the image space and activating the appropriate voxels within each slice, as shown in Figure 8.1.6.

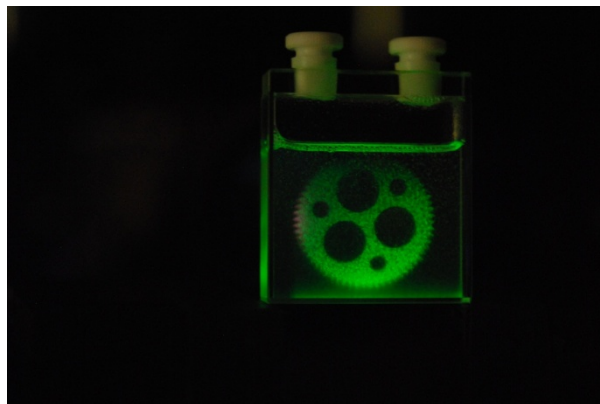


Figure 8.1.6. The desired image “gear” in 3D using CSpace[®] display.

Successive slices contain the cross-sectional 2D images of the 3D image. To generate

a flicker-free 3D image, all slices must be rendered in a time less than the processing time of the retina. This indicates that the complete scan of the image space must be achieved at least in less than 60 ms and preferably close to 30 ms. The display relies upon a special 3D graphics engine developed by 3DIcon Corporation to partition images into slices, and then provide the necessary control signals to the DLP systems. Figure 8.1.7 shows the constructed 3D image from several directions.

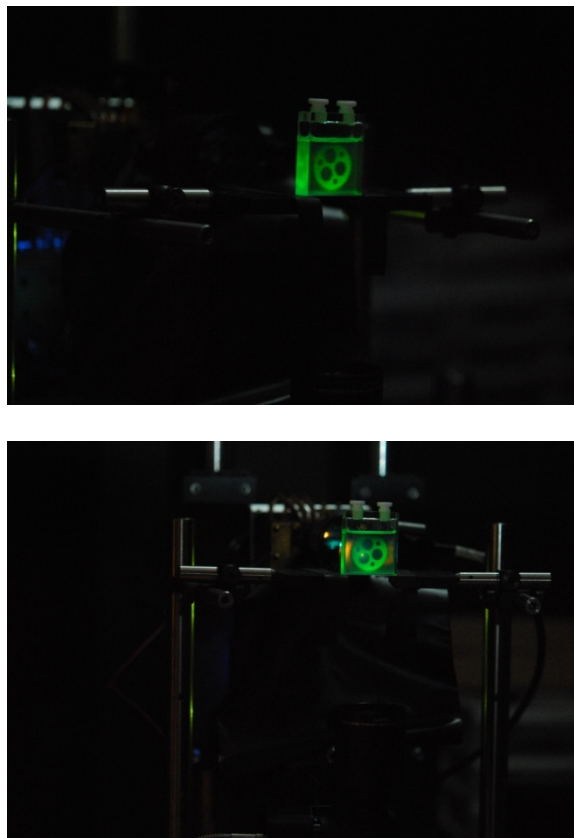


Figure 8.1.7. The desired image from different directions.

Chapter 9

Conclusion and Future Work

9.1 Conclusion

The goal of any 3D (volumetric) display is to present the viewer with a high resolution image that can be viewed from a wide range of angles and to provide both the level of detail and image size required for the target application. There are generally two difficulties encountered in producing a large 3D image; each is related to a particular method of image generation. For swept-volume displays, the imaging surface is physically swept through the intended image volume as addressing lasers project images onto the surface. The difficulty encountered for this type of display is the size of the surface required combined with the need to move the surface rapidly throughout the display volume. To the best of the author's knowledge, no practical demonstration of a large-volume 3D display based on this method has been reported. For static-volume displays, the image is generated in a static material by an interaction between the addressing lasers and the material itself. A commonly used approach is TSTF-UC, where two infrared lasers generate visible light emission from only the volumes where the two lasers intersect with sufficient power density [49] [50]. The difficulty encountered for this type of display is that the materials used for the display volume are almost exclusively high-quality optical crystals. Such crystals can be easily grown in small sizes (1 cm³, for example) but larger scale growth is more difficult to achieve [51]. Crystal volumes greater than 10 cm³ are also costly to grow and require high quality equipment and growing facilities. Even under optimal conditions there may be multiple failures before a crystal of sufficient quality for use in a 3D display is achieved. The cost of this process, both in time and materials, is impractical for use in

commercial applications. For relatively small displays, a greater volume may be achieved by cementing several smaller crystals together, but this process is not practically scalable and disruptions of the image at the crystal boundaries remains a problem.

An alternative method was presented for achieving a large-volume TSTF-UC based display using microcrystals dispersed within a liquid, index-matched host. The microcrystal were generated by quite simply growing Small crystals, grinding them into micro-size powder, and then dispersing them in an index matched host. Dispersion of these microcrystals was done in different refractive index liquids, including 1.45, 1.456, 1.46, 1.468, 1.47, 1.472, 1.474, 1.476, 1.478, 1.48, 1.484, and 1.49. The refractive index of the microcrystal candidates was identified. Green emission strength and scattering measurements were demonstrated. 0.5% Er:KY₃F₁₀ microcrystals dispersed in 1.49 liquid offered superior results. Increasing the particle concentrations was studied, as well. The prototype scalable medium 0.5% Er: KY₃F₁₀ microcrystal 30% wt dispersed in 1.49 oil demonstrated acceptable transparency and brightness. A 3D image was displayed on the prototype scalable medium that was created.

The prototype scalable medium achieved is effective. The liquid medium provides scalability and flexibility of the imaging volume and requires less time at a lower expense and is potentially lighter in weight than the traditional whole-crystal medium.

9.2 Future work

Although the prototype scalable medium 0.5% Er: KY₃F₁₀ microcrystal 30% wt dispersed in 1.49 oil provided the most acceptable transparency and brightness characteristics of all samples studied, it is expected that the levels achieved are not the upper limits possible. The materials studied for this work can be further improved by shaping particles, sieving them, and studying the effect of size and shape on scattering.

Since a high concentration of particles is necessary to increase brightness, increasing the particle concentration is recommended. However, it is important to remember that doing so will affect the transparency and increase scattering. Therefore, the use of smaller size particles could result in a significant reduction in scattering and, at the same time, increase brightness [52]. This result is due to the fact that the number of particles in the same volume will be much higher than that of the large particles.

The main disadvantages of the prototype sample were particle instability over time and internal scattering due to the non-transparency. One way to overcome this is utilizing polymer gel as the host material [53] [54]. Other materials (crystal hosts), such as ceramic crystal, can also be investigated.

References

- [1] B. G. Blundell, A.J. Schwarz, "Volumetric three dimensional display systems", Wiley-Interscience, 2000.
- [2] S. Y. Edgerton, "The Renaissance rediscovery of linear perspective", Basic Books, New York, 1975.
- [3] D. F. McAllister, "Display Technology: Stereo & 3D Display Technologies", Raleigh, NC: North Carolina State University, 2002.
- [4] Y. Yeh, Visual and perceptual issues in stereoscopic color displays. In "Stereo computer graphics and other true 3D technologies", Ed. D. McAllister, Princeton University Press, 1993.
- [5] C. Wheatstone, "Contributions to the Physiology of Vision. -Part the First. On some remarkable, and hitherto unobserved, Phenomena of Binocular Vision", Philosophical Transactions of the Royal society of London, 128, 371-394, June 1838.
- [6] I. P. Howard and B. J. Rogers, "Binocular Vision and Stereopsis", Oxford university press, New York, 1995.
- [7] B. Lane, "Stereoscopic displays", Proceedings of the SPIE, Vol. 367, Aug. 1982.
- [8] T. Okoshi, "Three- dimensional imaging techniques", Academic press, New York, 1976.
- [9] L. Sexton, P. Surman, " Stereoscopic and Autostereoscopic Display Systems", IEEE Signal Processing Magazine, Vol. 16, No. 3, May 1999.
- [10] K. Lizuka, "Welcome to the Wonderful World of 3D: Anaglyph Experiments", Optics & Photonics News, Vol. 18, No. 2, February 2007.
- [11] A. Schwerdtner, "Autostereoscopic 3D display", Stereoscopic Display and Virtual Reality Systems XIII, Proc. SPIE-IS&T, 6055, 2006.
- [12] B. Delaney, "Forget the Funny Glasses", IEEE computer graphics and applications, Vol. 25, No. 3, May-June 2005.
- [13] N. A. Dodgson, "Autostereoscopic 3D Display", IEEE computer magazine, Vol. 38, No. 8, August 2005.
- [14] N. A. Dodgson, "Autostereo displays: 3D without glasses", EID '97(Electronic Information Displays), Esher, Surrey, 18th-20th Nov.1997.

- [15] R-P.M. Berretty, F.J. Petersand G.T.G. Volleberg "Real-time rendering for "multiviewautostereoscopic Displays" Proc. SPIE 6055, 60550N, 2006.
- [16] P. Surman, I. Sexton, R. Bates, W. K. Lee, K. Hopf, T. Koukoulas, "Latest developments in a multi-user 3D display", Three-dimensional TV, Video, and Display IV, Proc. Of SPIE Vol. 6016, 2005.
- [17] J . Kim, K. Hong,J -H. Jung,G. Park, J. Lim, Y. Kim, J. Hahn, S-W. Min, and B. Lee, "High-definitionIntegral floating display with multiple spatial light modulators," P roc.SPIE 7 237, 7 237 OT, 2009.
- [18] <http://en.wikipedia.org/wiki/Holography>.
- [19] B. G. Blundell, A. J. Schwarz, "The Classification of Volumetric Display Systems: Characteristics and Predictability of the Image Space", IEEE Transactions on Visualization and Computer Graphics, Vol. 8, No. 1, January-March 2002.
- [20] G. E. Favalora, "Volumetric 3D Displays and Application Infrastructure", IEEE computer, Vol. 38, No. 8, August 2005.
- [21] G. E. Favalora, J. Napoli, D. M. Hall, R. K. Dorval, M. G. Giovinco, M. J. Richmond, W. S. Chun, "100 Million-voxel volumetric display", in Cockpit Displays IX: Displays for Defense Applications, Proceedings of SPIE, Vol. 4712, pp. 300-312, 2002.
- [22] http://www.actuality-medical.com/site/content/perspecta_display1-9.html
- [23] K. Langhans, D. Bezecny, D. Homann, D. Bahr, C. Vogt, C. Blohm, K. Scharschmidt, "New portable FELIX 3D display", Projection display IV, Proceedings of SPIE, Vol. 3296, 24-30 January 1998.
- [24] A. Sullivan, "DepthCube solid-state 3D volumetric display", Stereoscopic Displays and Virtual Reality Systems XI, Proceedings of SPIE, Vol. 5291, May 2004.
- [25] E. Downing, L. Hesselink, J. Ralston, R. Macfarlane, "A Three-Color, Solid State, Three- Dimensional Display", Science, Vol. 273, No. 5279, August 1996.
- [26] <http://www.3dicon.net/>
- [27] H. H. Refai, "CSpace- Static Volumetric Display," in Digital Holography and Three-Dimensional Imaging, OSA Technical Digest (CD) (Optical Society of America, 2010), paper DWB3.
- [28] H. H. Refai, "Static volumetric three-dimensional display," IEEE/OSA Journal of Display Technology, Vol. 5, Issue 10, PP. 319-397, October 2009.

- [29] N. Bloembergen, "Solid state infrared quantum counters", Physical review letters, Vol. 2, pp. 84-85, 1959.
- [30] F. Wang, X. Liu, Recent advances in the chemistry of Lanthanide-doped Upconversion Nanocrystals, Chem.Soc.Rev.38:976-989.
- [31] F. Azuel. The luminescence of inorganic solids. Plenum Press, New York, 1979.
- [32] A. Rappaport, J. Millez, M. Bass, A. Cassanho and H. Jenssen, "Review of the properties of up conversion phosphors for new emissive displays", Journal of display technology, VOL.2, NO.1, March 2006.
- [33] J. L. Sommerdijk, "On the excitation mechanisms of the infrared-excited visible luminescence in Yb, Er-doped fluorides," Journal of Luminescence, vol. 4, pp. 441-449, 1971.
- [34] A. Rapaport, V. David, M. Bass, C. Deka, and L. A. Boatner, "Optical spectroscopy of erbium-doped lutetium orthophosphate," Journal of Luminescence, vol. 85, pp. 155, 1999.
- [35] P. E. A. Mobert, E. Heumann, G. Huber, and B. H. T. Chai, "Green Er:YLiF upconversion laser at 551 nm with Yb codoping: a novel pumping scheme," Optics Letters, vol. 22, pp. 1412, 1997.
- [36] L. F. Johnson, H. J. Guggenheim, T. C. Rich, and F. W. Ostermayer, "Infrared-to-visible conversion by rare-earth ions in crystals," Journal of Applied Physics, vol. 43, pp. 1125-1137, 1972.
- [37] C. Wyss, W. Luthy, H. P. Weber, P. Rogin, and J. Hulliger, "Energy transfer in Yb:Er:YLF," Optics Communications, vol. 144, pp. 31, 1997.
- [38] A. Dienes, P. E.-A. Mobert, and G. Huber, "Diode-pumped continuous-wave, quasi-continuous-wave, and Q-switched laser operation of Yb,Tm: YLiF₄ at 1.5 and 2.3 μ m," Journal of Applied Physics, vol. 84, pp. 5900-5904, 1998.
- [39] B. Koudsi, J. J. Sluss, "Static 3D image space", Emerging Liquid Crystal Technologies SPIE 7618, February 2010.
- [40] <http://physicsworld.com/cws/article/news/2010/feb/24/crystal-control-moves-towards-3d-displays>
- [41] M. Bass, H. Jenssen, "Display medium using emitting particles dispersed in a transparent host", U.S. Patent 6,327,074 B1, 2001.
- [42] http://en.wikipedia.org/wiki/Magnetic_stirrer.

- [43] <http://www.cargille.com/>.
- [44] <http://www.engr.uvic.ca/~mech580/electronmicroscopy/Introduction%20SEM.pdf>.
- [45] http://www.rp-photonics.com/collimated_beams.html.
- [46] J. Cho, M. Bass, and H. P. Jenssen, (2007), "Volumetric three-dimensional up-conversion display medium". *Journal of the Society for Information Display*, 15: 1029–1036. doi: 10.1889/1.2825087.
- [47] http://www.starnacells.com/d_cells_f/T018F.html
- [48] Google SketchUp.
- [49] J. Milliez, A. Rapaport, F. Szipocs, M. Bass, A. Cassanho, and H. Jenssen, "Upconversion efficiency of potential candidates for photonic displays," in *SID'2003 International Symposium- Digest of technical papers*, vol. XXXIV. Baltimore, MD: Society for Information Display, May 2003, pp. 1230-1233.
- [50] P. Caro and P. Porcher, "Infra-red excitation of visible luminescence in upconverters rare earth materials," *Journal of Luminescence*, vol. 18-19, pp. 257-261, 1979.
- [51] H. J. Scheel, "Historical aspects of crystal growth technology," *Journal of Crystal Growth*, vol. 211, pp. 1, 2000.
- [52] C. F. Bohren and D. R. Huffman, *Absorption and Scattering of Light by Small Particles*: John Wiley & Sons, Inc, 1998.
- [53] J. Ballato, S. Foulger, and D. W. Smith, Jr., "Optical properties of perfluorocyclobutyl polymers," *Journal of the Optical Society of America B (Optical Physics)*, vol. 20, pp. 1838, 2003.
- [54] J.-P. Boilot, J. Biteau, F. Chaput, T. Gacoin, A. Brun, B. Darracq, P. Georges, and Y. Levy, "Organic-inorganic solids by sol-gel processing: optical applications," *Pure and Applied Optics*, vol. 7, pp. 169-177, 1998.